

Investigation of the use of Limestone Calcined Clay Cement (LC3) applied to Thailand

Thèse N° 9005

Présentée le 18 janvier 2019

à la Faculté des sciences et techniques de l'ingénieur
Laboratoire des matériaux de construction
Programme doctoral en science et génie des matériaux

pour l'obtention du grade de Docteur ès Sciences

par

WILASINEE HANPONGPUN

Acceptée sur proposition du jury

Prof. D. Damjanovic, président du jury
Prof. K. Scrivener, directrice de thèse
Prof. M. Geiker, rapporteuse
Dr D. Herfort, rapporteur
Dr B. Lothenbach, rapporteuse

2019

Acknowledgements

First of all, I would like to express my very great appreciation to Prof. Karen Scrivener for giving me the opportunity to be a member of the exceptional workplace, Laboratory of Construction Materials at EPFL. Thank you for her supervising my Ph.D. research, her guidance and her time for discussion on my work. It was a great honor for me to share her extraordinary scientific knowledge. Thank you very much!

Special thanks to SCG Cement-Building Materials Co., Ltd. for the sponsorship of my Ph.D. program and my expenses here in Switzerland. In particular, I would like to thank Dr. Prinya Sainamthip, Mr. Sanit Kessuwan, Mr. Santi Lorlowhakarn, Mr. Sompong Luankosolchai, Mr. Manasit Sarigaphuti, Dr. Sakprayut Sinthupinyo, Mr. Surachai Vangrattanachai, Asst. Prof. Sirithan Jiemsirilers and SRI-CAT family for their support and encourage me to study Ph.D. at EPFL. I also thank P'Dean for fluidized bed calcination, N'Ball & N'Arm for rotary kiln calcination and P'Arnon for carbonation testing in Thailand.

I would like to thank the members of my jury for their insightful comments and suggestions to finish my thesis: Prof. Damjanovic Dragan, Prof. Mette Geiker, Dr. Duncan Herfort, and Dr. Barbara Lothenbach. I also thank Prof. Paul Bowen for being a jury of my yearly exam.

My special thanks are extended to François for his tremendous help to correct my English, the scientific discussions and also a wonderful lunch and the hiking place, Thank you! Thank you!

I thank my fellow officemates, Wiola for being my officemate for 4 years. Also, I thank my short term officemates, Arnaud, John, Anuj, Yuvaraj, Sundar, Hong, Mariana and Sarra for their colors of my life.

I thank all of LMC people, you guys Rock! For the same generation: Julien for the IT solving, Alex for the MATLAB code, Fabien for the rate method, Emmanuelle for the beautiful SEM images, Xuerun for the XRD training, Hamed for the chloride testing, Aurélie for the ASR testing, Lily for training of MIP, Silas is a LC³ manager, Franco for becoming a Thai nah!, Yosra for a kaki, Alex-P for a cup of coffee, Monisha for a birthday cake, Solene for exchanging Cuban money, Mahsa for her volunteer, Shiyu for running, Yu Yan for having KFC in Geneva, Yan for a nice dinner, Marcelo and his wife for brigadieros, Hadi for hiding my iPhone, Elise for her suggestions, Berta for alkali discussion, Pawel for his sister who treats my little finger, Frank for Haribos, Aslam for Al(VI), Abhishek for C-S-H, William for a Mac charger. I also thank the visitors and the new generation of LMC: Vineet, Sreejith, Arun, Geetika, Adrian, Akin, Junjie, Josh, Andrea, Qiao, Khalil, and Baghath for refreshing LMC. It was fantastic to know and work with you guys. Brilliant!!!

I am also grateful to the following LMC staffs: Maude for her kind assistance and wonderful organization for the events, Anne-Sandra and Marie Alix for their unfailing support, Lionel, Jean, Antonio and Nathan for their technical help.

Also, I thank all my Thai friends. They made me feel like I am always at home. Ji for the trips and running event, Fern & Ake & Tar for their companion, N'Erng for her stories, P'Wynn for the wonderful place for dinner parties, P' Kiat for the inside news, N' Bank & N' Num for the special Thai food and sweets, N'Golf for the information of SCG.

Finally, I would love to acknowledge my beloved family: Khun Vibool, Khun Nalinee, Munjai and Jaurusup for their love, constant support and inspiration.

Lausanne, 16th November 2018

Wilasinee Hanpongpun (Mink)

Abstract

The replacement of clinker with supplementary cementitious materials (SCMs) is the most interesting solution to reduce the CO₂ emissions from cement production. The abundant availability of clays, which have a sufficient amount of kaolinite content in Thailand, has led to the development of an alternative SCM.

The raw materials in this study come from Thailand and are used to formulate limestone calcined clay cement (LC³). The objectives of this thesis are to investigate the influence of the substitution level, the cement composition and the calcination process of calcined clay on the hydration reaction, the mechanical, rheological and durability properties of LC³. The properties of LC³ were also investigated at 30°C simulating the climate conditions in Thailand for LC³ application.

Limestone and calcined clay can replace clinker up to 45% with excellent results. LC³-80(2:1), LC³-65(2:1) and LC³-50(2:1) correspond to blended cements containing 80%, 65% and 50% of clinker, respectively, 5% of gypsum and 15%, 30% and 45% of calcined clay and limestone with a fixed ratio of 2:1. The replacement of clinker with calcined clay and limestone leads to a significant porosity refinement. This refinement results in the improvement of chloride ingress resistance. Concerning strength development, the gel-space ratio permits to correlate strength with the phase assemblage. The compressive strength of all LC³ blended systems meets the standard value of OPC type I (ASTM C150) or CEM I 42.5N (EN 197-1). Increasing temperature from 20°C to 30°C promotes the clinker hydration and the pozzolanic reaction resulting in the enhancement of strength development at the early ages. LC³-65(2:1) is commercially promising in Thailand in term of maximum substitution level coupled with satisfying results in terms of durability and strength.

For the optimization of LC³ properties, the influence of the alkali content in cement is investigated. KOH or NaOH are used to adjust the alkali equivalent ($\%Na_2O_{eq} = \%Na_2O + 0.658 \cdot \%K_2O$) from 0.44% to 1.20%. Increasing alkalinity accelerates the clinker hydration and enhances the precipitation of hydration products at early ages but it shows the opposite at late ages. The lower gel-space ratio and the increase of porosity in high alkali condition cause the dramatical decrease of strength at later ages. NaOH is more harmful on the properties of LC³-65(2:1) than KOH. Therefore, the maximum alkali equivalent of LC³-65(2:1) is 0.77% Na₂O_{eq} (or 0.99% Na₂O_{eq} in PC) for KOH addition and 0.63% Na₂O_{eq} (or 0.79% Na₂O_{eq} in PC) for NaOH addition to prevent the negative effects at later ages.

Concerning the influence of the calcination method, calcined clay produced by the rotary kiln process has a lower surface area compared to the clay calcined from the fluidized bed because of a coarser pore width of calcined clay particles. Accordingly, the calcined clay produced by fluidized bed has a slightly higher reactivity at the beginning but there is no significant difference in the reactivity of calcined clay between these two processes later on. In terms of fineness, no increase of reactivity is found for calcined clay finer than 10 μm, i.e. there is no need of overgrinding for calcined clay. The different calcination processes and the variation of kaolinite content (45-50%) do not impact the activation energy (E_a) of calcined clays.

Keywords: Limestone calcined clay cement, LC³, SCMs, alkalis, calcination process

Résumé

Le remplacement partiel du clinker par des matériaux cimentaires de substitution est la meilleure approche pour réduire les émissions de CO₂ liées à la production de ciment. En Thaïlande, les argiles calcinées sont abondantes, et leur utilisation dans le ciment semble très prometteuse.

Les argiles utilisées dans cette étude proviennent de Thaïlande, et sont utilisées pour formuler les ciments calcaires argiles calcinées (LC³). Les objectifs de ce travail de thèse sont de promouvoir l'utilisation de LC³ en Thaïlande. Pour trouver la meilleure alternative possible, différents niveaux de substitution, compositions de ciment et méthodes de calcination de l'argile sont examinés. L'influence de ces paramètres sur les réactions d'hydratation, sur les propriétés rhéologiques, mécaniques et de durabilité est étudiée. De plus, pour répliquer les conditions climatiques de Thaïlande, des tests ont également été effectués à plus haute température, 30°C.

Trois niveaux de substitution ont été utilisés : LC³-80(2:1), LC³-65(2:1) et LC³-50(2:1), avec respectivement une fraction de clinker de 80%, 65% et 50%. 5% de gypse est présent dans chaque système. Le reste est composé d'une combinaison d'argile calcinée et de calcaire avec un ratio de 2 pour 1. Pour les trois niveaux de substitution, 15%, 30% et 45% d'argile calcinée et de calcaire sont ainsi considérés. Dans les ciments LC³, un important raffinement de la porosité est observé. Ce raffinement est responsable de l'excellente résistance aux chlorures. Concernant le développement des résistances mécaniques, les valeurs obtenues sont corrélées à l'assemblage de phase durant l'hydratation grâce à l'approche consistant à considérer le volume d'hydrates normalisé par l'espace disponible. Par ailleurs, tous les systèmes LC³ passent les standards OPC type I (ASTM C150) ou CEM I 42.5N (EN 197-1) en termes de performance. L'augmentation de la température de 20°C à 30°C accélère l'hydratation du clinker et la réaction du métakaolin dans l'argile calcinée. Les résistances à la compression sont améliorées à jeunes âges. Pour la Thaïlande, le système LC³-65 (2:1) est l'approche la plus prometteuse, avec le meilleur compromis en termes de résistances mécaniques et de durabilité.

Pour optimiser les propriétés du LC³, l'influence de la teneur en alcalis dans le ciment a été étudiée. KOH et NaOH ont été utilisés pour ajuster le contenu en alcalin ($\%Na_2O_{eq} = \%Na_2O + 0.658 \cdot \%K_2O$) de 0.44% à 1.20%. En augmentant le taux d'alcalin, l'hydratation est accélérée à jeunes âges mais l'effet opposé est observé pour des âges tardifs, où une augmentation de la porosité et une réduction des résistances à la compression sont observées. L'effet du NaOH est plus prononcé que le KOH. L'optimisation des propriétés du LC³-65 (2:1) est ainsi obtenue avec 0.77%Na₂O_{eq} pour l'addition de KOH et 0.63%Na₂O_{eq} pour le NaOH, sans pour autant dégrader les propriétés à âges tardifs.

Enfin, concernant l'influence du procédé de calcination, une surface spécifique moins élevée est mesurée pour l'argile calcinée par four rotatif par rapport au lit fluidifié. Cela conduit à une réactivité légèrement inférieure à jeune âge. En termes de broyage de l'argile, la réactivité de l'argile calcinée n'augmente plus en dessous d'une taille moyenne de 10 µm. Il n'y a par conséquent pas besoin de broyer trop finement l'argile calcinée. L'énergie d'activation de l'argile calcinée n'est en revanche pas influencée par les différents procédés de calcination.

Mots clés: Ciment calcaire argile calcinée, LC³, alcalins, procédé de calcination

Contents

Acknowledgements	iii
Abstract	v
Résumé	vii
List of Figures	xi
List of Tables	xv
Chapter 1. Introduction	1
1.1 Global situation of cement production	1
1.2 Kaolinite among clay types	2
1.3 Thermal activation of kaolinite	4
1.4 Combination of calcined clay and limestone	5
1.5 Properties of limestone calcined clay cement (LC ³)	5
1.5.1 Hydration reactions and microstructure development	5
1.5.2 Mechanical properties	7
1.5.3 Rheological properties	9
1.5.4 Durability properties	10
1.6 Motivation and objectives of the thesis	11
Chapter 2. Materials and Methods	13
2.1 Raw materials	14
2.2 Methods	15
2.2.1 Particle size distribution and specific surface analysis	15
2.2.2 Cement paste preparation	15
2.2.3 Isothermal calorimetry	15
2.2.4 X-Ray diffraction (XRD)	16
2.2.5 Thermogravimetric analysis (TGA)	17
2.2.6 Scanning electron microscopy (SEM)	18
2.2.7 Mercury Intrusion Porosimetry (MIP)	19
2.2.8 Pore solution extraction	21
2.2.9 Mass balance calculation	21
2.2.10 Compressive strength	22
2.2.11 Gel-Space ratio	22
2.2.12 Durability study	23
Chapter 3. Influence of substitution levels of calcined clay and limestone on the properties of LC³	25
3.1 Introduction	25
3.2 Formulations	25
3.3 Workability and mechanical properties	26
3.4 Hydration reaction and microstructure	28
3.4.1 Heat of hydration	28
3.4.2 Degree of reactions	29
3.4.3 Phase assemblage	30
3.4.4 Pore solution	31
3.4.5 Porosity	32
3.4.6 C-(A)-S-H composition	34
3.4.7 Microstructure	36

3.5	The relationship between compressive strength and porosity	39
3.6	The relationship between compressive strength and gel-space ratio	39
3.7	Summary	40
Chapter 4. The impact of alkalis on the properites of limestone calcined clay cement (LC³)...		41
4.1	Introduction	41
4.2	Formulations.....	42
4.3	Compressive strength	43
4.4	Kinetics.....	44
4.5	Degree of reaction.....	46
4.6	Phase assemblage	47
4.7	C-A-S-H composition	50
4.8	Porosity	52
4.9	Discussion	55
4.10	Summary.....	57
Chapter 5. Influence of calcination process on the reactivity of calcined clay and the properties of LC³		59
5.1	Introduction	59
5.2	Raw clays	60
5.3	Calcination and grinding process.....	61
5.4	Evaluation of quality of calcination.....	61
5.5	Calcined clay characterization.....	63
5.6	The reactivity of calcined clays	64
5.6.1	Influence of kaolinite content	64
5.6.2	Influence of particle size.....	65
5.6.3	Influence of calcination process.....	65
5.7	Workability of LC ³	67
5.8	Activation energy of calcined clays	70
5.8.1	Determination of activation energy of calcined clays.....	70
5.8.2	Results of activation energy of calcined clays.....	73
5.9	Summary.....	76
Chapter 6. Durability properites of LC³		77
6.1	Introduction	77
6.2	Carbonation.....	78
6.3	Chloride ingress.....	82
6.3.1	Migration testing	82
6.3.2	Ponding testing.....	83
6.4	Alkali silicate reaction (ASR)	86
6.5	Summary.....	88
Chapter 7. Conclusions and Perspectives		89
7.1	Conclusions.....	89
7.1.1	Substitution levels.....	89
7.1.2	Cement composition	89
7.1.3	Calcination process.....	90
7.1.4	Durability properties	90
7.2	Perspectives	91
7.2.1	Studying the durability properties	91
7.2.2	Understanding the workability of LC ³	91
Appendix		93
References		115
Curriulum Vitae		121

List of Figures

Figure 1.1 The amount of SCMs available worldwide	2
Figure 1.2 Diagrammatic sketch of Kaolinite, Montmorillonite, and Illite.....	3
Figure 1.3 Map showing locations of kaolinite deposits in Thailand and clays used in this study.....	3
Figure 1.4 ²⁷ Al NMR spectra of kaolinite, illite, and montmorillonite before and after calcination.....	4
Figure 1.5 XRD results of OPC, MK30, LS15, and MK-B45 at 1, 7, 28 and 90 days.....	6
Figure 1.6 MIP results of OPC and the blended cements at 28 days.	6
Figure 1.7 The critical pore entry radius plotted as a function of calcined kaolinite content (left) and the degree of clinker hydration as a function of time (right)	7
Figure 1.8 Relative compressive strength of B45 (LC ³ -50) varying metakaolin:limestone ratios.....	8
Figure 1.9 The relation between calcined kaolinite content and compressive strength of LC ³ -50 blends.....	8
Figure 1.10 Compressive strength of LC3-50 containing 15% of limestone (LC3), 15% of dolomite (DC3), and 15% of quartz (QC3)	9
Figure 1.11 The amount of superplasticizer used in LC ³ -50 mortars (left) and pastes (right).....	9
Figure 1.12 MIP results for PC and LC ³ -50 blends at 3 days and 28 days.....	10
Figure 1.13 Chloride profiles for PC and LC ³ -50 mortars	10
Figure 1.14 Correlation between the bound chloride and the critical pore entry radius with the apparent chloride diffusion coefficient	11
Figure 2.1 The overview of the samples and the main techniques used for the characterization /evaluation in this study.....	13
Figure 2.2 Heat evolution curve of OPC type I	16
Figure 2.3 TGA and DTG curves of a kaolinite clay	17
Figure 2.4 EDS point analysis of inner C-(A)-S-H	19
Figure 2.5 Determination of the C-(A)-S-H composition from the plot of Si/Ca versus Al/Ca	19
Figure 2.6 Dimensional range of phases and pores in a hydrated cement paste.....	20
Figure 2.7 MIP results showing derivative and cumulative curves of LC ³ -50(2:1) paste sample at 28 days	20
Figure 2.8 Procedure of mass balance calculation.....	21
Figure 2.9 The set-up of chloride migration test.....	23
Figure 3.1 The particle size distribution of raw materials	26
Figure 3.2 Flow test results of PC and LC ³ systems at 20°C.....	27
Figure 3.3 Compressive strength of PC and LC ³ systems at (a) 20°C and (b) 30°C	27
Figure 3.4 Heat flow of PC and LC ³ systems at 20°C (a) and 30°C (b) normalized per gram of solid (left) and per gram of clinker (right).....	28
Figure 3.5 Degree of clinker hydration of PC and LC ³ systems at (a) 20°C and (b) 30°C.....	29
Figure 3.6 Degree of metakaolin reaction of LC ³ systems at (a) 20°C and (b) 30°C.....	29
Figure 3.7 XRD patterns of PC and LC ³ systems at 20°C and 30°C for 1 day (a) 28 days (b).....	30
Figure 3.8 Volume of phase assemblage of PC and LC ³ systems evaluated by mass balance calculation cured for 3 days and 28 days at 20°C and 30°C	31
Figure 3.9 Pore size distribution of PC and LC ³ systems cured at 20°C and 30°C for 3 days and 28 days.....	33
Figure 3.10 Total porosity (a) and threshold pore radius (b) of PC and LC ³ systems.....	33
Figure 3.11 The critical pore radius of PC and LC ³ systems.....	34

Figure 3.12 Hc+Mc quantified by XRD-Rietveld analysis of PC and LC ³ systems at 20°C.....	34
Figure 3.13 The plot of Al/Ca vs Si/Ca of inner C-(A)-S-H of PC (a) LC ³ -80(2:1) (b), LC ³ -65(2:1) (c) and LC ³ -50(2:1) (d) cured at 20°C and 30°C for 28 days	35
Figure 3.14 The C-(A)-S-H composition of PC and LC ³ systems cured at 20°C and 30°C for 28 days showing Ca/Si (a) and Al/Si (b).....	36
Figure 3.15 BSE-SEM image (left) and its porosity analysis (right) of PC, LC ³ -80(2:1), LC ³ -65(2:1) and LC ³ -50(2:1) cured at 20°C for 28 days.....	37
Figure 3.16 BSE-SEM image (left) and its porosity analysis (right) of PC, LC ³ -80(2:1), LC ³ -65(2:1) and LC ³ -50(2:1) cured at 30°C for 28 days.....	38
Figure 3.17 The compressive strength of PC and LC ³ systems cured at 20°C and 30°C plotted as a function of total porosity.....	39
Figure 3.18 Compressive strength plotted versus gel space ratio considering C-(A)-S-H as the gel of PC and LC ³ systems cured at 20°C and 30°C.....	40
Figure 4.1 Compressive strength of PC and LC ³ -65(2:1) with various alkali contents.....	43
Figure 4.2 Relative compressive strength of LC ³ -65(2:1) with various alkali contents.....	43
Figure 4.3 Heat flow of PC and LC ³ -65(2:1) with various alkali contents (a) KOH addition and (b) NaOH addition	44
Figure 4.4 Determination of time to stop the hydration at the end of the acceleration period corresponding to the identical DoH of LC ³ -65(2:1)-0.44%Na ₂ O _{eq} (top left) and C-A-S-H morphology of LC ³ -65(2:1)-0.44%Na ₂ O _{eq} , LC ³ -65(2:1)-1.09%-K and LC ³ -65(2:1)-1.20%-N after stopped the hydration	45
Figure 4.5 Degree of clinker hydration of LC ³ -65(2:1) with various alkali contents.....	46
Figure 4.6 Degree of MK reaction of LC ³ -65(2:1) with various alkali contents.....	47
Figure 4.7 Volume of phase assemblage at 3 days and 28 days of LC ³ -65(2:1) with various alkali contents (a) KOH addition and (b) NaOH addition	48
Figure 4.8 Compressive strength vs gel-space ratio of LC ³ -65(2:1) systems, considering only C-A-S-H as the gel (a) and total volume of hydrated as the gel (b)	49
Figure 4.9 EDS analysis of LC ³ -65(2:1) with various alkali contents at 3 days (top) and 28 days (bottom).....	50
Figure 4.10 K/Si and Al/Si at 28 days of LC ³ -65(2:1) adjusted alkali content (a) KOH addition and (b) NaOH addition	51
Figure 4.11 Pore entry size distribution of LC ³ -65(2:1) with various alkali contents at 3 days for KOH addition (a) and NaOH addition (b)	52
Figure 4.12 Pore entry size distribution of LC ³ -65(2:1) with various alkali contents at 90 days for KOH addition (a) and NaOH addition (b).....	53
Figure 4.13 Compressive strength of LC ³ -65(2:1) with various alkali contents plotted as a function of total porosity (a) and threshold pore radius (b).....	54
Figure 4.14 Saturation index of C-S-H at 28 days of LC ³ -65(2:1) with various alkali contents.....	55
Figure 4.15 Comparison between the critical pore entry radius measured by MIP and the minimum pore radius for the growth of C-S-H calculated from saturation index at 28 days of LC ³ -65(2:1) with various alkali contents (a) KOH addition (b) NaOH addition	56
Figure 5.1 Pilot scale production for clay calcination (a) Rotary kiln (b) Fluidized bed.....	60
Figure 5.2 Visual observation of the raw clays for (a) rotary kiln and (b) fluidized bed.....	61
Figure 5.3 XRD of raw clays and calcined clays.....	62
Figure 5.4 TGA (a) and DTG (b) curves of raw clays and calcined clays	62

Figure 5.5 SEM images of raw clay with 45% kaolinite content and calcined clay taken by SEM-SE for morphology surface (top) and SEM-BSE for polishing surface (bottom)	63
Figure 5.6 The R ³ test (a) and compressive strength (b) of LC ³ -65(2:1) with different kaolinite content.....	64
Figure 5.7 R ³ test (a) and compressive strength of LC ³ -65(2:1) (b) with different size of calcined clay	65
Figure 5.8 R ³ test (a) and compressive strength of LC ³ -65(2:1) (b) with different calcination process.....	66
Figure 5.9 The correlation between heat release by R ³ test at 24 hr and the compressive strength of LC ³ -65(2:1) of all calcined clays used in this study	66
Figure 5.10 Flows of the mortar of PC and LC ³ -65(2:1) with the different condition of calcined clays (a) kaolinite content (b) particle size, and (c) calcination process	68
Figure 5.11 Spreads of PC and LC ³ -65(2:1) with the different condition of calcined clays (a) kaolinite content (b) particle size, and (c) calcination process	69
Figure 5.12 Fitting three heat accumulative curves for the superposition method.....	71
Figure 5.13 Determination of E_a from the plot of $\ln k(\tau)$ versus $1/T$ for the superposition method.....	72
Figure 5.14 Heat accumulative curve of R ³ test for the superposition method, before curve fitting (top) and after curve fitting (bottom)	73
Figure 5.15 Heat flow curve of R ³ test for the rate method.....	74
Figure 5.16 The E_a of calcined clays plotted as a function of heat releases for the rate method	74
Figure 5.17 The comparison of E_a using the different methods	75
Figure 6.1 The diagram showing the durability properties investigated in this study.....	77
Figure 6.2 The relative rate of carbonation as a function of the relative humidity of environment.....	78
Figure 6.3 Carbonation depth of PC, LC ³ -80(2:1), and LC ³ -65(2:1) for 6 months of exposure both indoor and outdoor conditions in (a) Switzerland and (b) Thailand.....	79
Figure 6.4 Carbonation depth of PC, LC ³ -80(2:1), and LC ³ -65(2:1) for 1 year of exposure both indoor and outdoor conditions in (a) Switzerland and (b) Thailand.....	79
Figure 6.5 Carbonation depth of PC, LC ³ -80(2:1), and LC ³ -65(2:1) for 2 years of exposure both indoor and outdoor conditions in (a) Switzerland and (b) Thailand.....	80
Figure 6.6 Carbonation depth plotted as a function of square root of time for samples cured for 28 days before exposure both indoor and outdoor conditions in (a) Switzerland and (b) Thailand	80
Figure 6.7 Carbonation coefficient of natural carbonation tested on mortars cured for 28 days before exposure.....	81
Figure 6.8 Chloride migration test results of PC and LC ³ systems (applied voltage = 20V)	82
Figure 6.9 MIP results of PC and LC ³ systems mortars cured at 20°C for 28 days before testing.....	83
Figure 6.10 The total chloride content as a function of depth of PC and LC ³ systems at 6 months and 1 year of exposure	83
Figure 6.11 The relation between chloride content at the top surface of mortars after 1 year of exposure in 3%NaCl solution and volume of AFm phases (Hc+Mc) analyzed on pastes cured for 28 days	84
Figure 6.12 Apparent chloride diffusion coefficient of PC and LC ³ systems.....	85
Figure 6.13 Apparent chloride diffusion coefficient of PC and LC ³ systems plotted as a function of threshold pore radius of mortars cured for 28 days before exposure	85
Figure 6.14 Mechanism of ASR damage in concrete.....	86
Figure 6.15 Expansion of PC and LC ³ -65(2 :1) soaked in 0.32 mol/L of NaOH at 38°C	87

List of Figures

Figure 6.16 MIP results at 28 days of cement pastes containing the same amount of cementitious materials with the tested mortars of PC and LC ³ -65(2:1) systems.....	87
Figure 6.17 The ions concentration of pore solution of cement pastes containing the same amount of cementitious materials with the tested mortars of PC and LC ³ -65(2:1) systems cured for 28 days (before exposure)	88
Figure 7.1 The optimal amount of alkali equivalent in PC and LC ³ -65(2:1) for KOH addition (a) and NaOH addition (b).....	90
Figure 7.2 Spread of LC ³ -65(2:1) paste after adding 0.25% and 0.5% of superplasticizer plotted as a function of BET surface area (a) and pore width (b) of the particle of calcined clay.....	91

List of Tables

Table 2.1 Chemical and physical properties of raw materials	14
Table 2.2 The phase composition of the PC	14
Table 2.3 Refractive index and absorption index of solutions and powders	15
Table 2.4 Phase density from GEMS	22
Table 2.5 The depth intervals of drilling	24
Table 3.1 Formulations of LC ³ blended cements	26
Table 3.2 Ion concentrations in pore solutions of PC and LC ³ systems cured at 20°C for 28 days	31
Table 3.3 Effective saturation indices of hydrates calculated using GEMS of PC and LC ³ systems	31
Table 4.1 Formulations and name of LC ³ -65(2:1) with various alkali contents	42
Table 4.2 The C-A-S-H composition of LC ³ -65 (2:1) with various alkali contents	51
Table 4.3 The minimum pore radius for the growth of C-S-H at 28 days	56
Table 5.1 Kaolinite and calcite content of raw clays by TGA	60
Table 5.2 The chemical composition of raw clays by XRF	60
Table 5.3 The mineralogical composition of raw clays by XRD	61
Table 5.4 The characterization of calcined clay particles	63
Table 5.5 Composition of materials for R ³ test	64
Table 5.6 The composition of R ³ test and the list of investigated calcined clays	70
Table 5.7 The parameters for curve fitting and evaluated E_a using the superposition method	73
Table 5.8 The E_a results using the rate method over the heat releases of 100 – 300 J/g	74
Table 6.1 Carbonation coefficient of PC, LC ³ -80(2:1) and LC ³ -65(2:1)	81
Table 6.2 The ions concentration in the pore solution of PC and LC ³ systems cured at 20°C for 28 days before exposure	82
Table 6.3 The pH of pore solution of cement pastes containing the same amount of cementitious materials with the tested mortars of PC and LC ³ -65(2 :1) systems cured for 28 days (before exposure)	87

Chapter 1. Introduction

1.1	Global situation of cement production	1
1.2	Kaolinite among clay types	2
1.3	Thermal activation of kaolinite	4
1.4	Combination of calcined clay and limestone.....	5
1.5	Properties of limestone calcined clay cement (LC ³)	5
1.5.1	Hydration reactions and microstructure development.....	5
1.5.2	Mechanical properties.....	7
1.5.3	Rheological properties	9
1.5.4	Durability properties	10
1.6	Motivation and objectives of the thesis.....	11

1.1 Global situation of cement production

The cement industry is a single industry that accounts for about 7% of global carbon dioxide (CO₂) emissions [1]. As environmental concerns mount up, the demand for more environmentally friendly construction materials keeps on rising. Supplementary cementitious materials (SCMs) can significantly decrease the amount of clinker required for the production of blended cement. In addition, the proper use of SCMs can improve the performance of the cementitious product made [2-5]. Therefore, the demand for SCMs has increased. Traditional SCMs such as fly ash, ground granulated blast furnace slag, or silica fume are potentially good for replacing part of the clinker, but their local availability can become a limiting factor and they are no longer sufficient for the demands of the construction industry [6]. The use of calcined clay, with sufficient kaolinite content, as an alternative SCM is becoming a commercially viable option because of the abundant supplies available worldwide as seen in Figure 1.1.

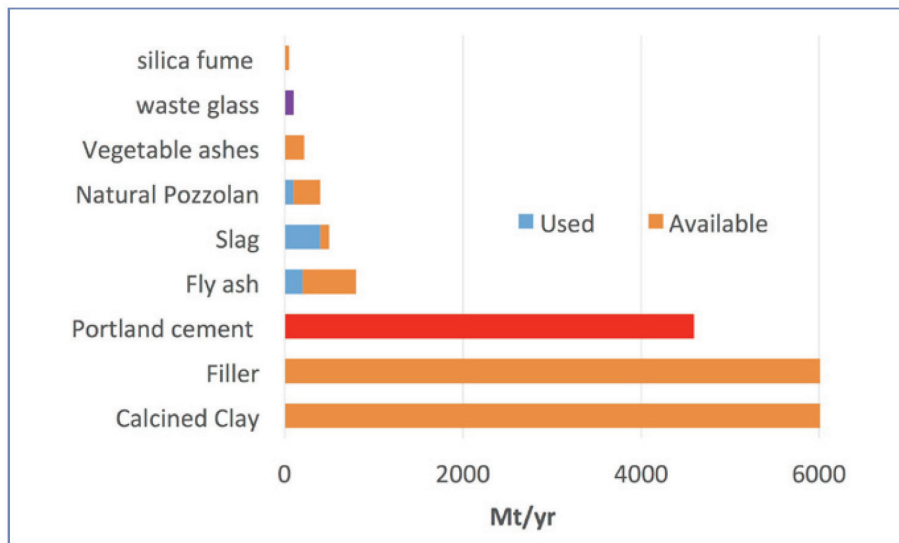


Figure 1.1 The amount of SCMs available worldwide [7]

Limestone Calcined Clay Cement (LC³) is a new type of ternary blend of limestone, calcined clay and clinker [8]. Although, calcined clay and limestone have been used for several decades in blended cements. The novelty of LC³ is to exploit from the synergy of the combined use of calcined clay and limestone. LC³ has properties similar to or better than typical Portland cement even at much lower levels of clinker. Accordingly, LC³ becomes very attractive for the cement industry to reduce CO₂ emission from cement production.

In Thailand, Siam Cement Group (SCG) places importance on the research and development of products and aims to develop innovative products that both are environmentally friendly and meet the demands of the consumer [9]. For SCG Cement-Building Materials business, the replacement of clinker with SCMs is of great interest to achieve the target of greenhouse gas emission reduction. The abundant availability of limestone and clays in Thailand makes the application of LC³ in Thailand of interest.

1.2 Kaolinite among clay types

There are several types of natural clay minerals differing in their structure. In general, the structure of the clay minerals consists of two basic units, an octahedral sheet and a tetrahedral sheet [10]. The octahedral sheet is composed of closely packed oxygens and hydroxyls in which mostly aluminum, but also iron or magnesium atoms are arranged in octahedral coordination. The tetrahedral sheet consists of four oxygens arranged in the form of a tetrahedron with the silicon atom in the center.

Clay minerals can be divided into two types:

- Two-layer type (a single tetrahedral sheet and a single octahedral sheet, 1:1)
 - E.g. Kaolinite, Dickite, Nacrite
- Three-layer type (two layers of silica tetrahedrons and one central dioctahedral or trioctahedral layer, 2:1)

- Expansive (e.g. Montmorillonite (smectitic), Nontronite)
- Non-expansive (e.g. Illite)

The diagrammatic sketch of Kaolinite, Montmorillonite, and Illite is shown in Figure 1.2.

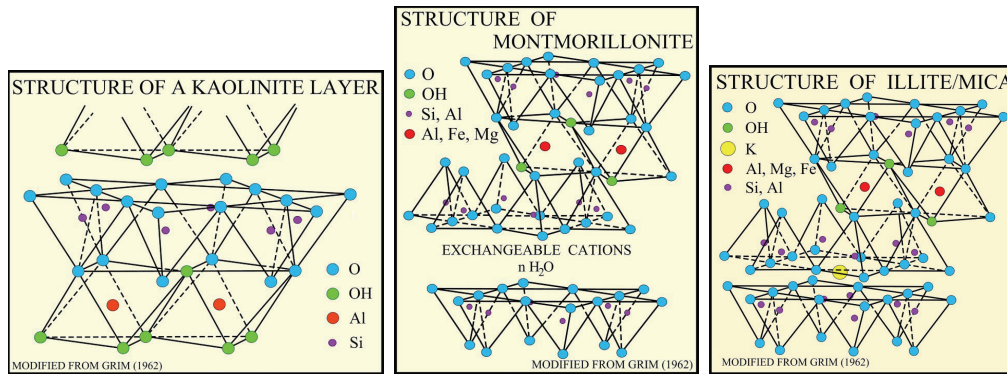


Figure 1.2 Diagrammatic sketch of Kaolinite, Montmorillonite, and Illite. Adapted from [11]

Among the different kinds of clays, kaolinite is the most suitable for use as an SCM [12], as explained in the next section. In Thailand, kaolinite is one of the major clay minerals and is distributed throughout the country as seen in Figure 1.3 where stars indicate the locations of kaolinitic clay quarries mainly used in the ceramic industry. The geological features of kaolinite sources can be divided into 3 types including sedimentary origin, hydrothermal/pneumatolytic origin and residual weathering origin [13]. The source of clays used in this study comes from the central part of Thailand, which comes from the hydrothermal degradation of rhyolite or volcanic tuff.

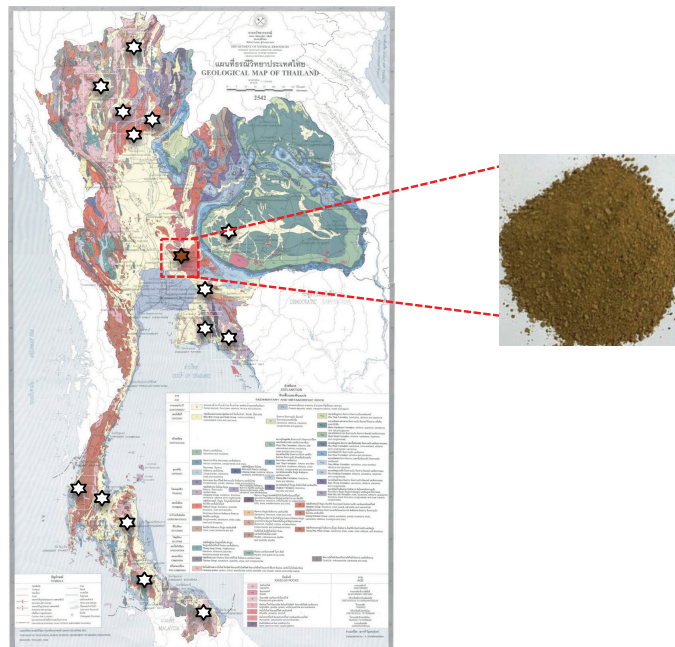


Figure 1.3 Map showing locations of kaolinite deposits in Thailand and clays used in this study.

Adapted from [14]

1.3 Thermal activation of kaolinite

Most of the raw clays in cement act as inert filler. To make clay reactive, the clay must be activated through a mechanical, a chemical or a thermal process [15]. However, the most economically viable and common technique to activate raw clays is the thermal activation through dehydroxylation /calcination of the clays. The conventional calcination process of clay is using a rotary kiln, similar to clinkerization process. Flash calcination is applied to produce the calcined clay, recently. This process is more thermally efficient process than the rotary calcination [16] and flash calcination seems to slightly enhance the reactivity of calcined clay compared with the rotary kiln [16-18].

The calcination of kaolinite (AS_2H_2) leads to the formation of a highly reactive metastable phase called metakaolin (AS_2), according to Equation 1.1. The adequate thermal range for clay calcination is between 700°C and 850°C [19].



The excellent reactivity of metakaolin was explained by the presence of Al(V) in the structure, as shown by ^{27}Al NMR spectra in Figure 1.4. For other types of clays, which are less reactive, only Al(IV) and Al(VI) are observed. This structural disorder is responsible for the pozzolanic reactivity of metakaolin [20]. Metakaolin also shows the highest reactive properties due to its higher content of dehydroxylated groups comparing with calcined illite and calcined montmorillonite [12, 21].

During hydration of blended cements, metakaolin reacts as a pozzolan with portlandite (CH) to form C-A-S-H and some aluminate hydrates such as strätlingite (C_2ASH_8) which starts to form after CH depletion [22]. The pozzolanic reaction of calcined clay or metakaolin (AS_2) is shown in Equation 1.2.

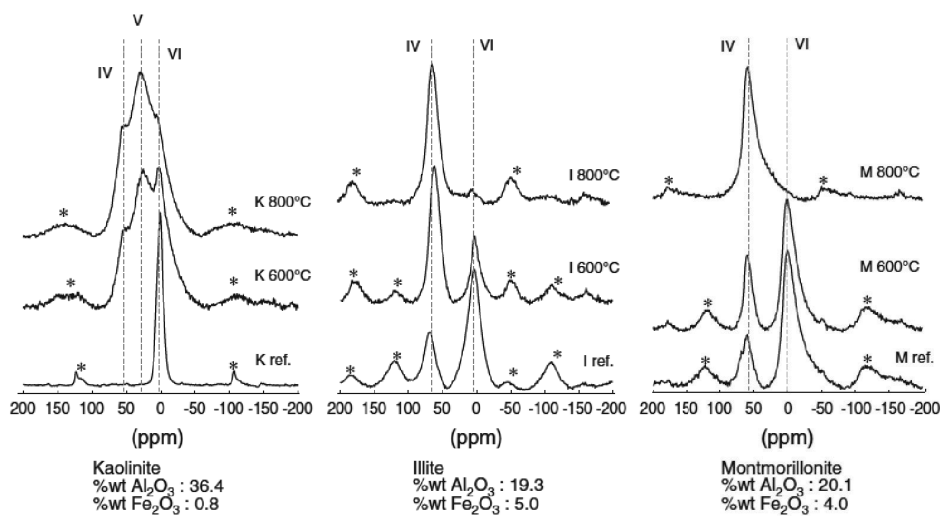
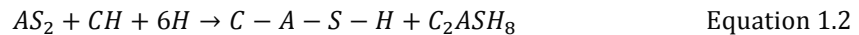
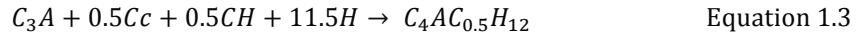


Figure 1.4 ^{27}Al NMR spectra of kaolinite, illite, and montmorillonite before and after calcination [12]

1.4 Combination of calcined clay and limestone

In presence of limestone in Portland cement, calcium carbonate (Cc) can react with C_3A from the clinker to form hemicarboaluminate ($C_4AC_{0.5}H_{12}$) and monocarboaluminate (C_4ACH_{11}) phases [23-25] according to Equation 1.3 and Equation 1.4. As a consequence of Hc and Mc formation, ettringite does not decompose to monosulfate in systems containing limestone [26]. However, the formation of carboaluminate hydrates is limited by the aluminate provided by the clinker [27].



When limestone and calcined clay are combined, in addition to the pozzolanic reaction of metakaolin and limestone reaction with C_3A , there is the synergetic effect between metakaolin and limestone resulting in the enhancement of limestone reaction thanks to the extra aluminates (A) provided by metakaolin [28]. The equation of the synergy effect is described in Equation 1.5.



1.5 Properties of limestone calcined clay cement (LC³)

1.5.1 Hydration reactions and microstructure development

Antoni [29] demonstrated the feasibility of using high-grade calcined clay (>95% of metakaolin) for blended cement and studied the hydration reaction of blended cement in several systems including OPC-metakaolin (MK30), OPC-limestone (LS15), and OPC-metakaolin-limestone (MK-B45) compared to OPC. The Phase assemblage for each system qualified using XRD is shown in Figure 1.5. It was found that the presence of metakaolin only (MK30) leads to the formation of strätlingite (strät) and monosulfate (Ms) along with less Portlandite (CH) from 7 days onwards. The presence of limestone (LS15) promotes the formation of carboaluminate hydrated (Hc and Mc) instead of Ms. The enhancement of ettringite (Etrr) and carboaluminate phases formation can be obtained from the system containing both metakaolin and limestone (MK-B45).

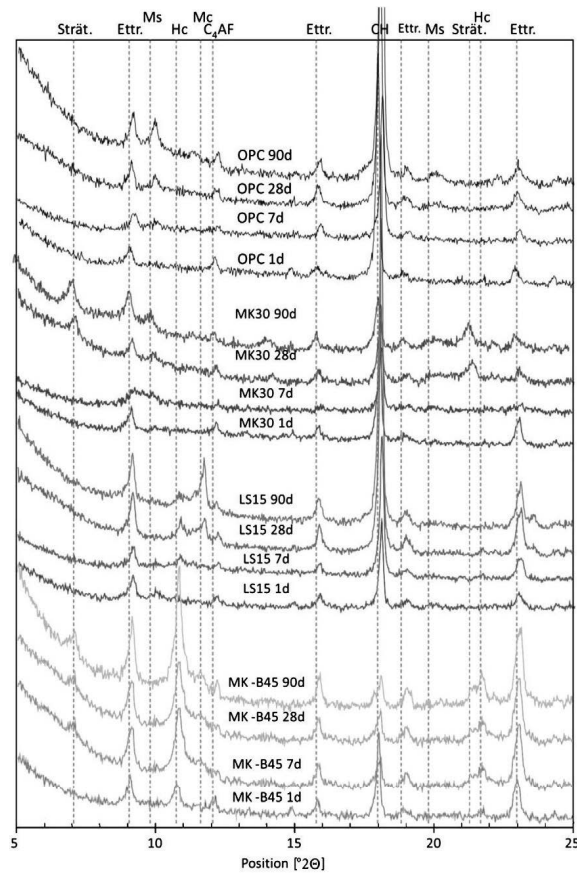


Figure 1.5 XRD results of OPC, MK30, LS15, and MK-B45 at 1, 7, 28 and 90 days [29].

The difference in phase assemblage results in the different microstructure development and influences the properties of cement. As seen in Figure 1.6, the MIP results show a porosity refinement for all the blended systems compared to OPC.

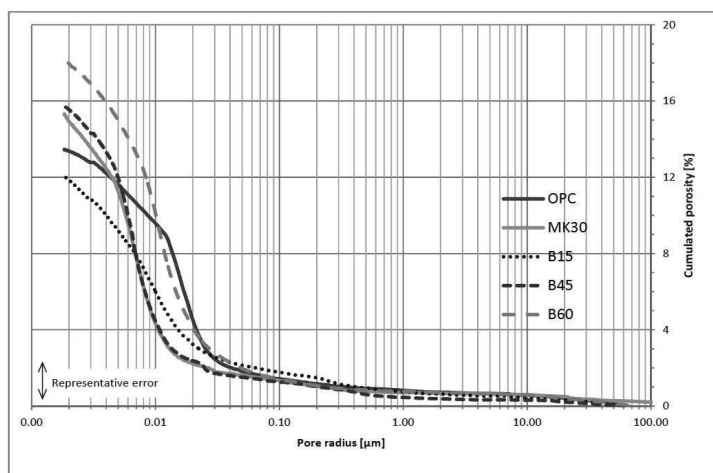


Figure 1.6 MIP results of OPC and the blended cements at 28 days [29].

For high-grade clays (high kaolinite content) in LC³-50, there is a refinement of the porosity to a limiting critical pore entry radius (about 3-5 nm [30]). This results in the slowing down of the clinker hydration as seen in Figure 1.7. As explained from Equation 1.6 (Correns equation) that the decrease of the pore size (r) results in the increase of the curvature at the solid/liquid interface (γ). Accordingly, to continue hydrated growth and continue hydration, it is necessary to increase the saturation index (SI).

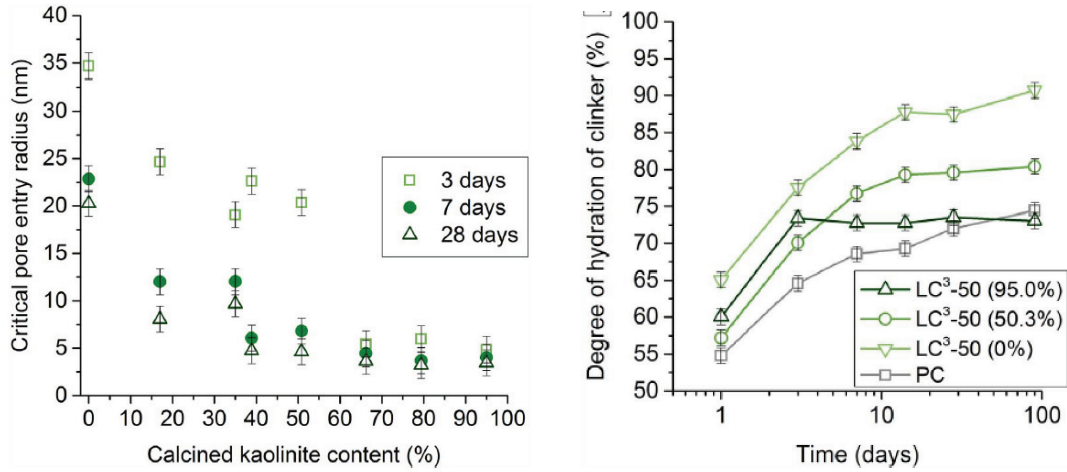


Figure 1.7 The critical pore entry radius plotted as a function of calcined kaolinite content (left) and the degree of clinker hydration as a function of time (right) [30]

$$P = \frac{RT}{V_m} \ln(10^{SI}) = \frac{RT}{V_m} \ln\left(\frac{K}{K_{sp}}\right) = \frac{2\gamma}{r} \quad \text{Equation 1.6}$$

where P is the pressure, K is the ion activity product, K_{sp} is the solubility product of the hydrate growing in the pore, R is the gas constant, T is the temperature, V_m is the molar volume of the hydration product growing in the pore. γ is the interfacial energy between the hydration product and the solution.

1.5.2 Mechanical properties

Antoni [29] studied a blended cement with 45% of clinker substitution by varying metakaolin to limestone weight ratios (B45 in [29] or called LC³-50). The optimal calcined clay to limestone ratio was found to be 2:1 which gave the best mechanical properties at 7 and 28 days, as shown in Figure 1.8. Moreover, Antoni also mentioned that the sulfate content should be adjusted in the system containing a high amount of calcined clay to prevent undersulfation. After 1.5% and 3% of gypsum addition, the 1-day strength of the blend was increased from 44% of the reference PC to 69% and 64% of the reference PC, respectively.

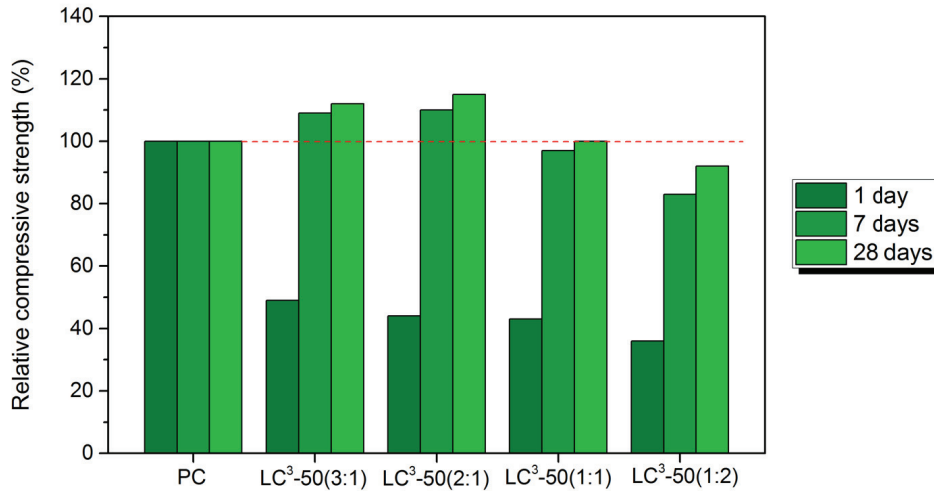


Figure 1.8 Relative compressive strength of B45 (LC³-50) varying metakaolin:limestone ratios. Adapted from [29]

Due to the high expense of high-grade calcined clays, Avet [31] investigated the influence of the calcined kaolinite content of calcined clays on the mechanical properties of LC³. For LC³-50 systems (50% clinker, 5% gypsum, 30% calcined clay and 15% limestone), strengths increase linearly with the calcined kaolinite content of calcined clays. LC³ blends containing based on clays with $\geq 40\%$ of calcined kaolinite reached equivalent strengths to reference PC (dotted lines) from 7 days onwards as seen in Figure 1.9. Thus, low-grade calcined clays containing $\geq 40\%$ of calcined kaolinite can be used in LC³. These clays are the most promising for LC³, since they are less expensive, and provide the best compromise between mechanical, rheological and durability properties [31].

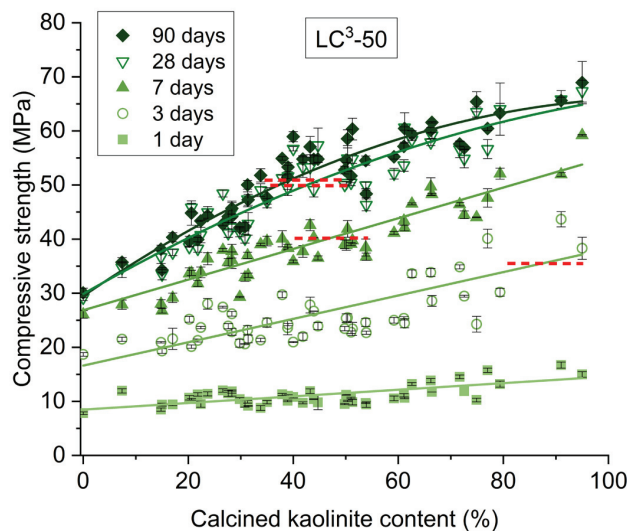


Figure 1.9 The relation between calcined kaolinite content and compressive strength of LC³-50 blends [30]

Considering the quality of limestone, Krishnan et al. [32] explored the use of dolomite as an alternative carbonate source to limestone in the LC³-50 system. He showed the similar trends observed in the compressive strength development of the LC3 (using limestone) and the DC3 (using dolomite) blends. Compared with quartz (QC3), limestone and dolomite provide a significant improvement of early age strength, as shown in Figure 1.10.

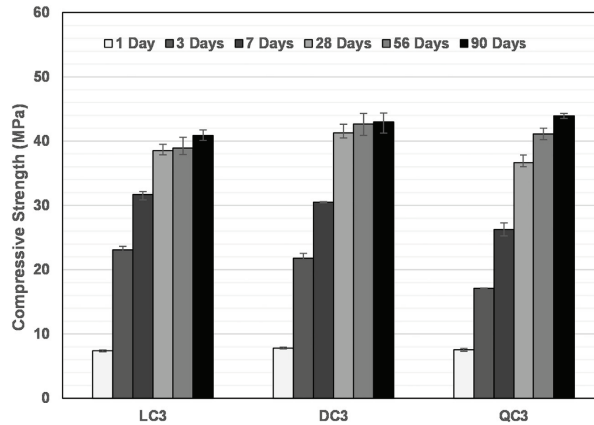


Figure 1.10 Compressive strength of LC3-50 containing 15% of limestone (LC3), 15% of dolomite (DC3), and 15% of quartz (QC3) [32]

1.5.3 Rheological properties

One of the issues concerning the use of calcined clay is the workability. Because of the high surface area of clay particles, the water requirement of LC³ blended cement may be higher than that of normal PC for similar workability properties. However, to improve the workability of LC³, the chemical admixtures can be used. Avet [31] presented the amount of superplasticizer needed for LC³ to get the comparable flowability with as plain PC as a function of the calcined kaolinite content in both cases of mortars and pastes. As seen in Figure 1.11, the higher the calcined kaolinite content the more superplasticizer required to achieve the same workability.

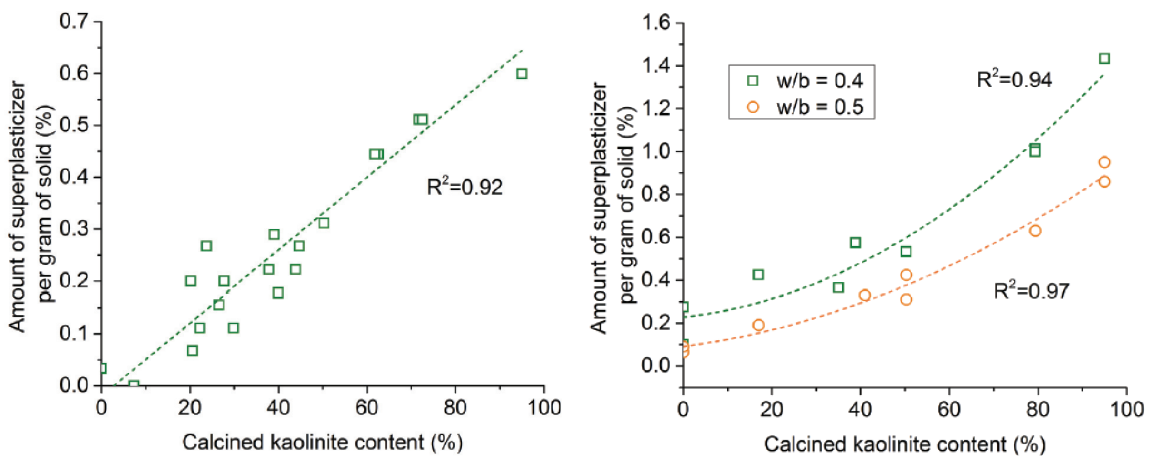


Figure 1.11 The amount of superplasticizer used in LC³-50 mortars (left) and pastes (right) [31]

1.5.4 Durability properties

The obvious advantage of LC³ is a very high degree of pore refinement compared to the plain PC as seen in Figure 1.12. The MIP results show the progressive porosity refinement of LC³-50 blends with an increasing percentage of kaolinite. This refined pore structure is beneficial in terms of transport properties, particularly chloride penetration. Figure 1.13 shows the chloride penetration depth of LC³-50 mortars containing >50% kaolinite is less than 10 mm after exposures in 3 wt% NaCl solution for 2 years. As discussed by Maraghechi et al. [33], it appears that the improvement in chloride resistance is due to the porosity refinement rather than differences in chloride binding capacity of the hydrated products as seen in Figure 1.14.

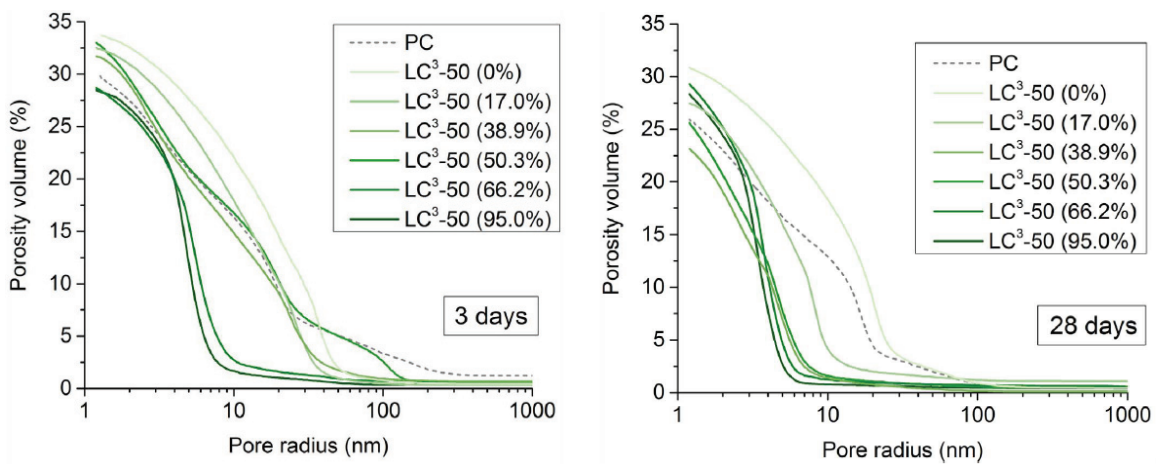


Figure 1.12 MIP results for PC and LC³-50 blends at 3 days and 28 days [30]

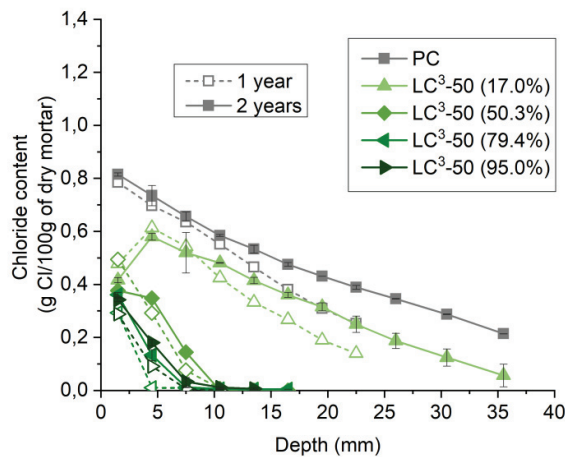


Figure 1.13 Chloride profiles for PC and LC³-50 mortars [33]

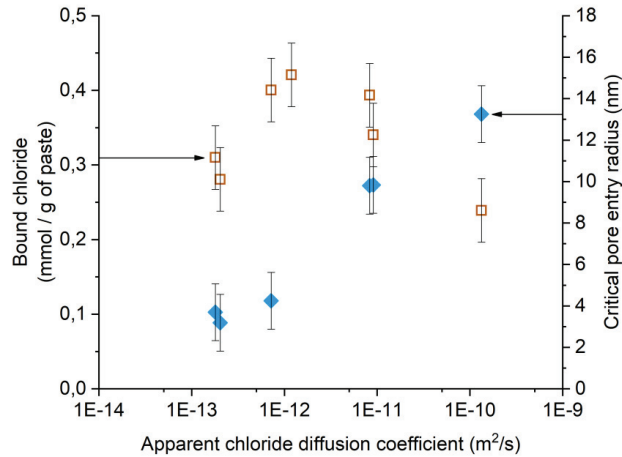


Figure 1.14 Correlation between the bound chloride and the critical pore entry radius with the apparent chloride diffusion coefficient [33]

1.6 Motivation and objectives of the thesis

Antoni's work has shown the positive effects of calcined clay with high kaolinite content and Avet's work investigated clay composition and properties and showed the satisfactory results obtained using low kaolinite calcined clay. Krishnan's work provided the information on limestone that even low-grade limestone could be used in LC³. However, there is a lack of information concerning the influence of cement composition. Due to the different clinkers existing in Thailand, the influence of the cement composition is crucial for optimizing the substitution level of clinker in LC³. Moreover, the study of hydration mechanisms of clays calcined from the different process has not been deeply studied.

Another important point is that all the previous tests were performed at room temperature of EPFL (20°C), which is lower than the normal working temperature in Thailand. The average temperature in Thailand is around 30°C. The impacts of temperature are also studied to mimic the climate conditions for LC³ in Thailand.

Therefore, in order to explore the potential of using calcined clays with low kaolinite content (approximately 50%) which are available in Thailand for LC³ production, the understanding of the influence of the substitution level, the cement composition, and the different calcination process on the properties of LC³ were studied. Also, LC³ systems were investigated the properties at 30°C in the laboratory to simulate using LC³ in real environments.

Thus, the aims of this thesis are:

1. To maximize SCMs levels in LC³ to get comparable properties to PC
2. To study the effect of cement composition particularly alkalis content on the reactions of LC³
3. To study the reactivity of calcined clay from different calcination process
4. To study the effect of the temperature on the properties of LC³

The overall outline of the thesis is summarized as follows

Chapter 2. describes the materials and methods used

Chapter 3. presents the influence of substitution level on the properties of LC³.

Chapter 4. investigates the impact of alkalis on the properties of LC³.

Chapter 5. details the influence of calcination process on the reactivity of calcined clay and consequently the properties of LC³.

Chapter 6. monitors the durabilities properties of LC³.

Chapter 7. provides the conclusions and the perspectives for future work.

Chapter 2. Materials and Methods

2.1	Raw materials.....	14
2.2	Methods.....	15
2.2.1	Particle size distribution and specific surface analysis	15
2.2.2	Cement paste preparation	15
2.2.3	Isothermal calorimetry	15
2.2.4	X-Ray diffraction (XRD)	16
2.2.5	Thermogravimetric analysis (TGA).....	17
2.2.6	Scanning electron microscopy (SEM).....	18
2.2.7	Mercury Intrusion Porosimetry (MIP).....	19
2.2.8	Pore solution extraction	21
2.2.9	Mass balance calculation.....	21
2.2.10	Compressive strength.....	22
2.2.11	Gel-Space ratio.....	22
2.2.12	Durability study	23

The overview of the samples and the main techniques used for the characterization/evaluation in this study is shown in Figure 2.1.

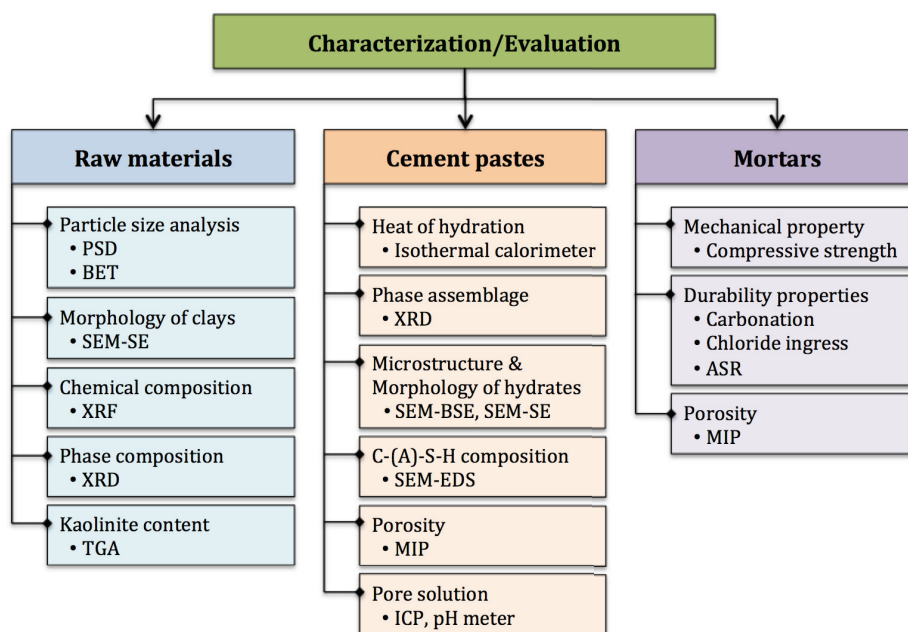


Figure 2.1 The overview of the samples and the main techniques used for the characterization /evaluation in this study

2.1 Raw materials

The cement (PC) used was OPC type I (ASTM C150) produced by Siam Cement Group (SCG), Thailand. The calcined clay used in this study has a kaolinite content of 50%, determined by TGA using a tangent method. This clay was calcined at 750°C for 5 sec in a fluidized bed combustor. Limestone used is a commercial product (Durcal 5, Omya). Gypsum for sulfate adjustment was reagent grade powder (>98% extra pure, AcrosOrganics). The chemical composition of raw materials obtained by X-Ray Fluorescence (XRF) is given in Table 2.1, as well as the volume median diameter measured by laser diffraction and the specific surface area determined by nitrogen adsorption with BET model. The phase composition of the PC is also shown in Table 2.2.

Table 2.1 Chemical and physical properties of raw materials

Oxides(%)	PC	Calcined clay	Limestone
SiO ₂	19.21	40.70	0.11
Al ₂ O ₃	4.92	30.36	0
Fe ₂ O ₃	3.26	20.13	0.04
CaO	65.24	2.07	54.96
MgO	1.24	0.55	0.15
SO ₃	2.37	0.01	0.03
Na ₂ O	0.22	0.31	0.06
K ₂ O	0.47	0.12	0
TiO ₂	0.29	2.67	0
P ₂ O ₅	0.04	0.63	0
Mn ₂ O ₃	0.07	0.12	0
LOI	2.56	2.49	42.5
%Na ₂ O _{eq}	0.52	0.39	0.06
Particle analysis			
D(v,0.5) (μm)	12.83	4.02	7.21
BET specific surface (m ² /g)	N/A	30.2	1.8

Table 2.2 The phase composition of the PC

Phase (%)	PC
C ₃ S	67.72
C ₂ S	7.95
C ₃ A	6.57
C ₄ AF	9.21
Calcite	4.09
Gypsum	0.93
Bassanite	4.02

2.2 Methods

2.2.1 Particle size distribution and specific surface analysis

The particle size of raw materials was analyzed using laser diffraction (Malvern MasterSizer S). The particles were dispersed in isopropanol for cement, in Na_2CO_3 solution ($\text{pH} \approx 10$) for calcined clays and in 0.01%PAA solution for limestone. Mie theory was used to predict the size of the particle. The parameters for the calculation are shown in Table 2.3.

Table 2.3 Refractive index and absorption index of solutions and powders

	Refractive index	Absorption index
Solutions		
Isopropanol	1.40	-
Na_2CO_3	1.33	-
PAA	1.51	-
Powders		
PC	1.68	0.10
Calcined clay	1.53	0.01
Limestone	1.50	0.01

The specific surface area of powder was carried on using gas adsorption technique. Micromeritics TriStar II Plus was used. The powder was degassed at 200°C under constant N_2 flow for 2-4 hr before the experiment. The BET equation [34] was employed to determine the specific surface area. The method of BJH [35] was used for calculating pore diameter, volume, and distribution. It is suitable for the determination of the mesopore and small macropore size ranges.

2.2.2 Cement paste preparation

Cement pastes were prepared for studying the hydration reaction, phase assemblage, microstructure, and porosity. The water to binder ratio was fixed at 0.4. 100 g of binder powder was mixed with water using a high-speed mixer at 1,600 rpm for 2 minutes in a plastic cup. Approximately, 10 g of the paste was placed in a calorimetry ampoule. The rest of fresh pastes was poured in 50 mL cylindrical polyethylene containers (35 mm in diameter) then sealed and stored at 20°C or 30°C for curing until testing.

At the required time of testing, hardened pastes were taken from the plastic container and three 2 mm-thick slices were cut with a diamond saw using deionized water as a lubricant. A fresh slice was directly used for X-Ray Diffraction and the other two slices were put in isopropanol for 7 days for stopping hydration. Isopropanol was changed after 1 hour, 1 day, and 3 days and then the slices were stored in a vacuum desiccator for at least 2 days.

2.2.3 Isothermal calorimetry

This technique is used for measuring the heat release from the hydration process of cementitious materials. A typical heat evolution curve of Portland cement is shown in Figure 2.2. The shape of the heat flow curve reflects the hydration process and the integrated heat flow (heat accumulation) curve relates to the magnitude of heat evolved.

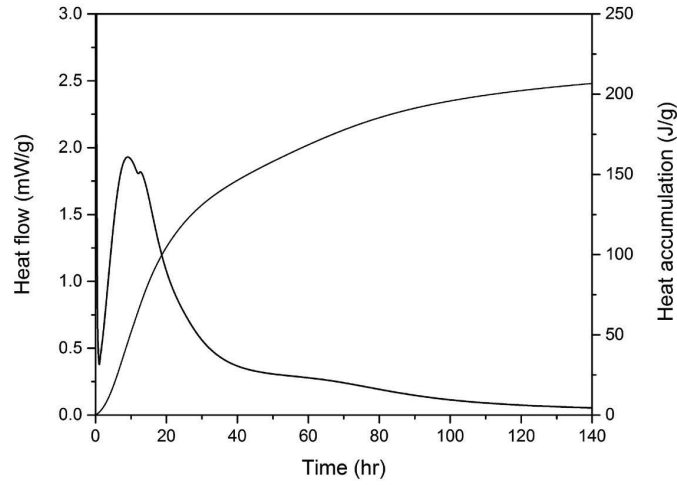


Figure 2.2 Heat evolution curve of OPC type I

To measure the heat evolution of samples, 10 g of paste was put into a specific ampoule. This ampoule was sealed with a lid and then was placed inside the isothermal calorimeter (TAM Air, TA instrument). The heat evolution was monitored at 20°C or 30°C for 7 days to investigate the hydration reaction. The reference sample used in this study had the same specific heat as the paste and was composed of 4.14 g of water.

2.2.4 X-Ray diffraction (XRD)

X-Ray diffraction was used to identify and quantify the phase composition of raw materials and hardened cement pastes. Raw materials and cement paste sample experiments were carried out on powder samples and fresh slices, respectively. The measurement was performed using PANalytical X'pert Pro MPD with a step width 0.0167° from 5° to 70° and time per step of 59.65 s for the raw materials or 29.84 s for the paste slices. The X-ray source was run at 45 kV, 40 mA using CuK α radiation ($\lambda=1.54 \text{ \AA}$). The phase quantification based on Rietveld analysis was carried out with X'Pert HighScore Plus program using rutile powder (Kronos-2300 Titanium dioxide) as an external standard.

The degree of clinker hydration (DoH) was calculated from the mass fractions of the C₃S (Alite), C₂S (Belite), C₃A (Aluminate), and C₄AF (Ferrite) reacted. The formula for calculation is shown in Equation 2.1.

$$DoH (\%)_t = \left(\frac{\sum(C_3S, C_2S, C_3A, C_4AF)_{t_0} - \sum(C_3S, C_2S, C_3A, C_4AF)_t}{\sum(C_3S, C_2S, C_3A, C_4AF)_{t_0}} \right) \times 100 \quad \text{Equation 2.1}$$

where $\sum(C_3S, C_2S, C_3S, C_4AF)_{t_0}$ was the sum of clinker phases at initial time

$\sum(C_3S, C_2S, C_3S, C_4AF)_t$ was the sum of the remaining clinker phases at time of interest

The XRD/Rietveld results can be expressed as either per 100 g of dry basis (carried on cement powder at initial) and per 100 g of paste basis (carried on fresh slices at time of interest). The DoH calculation should be done on the same basis to achieve the accurate results. The recalculation between dry basis and paste basis is given as follows.

$$\%Mass_{paste} = \%Mass_{dry} \times (1/1 + w/c) \quad \text{Equation 2.2}$$

$$\%Mass_{dry} = \%Mass_{paste} \times (1 + w/c) \quad \text{Equation 2.3}$$

2.2.5 Thermogravimetric analysis (TGA)

Thermogravimetric analysis was mainly used to determine the kaolinite content of the clays in this study. The characteristic TGA and DTG curves of the kaolinite clay can be seen in Figure 2.3. The mass loss at a temperature lower than 200°C can be due to the loss of moisture and the decomposition of organic compounds. The loss in the range of 220°C and 330°C corresponds to iron hydroxide decomposition [36]. The dehydroxylation of kaolinite clay takes place in the range of 400°C – 600°C depending on the crystallinity or particle size distribution [12]. And the mass loss between 650°C and 750°C is usually CaCO₃ decomposition. The other clay types can also contribute to the mass loss in the range of 350°C to 850°C [36]. The kaolinite content was calculated from the weight loss during clay dehydroxylation using the tangent method. The equation for calculating the percentage of kaolinite content is shown in Equation 2.4.

$$wt\%_{kaolinite} = wt\%_{water} \times \frac{M_{kaolinite}}{2M_{water}} \quad \text{Equation 2.4}$$

where, $wt\%_{kaolinite}$ was the percentage of kaolinite content, $wt\%_{water}$ was the mass loss during the dehydroxylation period, $M_{kaolinite}$ and M_{water} referred to the molecular mass of kaolinite and water, respectively.

TGA was also used to examine the phase assemblage of hydrated samples. The measurement was carried on powder samples using a Mettler-Toledo TGA/SDTA 851. Samples were crushed to obtain fine powder in an agate mortar. Approximately, 50 mg of powder was filled in a specific alumina crucible. The program was run at a ramp rate of 10°C/min from 30°C to 1,000°C under a 30 ml/min flow of N₂.

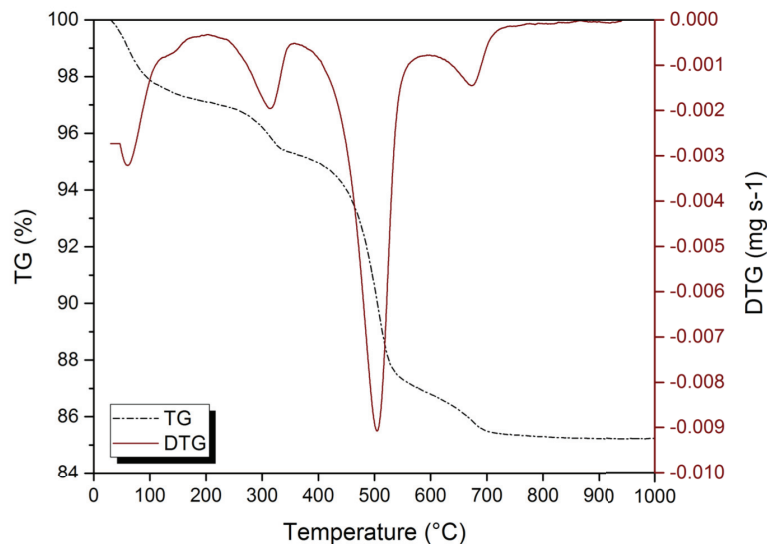


Figure 2.3 TGA and DTG curves of a kaolinite clay

2.2.6 Scanning electron microscopy (SEM)

Scanning electron microscopy is a useful technique for observing the microstructure of materials with information about the topography, morphology, and composition. The morphology of clay particles or hydration products were observed using a FEI XLF-30 SFEG-SEM in secondary electron mode (SEM-SE). Ir-metal coating was applied to achieve a conductive surface. The backscattered electron imaging (SEM-BSE) and energy dispersive X-ray spectroscopy (SEM-EDS) were carried out on polished cross-section using a FEI Quanta 200 equipped with Bruker XFlash 4030 EDS detector. Carbon was used as coating especially for the composition analysis because it is a light element ($Z = 6$) that does not interfere with the main elements present in hydration products.

2.2.6.1 Polished sample preparation

For the powder sample such as observing the agglomeration of clay particles, 0.1 g of clay powder was mixed with 10 g of a low viscosity epoxy resin (EpoTek 301) by hands in a plastic cup. The mixture was cast into a rubber mould and the resin allowed to set. The automatic polishing machine (MD Largo Struers) with a speed of 150 rpm and 20N force for pressing samples was used. To obtain a mirror-like sample surface, polishing started with 9 μm diamond spray for 30 min and then changed to 3 μm for 2 hr and finished with 1 μm for 2 hr. The petroleum and diamond sprays (Struers) were used as lubricant and polishing agent, respectively. Polished samples were cleaned using isopropanol in an ultrasonic bath and were kept in a desiccator. Before SEM investigations, a 15 nm thick carbon layer was applied in order to provide a conductive surface.

For hydrated samples, a small piece of sample was impregnated under vacuum with a low viscosity and transparent epoxy resin (EpoTek 301). After resin set, pre-polishing was done on an abrasive sandpaper grade P1200 using isopropanol as a lubricant. Once the resin-covered on the interested area was removed, the impregnated samples were moved to the step of fine polishing, similarly to powder samples.

2.2.6.2 The determination of C-A-S-H compositions

The composition of the C-(A)-S-H was determined by the EDS point analysis following the work of Rossen et al. [37] and observed on the polished surface of cement pastes. An acceleration voltage of 15 kV and a working distance of 12.5 mm were used. Due to the variability of the C-(A)-S-H composition and to achieve the better statistics, 200 points of the EDS analysis were collected from the inner product of C-(A)-S-H as seen the red point in Figure 2.4. The typical plot between the atomic ratio of Si/Ca versus Al/Ca to define the composition is shown in Figure 2.5. The other phases (AFt, Afm, and CH) can be possibly intermixed with C-(A)-S-H. Thus, the estimation of the C-(A)-S-H composition is the extrem point of the cloud as seen the red point in Figure 2.5.



Figure 2.4 EDS point analysis of inner C-(A)-S-H

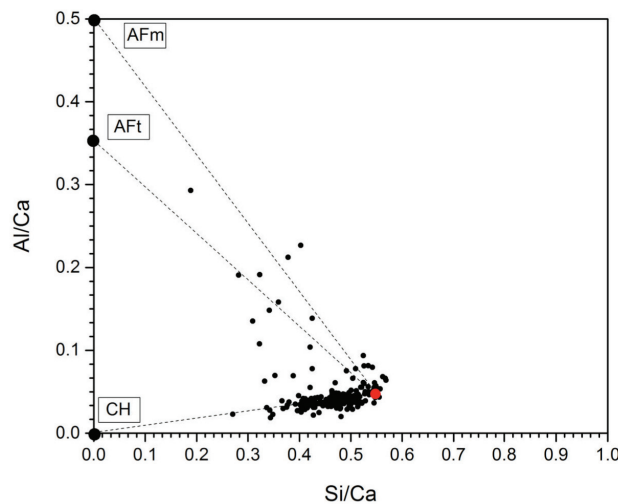


Figure 2.5 Determination of the C-(A)-S-H composition from the plot of Si/Ca versus Al/Ca

2.2.7 Mercury Intrusion Porosimetry (MIP)

The dimensional range of phases and pores in a hydrated cement paste is shown in Figure 2.6. The porosity parameters characterized using MIP are shown in Figure 2.7. The critical pore radius is the point where the intrusion of mercury increases the most rapidly corresponding to the maximum of the sharp peak of the derivative curve. The threshold pore radius or the onset of percolation is the first inflection point where the curve at which the slope of cumulative curve increase abruptly. The total porosity is the fraction of the volume of voids over the total volume of samples. In this study, all porosity parameters were used to investigate the physical properties, mechanical properties and durability properties of LC³ compared to PC.

To characterize porosity, MIP (POROTEC GmbH PASCAL 140 and PASCAL 440 instruments) was used on samples dried by solvent exchange. Pastes of 0.8 - 1 g were broken into small pieces and were tested up to a maximum pressure of 400 MPa. The Washburn equation was used to calculate the pore entry diameter/radius using 0.485 N/m for the surface tension of mercury and 140° for contact angle between mercury and cement paste.

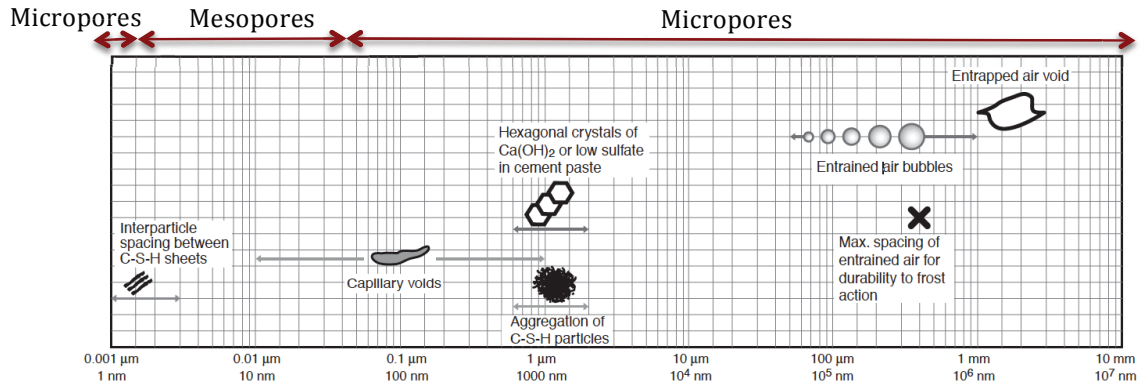


Figure 2.6 Dimensional range of phases and pores in a hydrated cement paste. Adapted from [38].

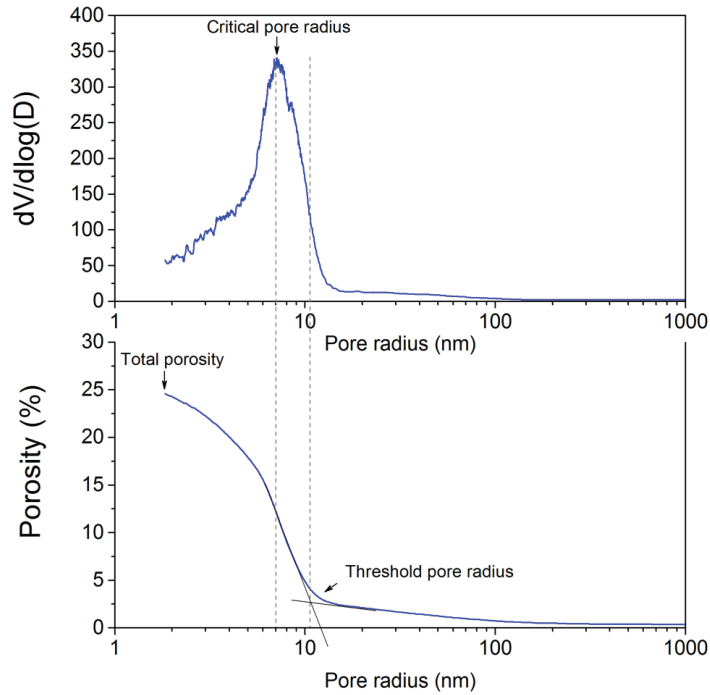


Figure 2.7 MIP results showing derivative and cumulative curves of LC³-50(2:1) paste sample at 28 days

2.2.8 Pore solution extraction

To extract the solution, cement pastes were mixed at a water/binder ratio of 0.4 and were cast into plastic bottles (55 mm in diameter, 100 mm height). The pastes were stored at 20°C in sealed conditions for 1, 3 and 28 days before testing. The extraction was carried out using a steel die press. The pore solution was extracted using 500 kN of pressure for 1-day, 3-day samples and 1200 kN for 28-day samples. To prevent precipitation, the pore solution was filtered with a 0.2 µm filter and 3.3 mL were diluted immediately in a plastic tube containing 6.47 mL of ultra-pure water and 0.2 ml of 8M HNO₃ and then they were kept at 4°C until testing. The cation concentrations of Ca, Al, Si, K, and Na were measured using an inductively coupled plasma/optical emission spectroscopy (ICP/OES, Shimadzu ICPE 9000). The pH of the extracted solution was measured at room temperature using a pH meter suitable for high pH (Knick pH-Meter 766 equipped with a Knick SE100 electrode). The concentration of OH⁻ was calculated according to Equation 2.5.

$$[OH^-] = 10^{(pH-14)} \quad \text{Equation 2.5}$$

2.2.9 Mass balance calculation

Some hydrated phases that are nanocrystalline, poorly crystalline and amorphous phase cannot be accurately quantified by XRD-Rietveld. Mass balance calculation is a useful method to determine the whole phase assemblage [31, 39] and it can be used to examine the degree of metakaolin reaction. The calculation requires the oxides converted from the reacted anhydrous phases and the ratio of Al/Ca and Si/Ca of C-(A)-S-H analyzed by SEM-EDS. The reacted anhydrous phases include clinker phases, limestone, and calcined clay. The amount of reacted calcined clay (metakaolin) is the independent variable for the calculation. The steps of the calculation are shown in Figure 2.8. The obtained results are in the unit of grams per 100 grams of binders. In order to convert to volume (cm³) per 100 grams of binders, the density of each phase in Table 2.4 was used.

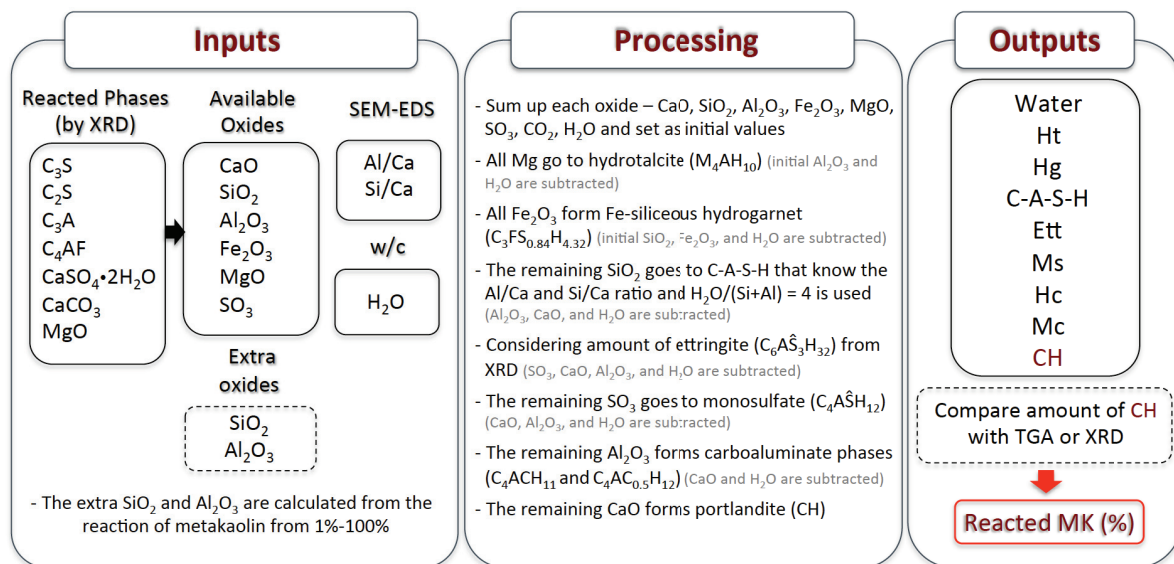


Figure 2.8 Procedure of mass balance calculation

Table 2.4 Phase density from GEMS

Phase	Formula	Notation	Density (g/cm ³)
Alite	M3-C ₃ S	C ₃ S	3.15
Belite	β-C ₂ S	C ₂ S	3.33
Aluminate	C ₃ A	C ₃ A	3.03
Ferrite	C ₄ AF	C ₄ AF	3.71
Metakaolin	AS ₂	MK	2.50
Limestone	CaCO ₃	LS	2.71
Unreacted calcined clay	-	CC	2.80
Quartz	SiO ₂	Q	2.64
Portlandite	Ca(OH) ₂	CH	2.25
Ettringite	C ₆ A ₃ H ₃₂	Ett	1.78
Monosulfate	C ₄ A ₁ H ₁₂	Ms	2.02
Monocarbonate	C ₄ AcH ₁₁	Mc	2.18
Hemicarbonate	C ₄ Ac _{0.5} H ₁₂	Hc	1.99
Hydrotalcite	M ₄ AH ₁₀	Ht	2.04
Hydrogarnet	C ₃ FS _{0.84} H _{4.32}	Hg	3.06
C-(A)-S-H	C _x A _y S _(1-y) H ₄	C-(A)-S-H	2.00
Water	H ₂ O	Water	1.00

2.2.10 Compressive strength

The mortars were formulated and mixed according to EN 196-1. The ratio of binder to sand ratio was 1:3 and water to binder was fixed at 0.5. After mixing, the mortars were cast into a three-prism steel mould 40 x 40 x 160 mm and kept in the molds for 24 hr. After demoulding, the mortars were cut to get 40x40x40 cubes. Mortar cubes were kept in non-sealed plastic bags and cured in fog room at >95% relative humidity until the day of testing (1, 2, 3, 7, 28, and 90 days). The compressive strength data for each system and for each age were averaged based on 4 cubes tested on a universal testing machine with a speed rate of 1.50 kN/s.

For testing at 30°C, mortar mixing was carried out at room temperature. The steel moulds were placed in an oven at a temperature of 30°C right after casting. Since the mortars were demoulded and were cut after 24 hr, cube samples were kept in sealed plastic bags to prevent moisture evaporation and then were cured in the oven until the day of testing.

2.2.11 Gel-Space ratio

The gel-space ratio is a way to compare strength with phase assemblage [40]. It is the ratio of the hydrates to the space available. A higher gel-space ratio reduces the porosity and therefore increases the strength. There are several definitions of gel in the previous works [40-42]. Nevertheless, two definitions of the gel were used in this study to investigate how the phase assemblage and space available influence the strength of LC³. The first was only C-(A)-S-H as a part of gel because it acts as a main of the hydration products. The second was considering all of the hydrated products (C-(A)-S-H, CH, Ett, Hc, Mc, Ht, and Hg) as gel. In both cases, space was defined as the sum of the initial volume of water and the volume of reacted binders (clinker, metakaolin, limestone). The calculation based on the results of the mass balance calculations and the formula for calculating is shown in Equation 2.6 and Equation 2.7.

$$Gel - Space\ ratio = \frac{\sum vol_{C-(A)-S-H}}{(\sum vol_{(react\ binders)_{t_0}} - \sum vol_{(react\ binders)_{t_t}}) + vol_{water}} \quad \text{Equation 2.6}$$

$$Gel - Space\ ratio = \frac{\sum vol_{hydration\ products}}{(\sum vol_{(react\ binders)_{t_0}} - \sum vol_{(react\ binders)_{t_t}}) + vol_{water}} \quad \text{Equation 2.7}$$

Where, $\sum vol_{C-(A)-S-H}$ was the volume of C-(A)-S-H, $\sum vol_{hydration\ products}$ was the sum of the volume of hydrated products including (C-(A)-S-H, portlandite, ettringite, hemicarbonate, monocarbonate, hydrotalcite, and hydrogarnet), $\sum vol_{react\ binders}$ was the sum of the volume of reacted binders including clinker, metakaolin, and limestone, vol_{water} was the initial volume of water

2.2.12 Durability study

2.2.12.1 Carbonation evaluation

Natural carbonation was studied on mortar cubes, using the same protocol as compressive strength test samples. After demoulding and cutting, the 40x40x40 cubes were stored in non-sealed plastic bags and cured at 20°C in fog room for 1, 3, and 28 days before exposure. The mortar cubes were then stored under indoor and outdoor conditions both in Switzerland and Thailand. The carbonation depth was measured using thymolphthalein or phenolphthalein after 6 months, 1 year and 2 years of exposure.

2.2.12.2 Chloride ingress

For chloride ingress measurements, the mortars were cast in cardboard cylinder moulds - 110 mm diameter and 230 mm height. After 24 hr, the mortar cylinders were demoulded and then cured at 20°C for 28 days in a fog room.

For migration testing, the experimental procedure was modified from ASTM C1202-97 by SIMCO using the set-up shown in Figure 2.9. The solution for the upstream cell was the mix of 0.3M NaOH and 0.5M NaCl and for the downstream cell was 0.3M NaOH. The cylinders were cut and ground to get a thickness of 27 mm, approximately. Before placing the mortar slice between the two cells, the mortars were soaked in 0.3M of NaOH solution under vacuum for 24 hr to be saturated. A voltage of 20 volts was applied and run for 14 days. The current was measured to estimate the diffusion coefficient of ions in cementitious materials.

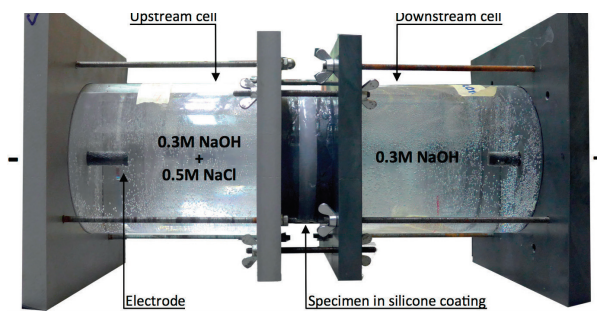


Figure 2.9 The set-up of chloride migration test [39].

Chloride ponding tests were performed following ASTM-C1543. The cylindrical mortars were cut in half and all surfaces except the cut side were covered with epoxy to prevent any penetration of chloride. The mortars were then ponded in a big plastic container with a 3% by mass NaCl solution for 6 months, 1 year and 2 years. The solution was exchanged every 2 months. At the time of interest, the samples were removed from the solution. The surface was dried for 24 h. The ponded samples were drilled perpendicular to the surface at different depths to obtain powdered samples. Depth intervals are shown in Table 2.5. The determination of chloride content was made according to ASTM-C1152/C1152M using AgNO_3 titration.

Table 2.5 The depth intervals of drilling

Layer	Depth (mm)
1	0.1 – 3.0
2	3.1 – 6.0
3	6.1 – 9.0
4	9.1 – 12.0
5	12.1 – 15.0
6	15.1 – 18.0
7	18.1 – 21.0
8	21.1 – 24.0
9	24.1 – 27.0
10	27.1 – 30.0
11	31.1 – 33.0
12	33.1 – 35.0

2.2.12.3 Alkali silicate reaction (ASR)

The highly reactive aggregate from North America called JOBE was used to investigate ASR. 40x40x160 mm mortar bars were cast using 1:3 binder to aggregate ratio and 0.46 as water to binder ratio. After curing for 28 days in fog room at 20°C, mortar bars were soaked in 0.32 mol/L of NaOH solutions at 38°C and the length changed was measured regularly over 12 months. The expansion has been determined according to ASTM C 1293.

Chapter 3. Influence of substitution levels of calcined clay and limestone on the properties of LC³

3.1	Introduction	25
3.2	Formulations.....	25
3.3	Workability and mechanical properties	26
3.4	Hydration reaction and microstructure.....	28
	3.4.1 Heat of hydration.....	28
	3.4.2 Degree of reactions.....	29
	3.4.3 Phase assemblage.....	30
	3.4.4 Pore solution	31
	3.4.5 Porosity.....	32
	3.4.6 C-(A)-S-H composition	34
	3.4.7 Microstructure.....	36
3.5	The relationship between compressive strength and porosity	39
3.6	The relationship between compressive strength and gel-space ratio.....	39
3.7	Summary.....	40

3.1 Introduction

The aim of this study is to investigate the influence of the substitution level focusing on the raw materials from Thailand in order to optimize the replacement of clinker by calcined clay and limestone. In addition to studying at the usual reference temperature of 20°C, the development of properties were also investigated at 30°C, which is more representative of ambient conditions in Thailand.

3.2 Formulations

The cement (PC) used was OPC type I (ASTM C150) produced by Siam Cement Group (SCG), Thailand. The calcined clay was also from Thailand with a calcined kaolinite content of 50% and this clay was calcined at 750°C for 5 sec in fluidized bed combustor. A commercial limestone powder (Durcal 5, Omya) was used in this study. The volume median diameter, $D(v,0.5)$, of PC, calcined clay, and limestone are 12.8 μm , 4.6 μm and 7.2 μm , respectively. The particle size distributions of raw materials are given in Figure 3.1. A typical bimodal distribution of calcined clay is observed, with metakaolin mainly present in the fine fraction (softer than secondary phases during grinding).

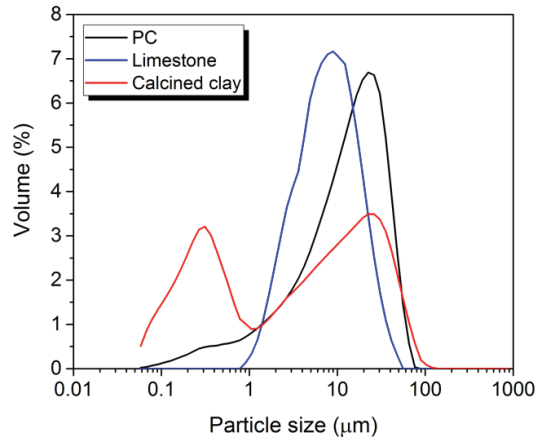


Figure 3.1 The particle size distribution of raw materials

In previous work [28], it was found that the ratio of calcined clay to limestone giving the best mechanical properties was 2:1, for 45% of clinker substitution. Therefore, this ratio of 2:1 was retained for this study. The replacement of clinker with limestone and calcined clays from 15-45% was studied. LC³-80(2:1), LC³-65(2:1) and LC³-50(2:1) correspond to blended cements with approximately 80%, 65% and 50% of clinker content, 5% of gypsum and with a replacement by calcined clay and limestone fixed ratio of 2:1 at 15%, 30% and 45%, respectively. Separate grinding was performed to prepare LC³ blended cements in this study. PC was directly used as a part of clinker. To obtain around 5% overall gypsum for each system of LC³, 0.25%, 0.5%, and 1% of calcium sulfate dihydrate (>98%, AcrosOrganics) was added to LC³-80(2:1), LC³-65(2:1) and LC³-50(2:1), respectively. The formulations of each batch are given in Table 3.1.

Table 3.1 Formulations of LC³ blended cements

Name	wt. %			
	PC	Calcined clay	Limestone	Gypsum addition
PC	100.00	0	0	0
LC ³ -80(2:1)	84.79	9.98	4.99	0.25
LC ³ -65(2:1)	69.65	19.90	9.95	0.50
LC ³ -50(2:1)	54.45	29.70	14.85	1.00

3.3 Workability and mechanical properties

The flow test was carried out following ASTM C1437-15. Figure 3.2 shows the flow of the fresh mortars measured after tapping 25 times in 15 seconds on a flow table. The flow of the PC reference is about 19.5 cm. It is interesting that replacing PC with calcined clay and limestone at all levels yields the flow values similar for all systems using the same water to binder ratio and without any superplasticizer. The flow of LC³ systems is in the range of 17.7-19.1 cm close to that of the PC.

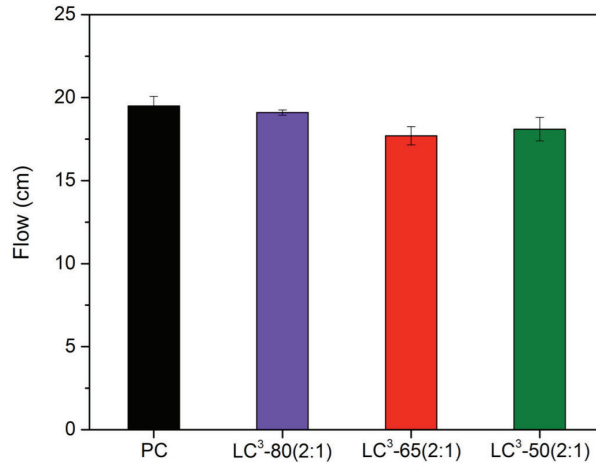


Figure 3.2 Flow test results of PC and LC³ systems at 20°C

The influence of the substitution level on the mechanical properties of LC³ at 20°C and 30°C is shown in Figure 3.3. It shows that at 20°C, the compressive strength of LC³-80(2:1) and LC³-65(2:1) is comparable to PC from 7 days onwards. Increasing temperature improves the strength development of LC³. Similar strength of LC³-80(2:1) and LC³-65(2:1) to PC is obtained from 2 days onwards. LC³-50(2:1) blend did not reach the same strength as PC at either temperature, it still has a strength in excess of that specified for OPC type I (ASTM C150) or CEM I 42.5N (EN197-1). According to ASTM C150, 3 days strength of this cement is equal or greater than 12 MPa and 7 days strength is equal or greater than 19 MPa. For EN197-1 (CEM I 42.5N or 52.5N), it is specified that 2 days strength and 28 days strength should not be less than 10 MPa or 20 MPa and 42.5 MPa or 52.5 MPa, respectively.

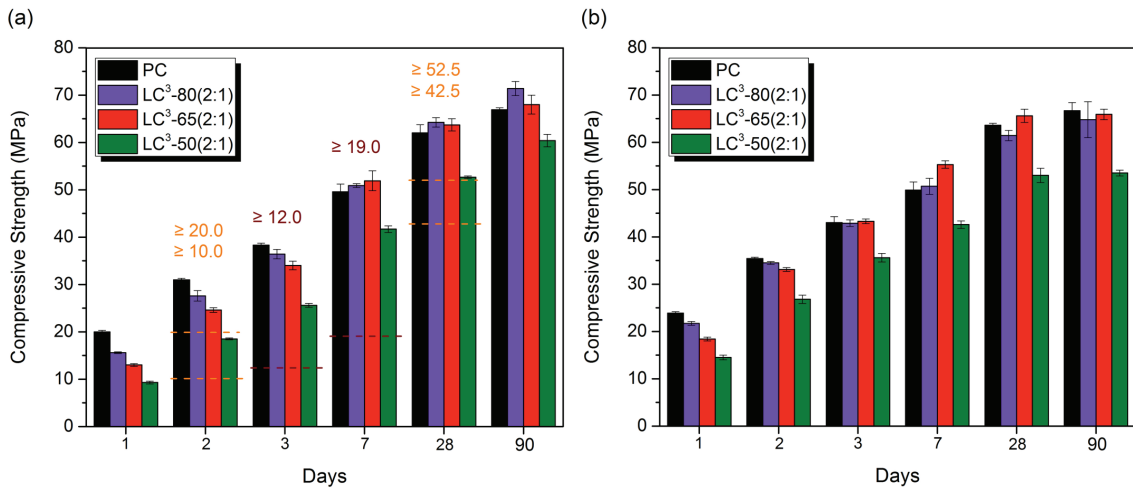


Figure 3.3 Compressive strength of PC and LC³ systems at (a) 20°C and (b) 30°C

3.4 Hydration reaction and microstructure

3.4.1 Heat of hydration

The heat flows of PC and LC³ systems normalized per gram of solid and normalized per gram of clinker during the first 24 hours of hydration at 20°C and 30°C are shown in Figure 3.4. Increasing temperature accelerates the cement hydration as seen by the higher intensities of the main peaks and the shorter induction and acceleration periods. The hydration of the silicate phase is accelerated for LC³ blends due to the filler effect [43] of calcined clay and limestone as observed by the shift of the 1st peak when replacing the clinker with SCMs. Moreover, it can be observed that the height of the 2nd peak corresponding to the aluminate phase reaction is significantly increased when increased the addition of SCMs.

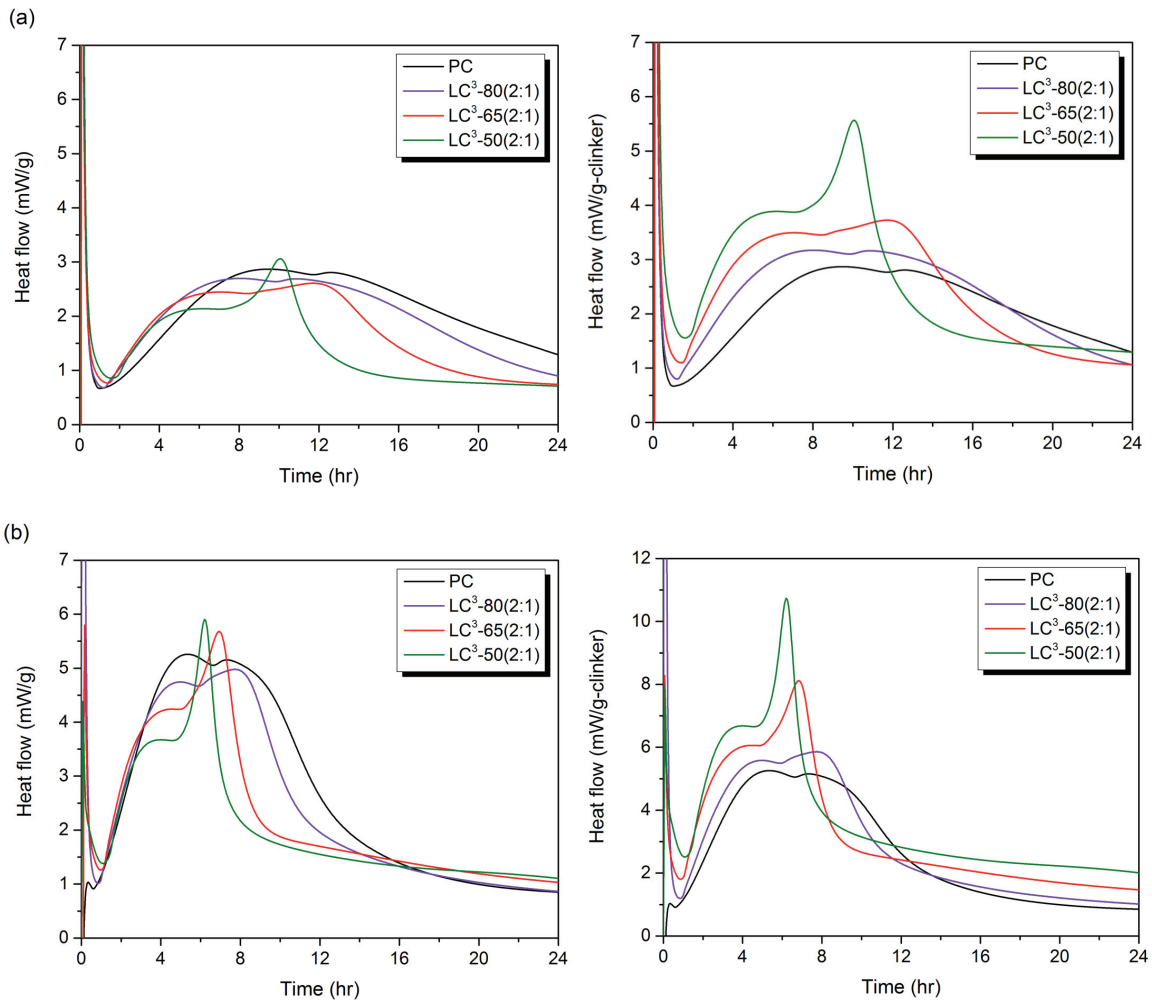


Figure 3.4 Heat flow of PC and LC³ systems at 20°C (a) and 30°C (b) normalized per gram of solid (left) and per gram of clinker (right)

3.4.2 Degree of reactions

The degree of clinker hydration (DoH) and the degree of metakaolin reaction (DoR) are shown in Figure 3.5 and Figure 3.6, respectively. The substitution levels of SCMs, which are 15-45% in this study, significantly affect the DoH at both temperatures. The DoH increases with increasing the addition of SCMs at early ages but the opposite is observed at later ages, as shown in Figure 3.5. The increase in temperature means this turnover occurs earlier.

The DoR of LC³ system evaluated by mass balance calculation shows similar trends to DoH at 20°C and 30°C as seen in Figure 3.6. At 20°C, there is no significant different DoR among LC³ blended cement at 3 days and 7 days of hydration but at 28 days the DoR of LC³-50(2:1) is lower than the others. Not only DoH is promoted by elevated temperature, but also the pozzolanic reaction. The DoR of LC³-65(2:1) and LC³-80(2:1) reaches 80% and 60% for LC³-50(2:1) at 3 days when increasing the temperature from 20°C to 30°C.

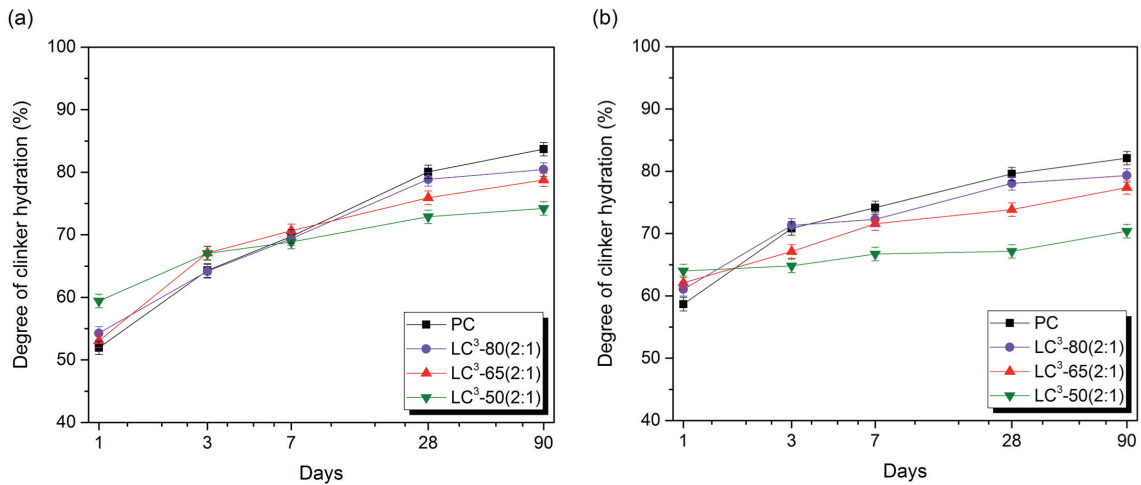


Figure 3.5 Degree of clinker hydration of PC and LC³ systems at (a) 20°C and (b) 30°C

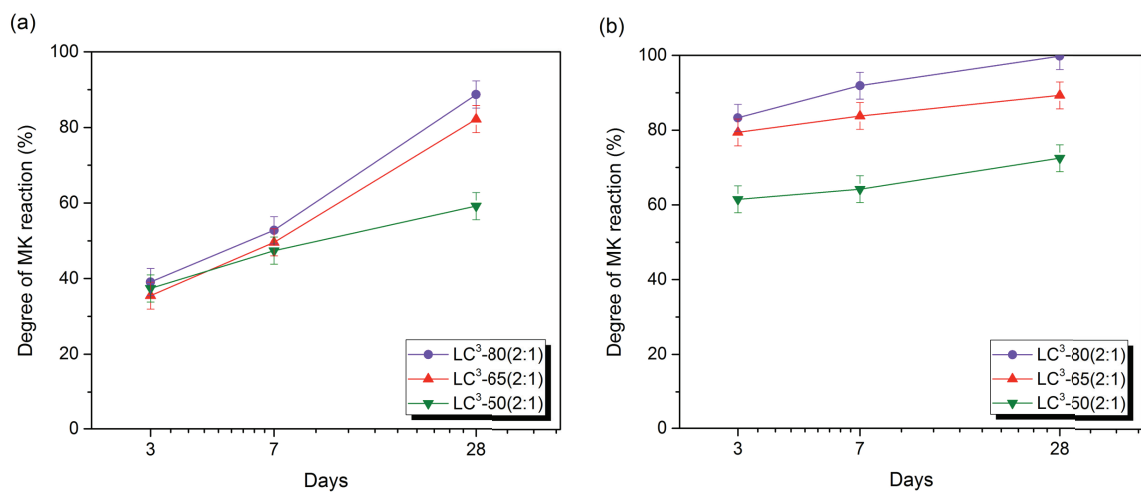


Figure 3.6 Degree of metakaolin reaction of LC³ systems at (a) 20°C and (b) 30°C

3.4.3 Phase assemblage

For the study of the phase assemblage, the XRD patterns are shown in Figure 3.7. The results show that ettringite (Ett, $2\theta \approx 9^\circ$) in all systems is retained after formation thanks to the presence of limestone [23, 24], this is also the case for PC which initially contains about 4% of limestone. However, the increase in curing temperature reduces the formation of Ett as seen by the peak intensity of Ett at 30°C is lower than at 20°C. The level of SCMs substitution affects the formation of carboaluminate phases, hemicarboaluminate (Hc, $2\theta \approx 10.7^\circ$) and monocarboaluminate (Mc, $2\theta \approx 11.6^\circ$). An increase of SCMs content increases the formation of Hc at 1 day and this is emphasized at 30°C. From the thermodynamic perspective, Hc is less stable compared to Mc, with time it will transform to Mc [25, 44]. However, these results show, that as the level of substitution increases, there is more persistence of Hc. Figure 3.7(b) shows the peak intensity of Hc phase of LC³-50(2:1) is higher than the others at 28 days. Higher temperature accelerates the transformation; the Hc peak in LC³-80(2:1) has almost disappeared at 28 days.

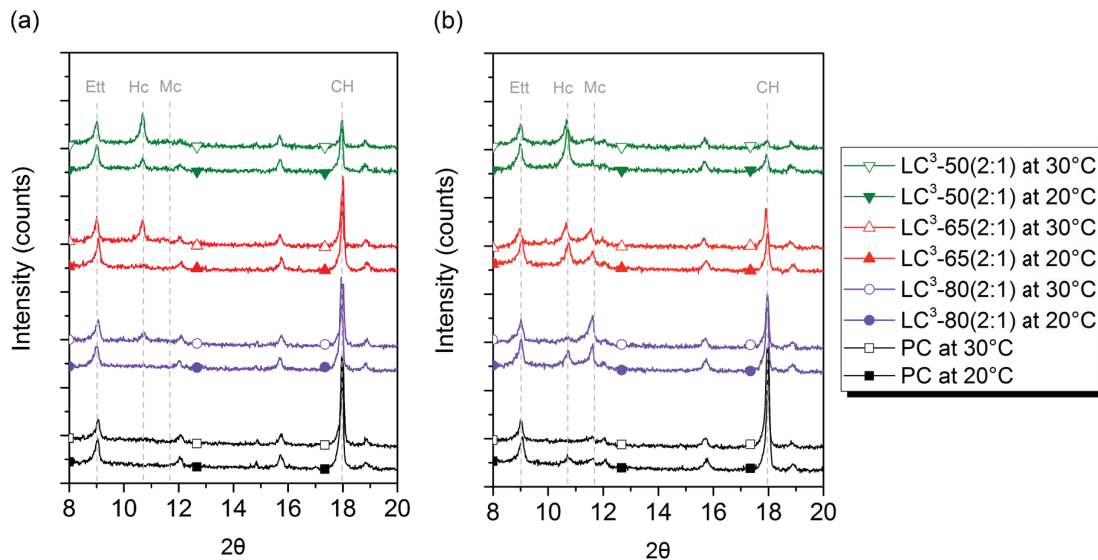


Figure 3.7 XRD patterns of PC and LC³ systems at 20°C and 30°C for 1 day (a) 28 days (b)

The solid phases of PC and LC³ systems on the basis of cm³ pre 100g of anhydrous was evaluated using mass balance calculation. The results for PC and LC³ systems are shown in Figure 3.8. At 20°C, it is observed that the highest substitution levels which are LC³-65(2:1) and LC³-50(2:1) show the highest volume of carboaluminate phases (Hc and Mc) at 3 days. When temperature raised up to 30°C, not only more Hc and Mc form in LC³-65(2:1) and LC³-50(2:1), but also PC and LC³-80(2:1). Moreover, the degree of clinker hydration and the pozzolanic reaction was promoted by increasing the temperature from 20°C to 30°C, with a higher volume of hydrated products since 3 days of hydration. Although the elevated temperature lowers the amount of ettringite, the formations of C-(A)-S-H and carboaluminate phases are increased at early ages.

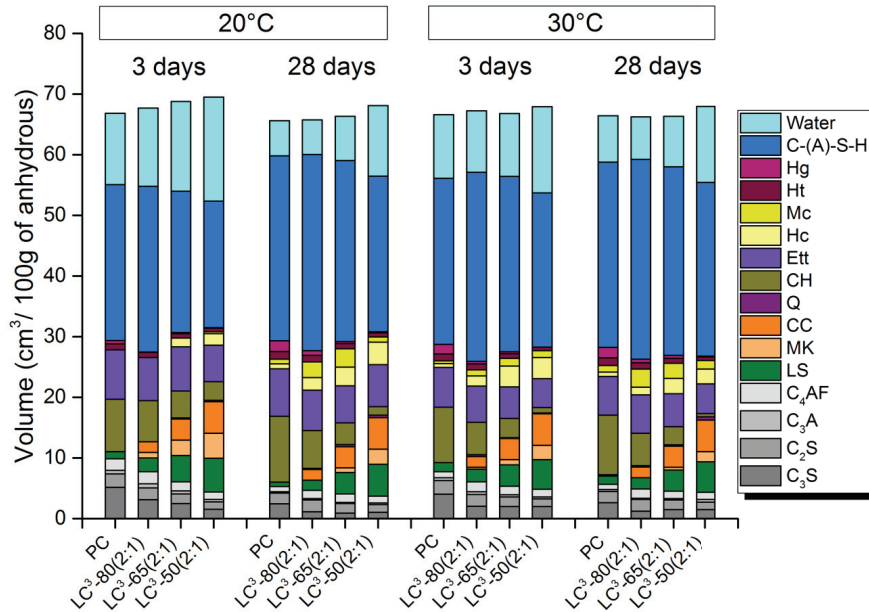


Figure 3.8 Volume of phase assemblage of PC and LC³ systems evaluated by mass balance calculation cured for 3 days and 28 days at 20°C and 30°C

LS = limestone, MK = unreacted metakaolin, CC = other components in calcined clay, Q = quartz, CH = portlandite, Ett = ettringite, Hc = hemicarbonat, Mc = monocarbonat, Ht = hydrotalcite, Hg = hydrogarnet

3.4.4 Pore solution

The ion concentrations of pore solutions for PC and LC³ systems cured at 20°C for 28 days are given in Table 3.2. The aluminum (Al) concentration increases with increasing the levels of calcined clay and the OH⁻ calculated from the pH decreases with increasing the levels of clinker substitution. Based on the results from pore solution, the effective saturation indices (SI) of the main hydration products of interest are calculated using GEMS [45] with CEMDATA 18 [46] for PC and LC³ systems presented in Table 3.3. The positive SI means the pore solution is oversaturated with regard to the formation of that hydrated phases and the negative SI indicates the pore solution is undersaturated with regard to that hydrates should not form.

Table 3.2 Ion concentrations in pore solutions of PC and LC³ systems cured at 20°C for 28 days

Samples	Al (mmol/l)	Ca (mmol/l)	K (mmol/l)	Na (mmol/l)	SO ₄ (mmol/l)	Si (mmol/l)	OH ⁻ (mmol/l)
PC	0.11	0.95	227.10	105.57	6.39	0.22	227.83
LC ³ -80(2:1)	0.10	1.42	133.50	80.77	4.04	0.21	188.89
LC ³ -65(2:1)	0.23	1.50	63.53	38.89	1.19	0.20	95.64
LC ³ -50(2:1)	0.56	1.44	38.36	20.10	0.53	0.18	58.23

Table 3.3 Effective saturation indices of hydrates calculated using GEMS of PC and LC³ systems

Samples	C-S-H	Strätlingite	Ettringite	Al(OH) ₃	Portlandite	Monocarbonat
PC	0.08	-0.27	0.10	-1.39	-0.06	0.03
LC ³ -80(2:1)	0.09	-0.21	0.15	-1.32	-0.08	0.04
LC ³ -65(2:1)	0.07	-0.04	0.14	-0.99	-0.19	0.07
LC ³ -50(2:1)	0.04	0.10	0.13	-0.68	-0.30	0.09

All systems have positive SI for C-S-H, ettringite, and monocarbonate (Mc). The highest degree of oversaturation of Mc and the positive SI with respect to strätlingite are observed in LC³-50(2:1). These indicate that Mc and strätlingite should form in this system. However, it is in contrast with the XRD result as shown in Figure 3.7. A smaller amount of Mc is formed and the formation of strätlingite is not observed for LC³-50(2:1). It is possible due to the lack of space for the hydration products to form which is discussed in the next section.

3.4.5 Porosity

The variation of phase assemblage influences the porosity development of the hardened cement pastes. Figure 3.9 shows the pore size distribution analyzed by MIP of PC and LC³ systems at 20°C and 30°C. The most marked change is the decrease in the pore entry radius (refinement). The strongest refinement of porosity is obtained for LC³-50(2:1) which is observed from 3 days of hydration. It is possible due to the proper physical structure of the products formed into the interstitial space. Temperature clearly affects both PC and LC³ cements. Figure 3.10 shows the total porosity and threshold pore radius – the first inflection point where the slope of the cumulative curve increases rapidly, for all systems. Increasing temperature decreases the total porosity at 3 days but it does slightly impact at 28 days because the larger amounts of hydrated products are promoted to form since the early ages of hydration. However, there is a different trend in the threshold pore radius at 28 days. For the PC and LC³-80(2:1) systems, the threshold pore radius increases with increasing the curing temperature but in the case of the LC³-65(2:1) and LC³-50(2:1) systems, there is not much difference in the threshold pore radius between 20°C and 30°C. The increase of the threshold pore radius reflects the coarsening porosity and it is clearly seen in the system of PC and LC³-80(2:1) when increasing the curing temperature. It can be possible due to the modification of the hydrated product microstructure, particularly calcium silicate hydrate (C-(A)-S-H) as widely reported elsewhere [47-51].

The critical pore radius – the point where the intrusion of mercury starts to increase rapidly, of all systems are shown in Figure 3.11. The critical pore radius decreases with increasing the substitution levels. It can be noticed that the critical pore entry radius of LC³-50(2:1) for both curing temperatures at 28 days is about 6-7 nm which is in the range of limiting pore entry radius (as seen the red dash line about 6 nm) for the growth of hydration products as discussed in the previous works [30, 52, 53].

Once the limit critical pore size is reached, higher levels of supersaturation are needed for hydrates to continue growing [30, 31, 54, 55]. As seen in Figure 3.12, Hc and Mc phases in LC³-50(2:1) quantified by XRD-Rietveld analysis are stop forming after 28 days in spite of a positive saturation index with respect to Mc of 0.09 (Table 3.3) indicated that Mc could form in this system. Likewise, strätlingite should form in LC³-50(2:1) at 28 days as seen the positive SI for this system but there is no evidence from XRD. The lack of space for the growth of hydration products could also explain the absence of this phase in the system of LC³-50(2:1), as also observed in Avet's work [30].

Moreover, the extreme refinement of porosity is observed in LC³-50(2:1) system which is correlated to the slowdown of the clinker hydration and the metakaolin reaction for this system. It is possible that the hydrates do not grow due to the lack of space, so no ions consumption and therefore no further dissolving of anhydrous phases. Thus, the lack of space could be an explanation of the slowdown of DoH and DoR for this system as it also found in earlier work [30].

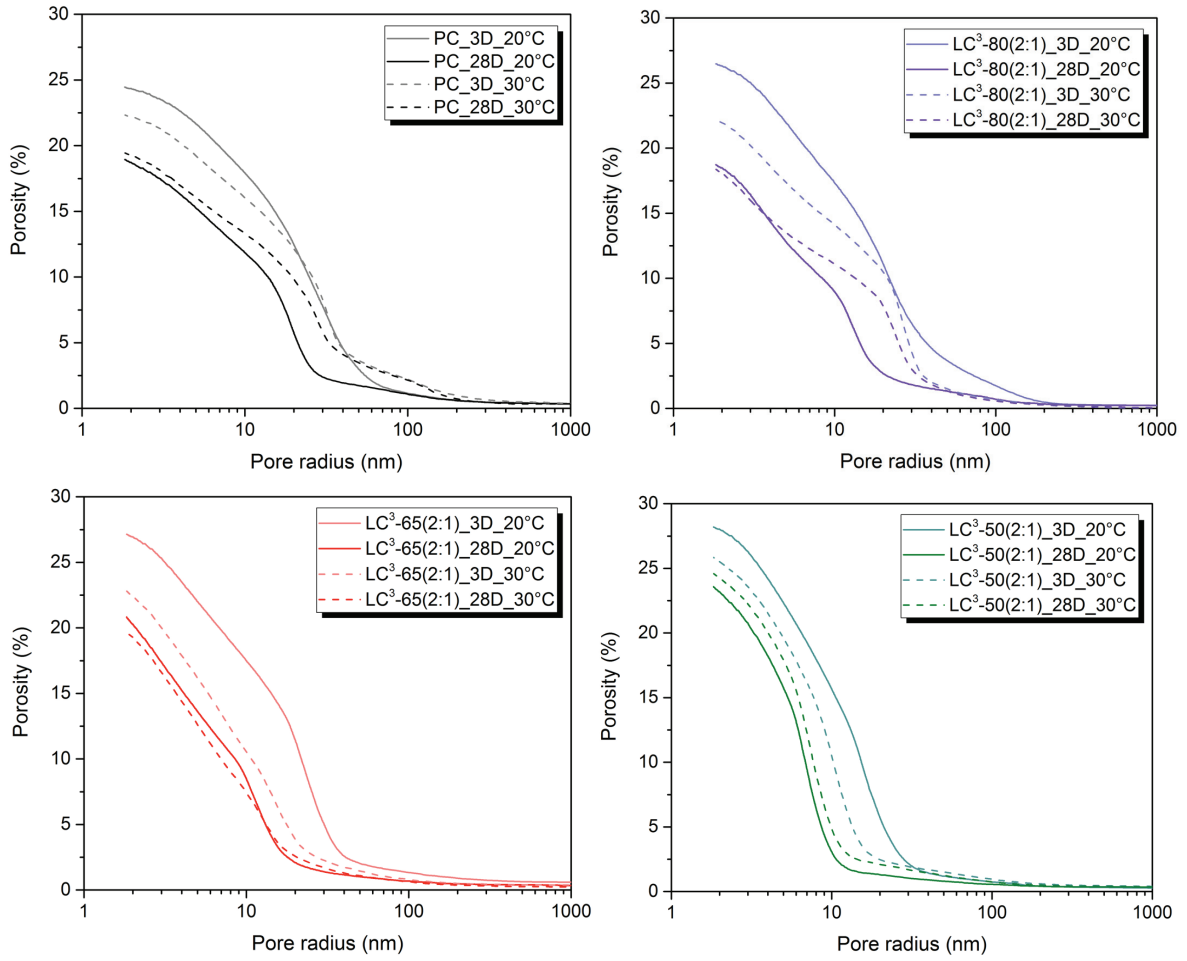


Figure 3.9 Pore size distribution of PC and LC³ systems cured at 20°C and 30°C for 3 days and 28 days

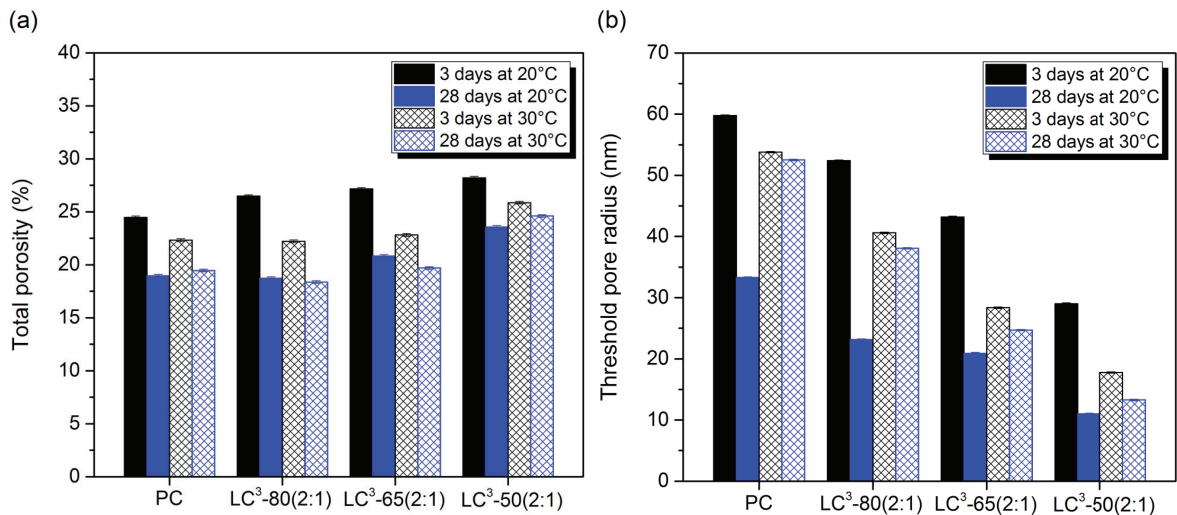
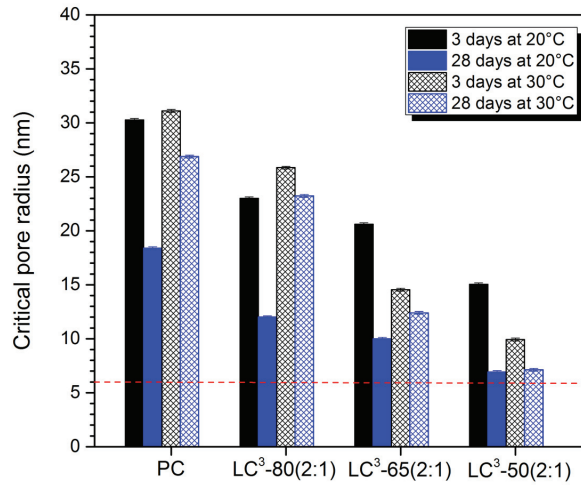
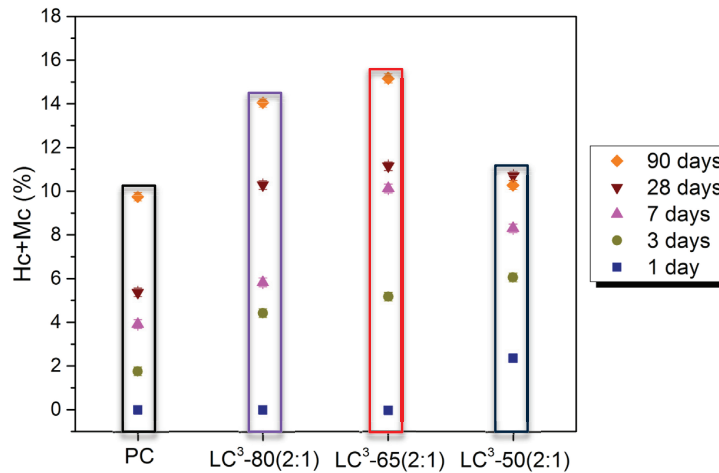


Figure 3.10 Total porosity (a) and threshold pore radius (b) of PC and LC³ systems

Figure 3.11 The critical pore radius of PC and LC³ systemsFigure 3.12 Hc+Mc quantified by XRD-Rietveld analysis of PC and LC³ systems at 20°C

3.4.6 C-(A)-S-H composition

Figure 3.13 shows the SEM-EDS point analysis results performed on inner C-(A)-S-H of PC and LC³ systems curing at 20°C and 30°C. The Si/Ca and Al/Ca ratio increase with increasing the level of SCMs substitution. This change results from the contribution of Si and Al provided by calcined clay. The higher Si incorporated in C-S-H causes the longer chain length of C-S-H [56] and this allows the higher Al uptake in C-(A)-S-H. In general, Al substitutes Si in the bridging site of silicate chains [57]. Raising temperature also influences the composition of C-(A)-S-H as seen the cloud point slightly shifted to the left in the systems of PC and LC³-80(2:1) and shifted up in LC³-65(2:1) and LC³-50(2:1) systems.

Figure 3.14 shows C-(A)-S-H composition in term of Ca/Si and Al/Si for all systems at 28 days. The pozzolanic reaction results in a decrease of Ca/Si and an increase of Al/Si in the systems of LC³. Raising temperature promotes the pozzolanic reaction [58, 59] and causes a higher Al/Si which is easily observed in the system with high substitution level. However, the higher Ca/Si is observed only in the systems of PC and LC³-80(2:1). It can be possible due to the inclusion of portlandite (CH) in the inner C-(A)-S-H.

The inclusion of CH with the inner C-(A)-S-H of PC and LC³-80(2:1) systems at higher temperature can be investigated in Figure 3.13, as seen the EDS points toward to CH in these systems. This is due to the higher precipitation rate of hydration products at an initial period resulted in the portlandite precipitating nearby the cement grains and leads to form unevenly C-(A)-S-H. The particular layout of these products induces the formation of heterogeneous microstructures and resulted in coarsening porosity [50]. However, in the case of the LC³-65(2:1) and LC³-50(2:1) systems, a fewer portlandite is observed in inner C-(A)-S-H due to the faster kinetics of the pozzolanic reaction at a higher temperature.

Thus, the modification of C-(A)-S-H caused by the inclusion of CH could explain coarsening porosity at a higher temperature in the case of PC and LC³-80(2:1) in this study.

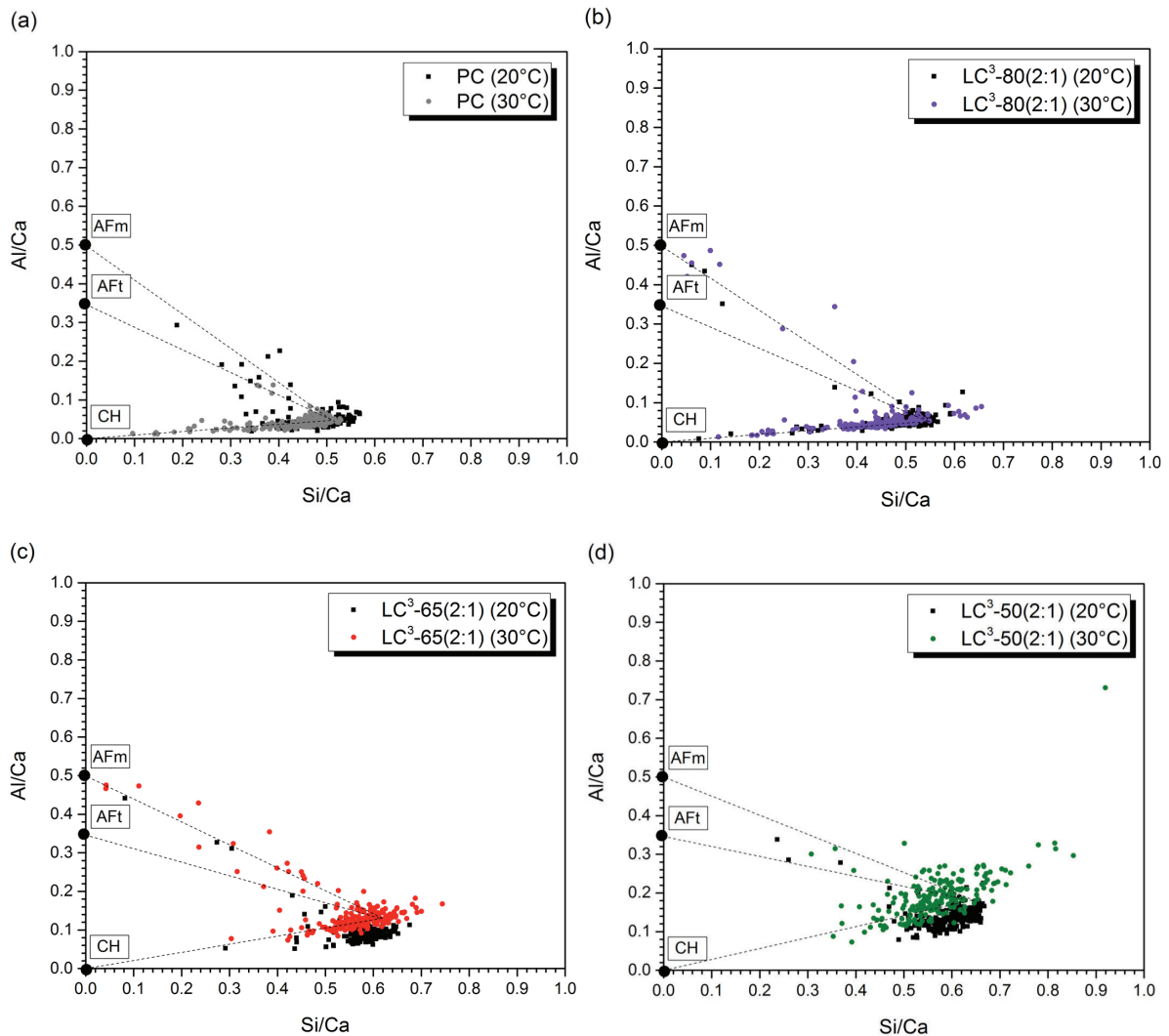


Figure 3.13 The plot of Al/Ca vs Si/Ca of inner C-(A)-S-H of PC (a) LC³-80(2:1) (b), LC³-65(2:1) (c) and LC³-50(2:1) (d) cured at 20°C and 30°C for 28 days

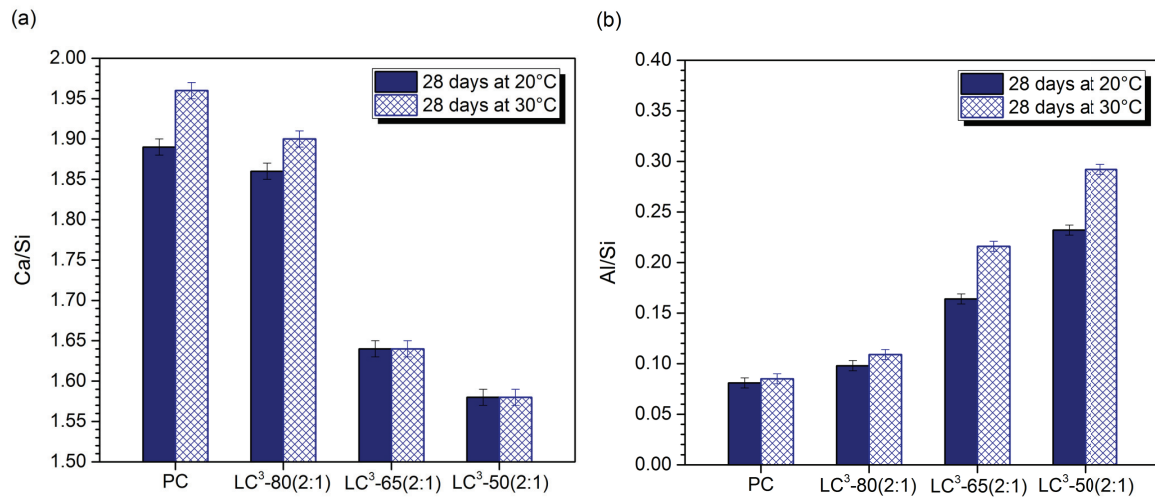


Figure 3.14 The C-(A)-S-H composition of PC and LC³ systems cured at 20°C and 30°C for 28 days showing Ca/Si (a) and Al/Si (b)

3.4.7 Microstructure

The microstructures of PC and LC³ systems cured at 20°C and 30°C for 28 days investigated using SEM-BSE are shown in Figure 3.15 and Figure 3.16. The percentage of porosity was estimated by image analysis. It is corresponding to 0-50 levels of gray level (max 255) analyzed by ImageJ software using thresholding technique.

The denser microstructure is observed at the higher level of substitution in both curing temperatures. LC³-50(2:1) shows the most densification of microstructure as seen the lowest percentage of porosity. Increasing temperature affects the microstructure of all systems. The microstructures appear more coarsening porosity at 30°C compared to 20°C. This is in agreement with the MIP results which show the increase of threshold pore radius and critical pore radius when increased the temperature.

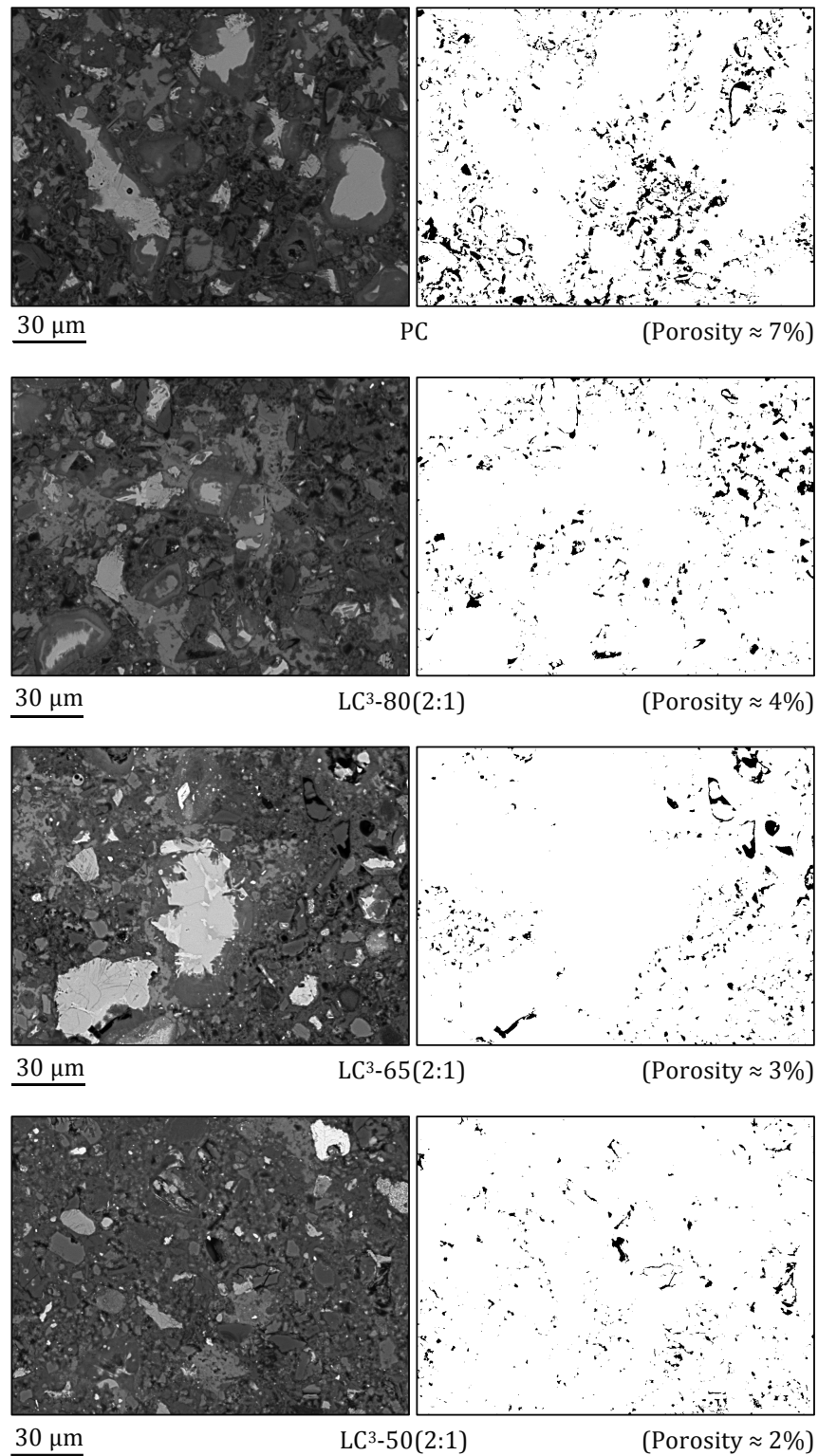


Figure 3.15 BSE-SEM image (left) and its porosity analysis (right) of PC, LC³-80(2:1), LC³-65(2:1) and LC³-50(2:1) cured at 20°C for 28 days

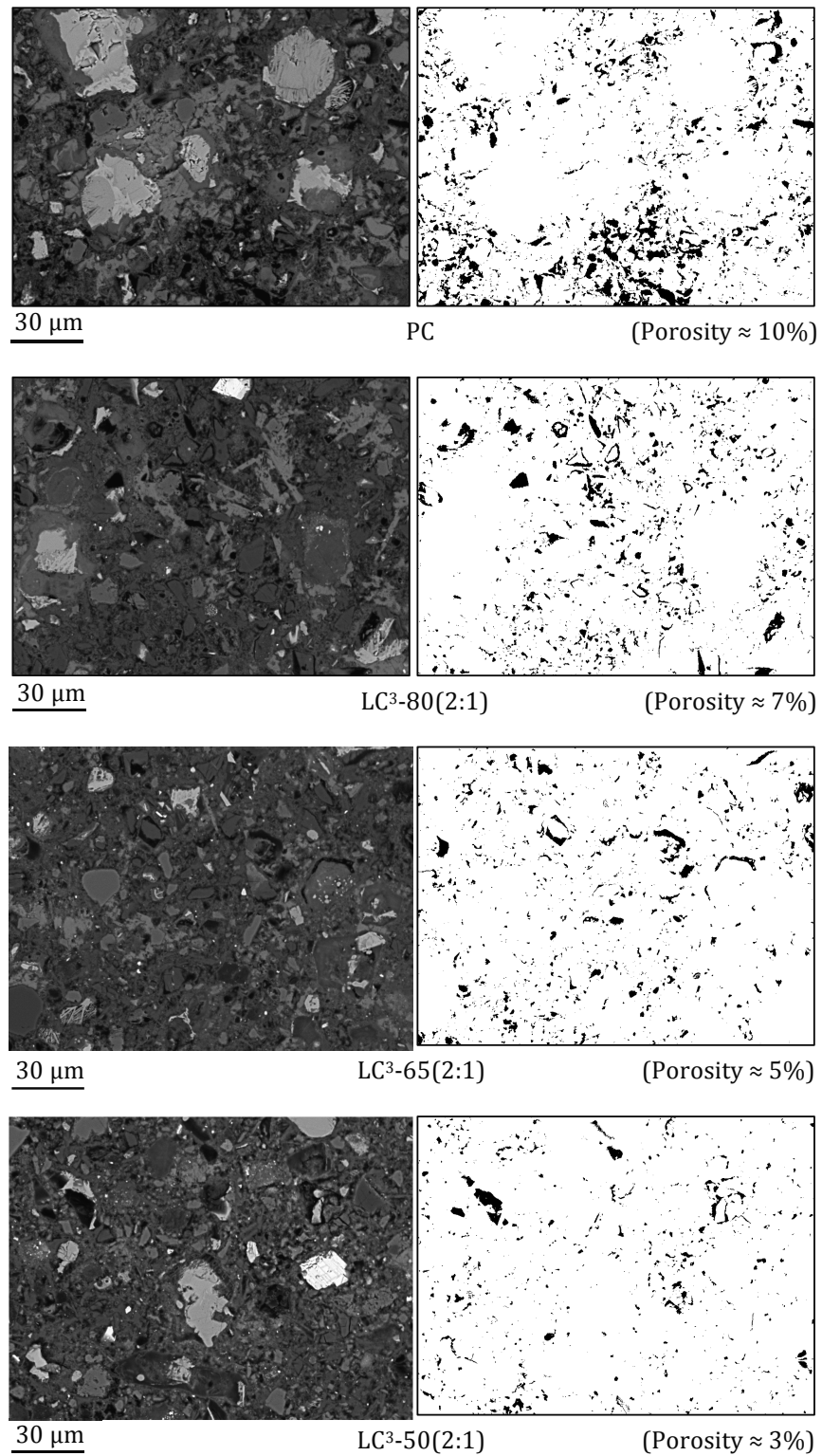


Figure 3.16 BSE-SEM image (left) and its porosity analysis (right) of PC, LC³-80(2:1), LC³-65(2:1) and LC³-50(2:1) cured at 30°C for 28 days

3.5 The relationship between compressive strength and porosity

The relationship between compressive strength and porosity of PC and LC³ systems curing at 20°C and 30°C shows in Figure 3.17. The strength was carried on mortar samples and the total porosity results were carried on cement pastes and they were tested at 3, 7, 28 and 90 days for curing at 20°C and at 3 and 28 days for curing at 30°C. In this study, the total porosity can explain the strength development of PC and LC³ systems as seen the linear relationship between the compressive strength and the total porosity. Both temperatures show a similar trend, the higher the total porosity, the lower the strength. LC³-50(2:1) includes the greater amount of total porosity resulting in the lower compressive than the others in this study.

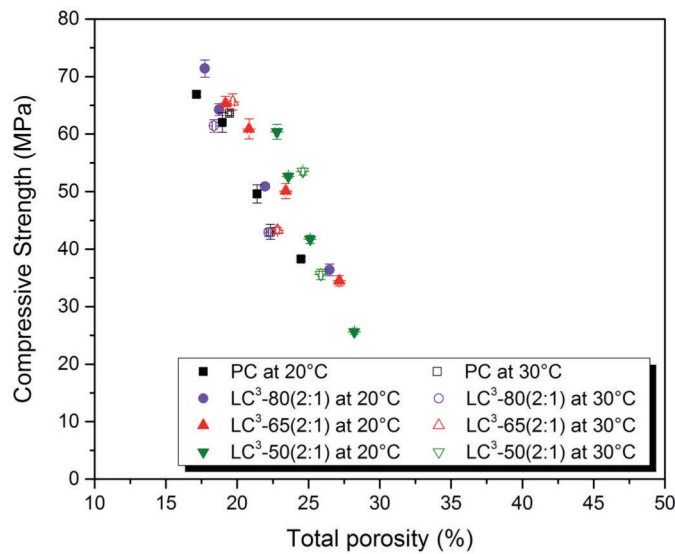


Figure 3.17 The compressive strength of PC and LC³ systems cured at 20°C and 30°C plotted as a function of total porosity

3.6 The relationship between compressive strength and gel-space ratio

Another approach promising to explain the strength development of PC and LC³ systems is the gel-space ratio. Powers [40] and Termkhajornkit [41] defined C-(A)-S-H which is the main hydration product as the gel. Space was the sum of the initial volume of water and the volume of reacted binders including clinker, metakaolin, and limestone. The calculation of the gel-space ratio is shown in Equation 3.1. The good relationship illustrated in Figure 3.18 guides that the compressive strength could be explained by the gel-space ratio.

$$Gel - Space\ ratio = \frac{\sum vol_{C-(A)-S-H}}{(\sum vol_{(react\ binders)_{t_0}} - \sum vol_{(react\ binders)_{t_t}}) + vol_{water}} \quad \text{Equation 3.1}$$

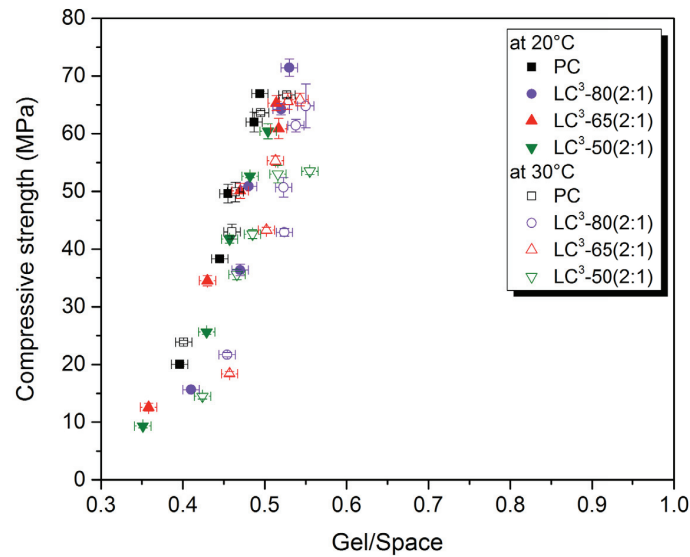


Figure 3.18 Compressive strength plotted versus gel space ratio considering C-(A)-S-H as the gel of PC and LC³ systems cured at 20°C and 30°C

3.7 Summary

- Limestone and calcined clay can replace clinker up to 45% to produce LC³ blended cement and give satisfactory results. The compressive strength of all LC³ blended systems meets the standard value of OPC type I and CEM I 42.5N. LC³-80(2:1) and LC³-65(2:1) show similar strength to PC from 7 days onwards. Increasing temperature stimulates the hydration of clinker and the pozzolanic reaction resulting in the enhancement of strength development at the early ages.
- The ettringite is retained in all systems thanks to the presence of limestone. The increase of SCMs content enhances the formation of carboaluminate phases and presents more persistence of Hc.
- The critical pore entry radius decreases with increasing the substitution levels and the size of LC³-50(2:1) reaches to about 6-7 nm which is in the range of limiting pore entry radius for precipitation and growth of hydration products. This results in the slowdown of DoH and DoR of LC³-50(2:1).
- The strengths show a good correlation to the gel-space ratio, so the lower strength of LC³-50(2:1) can be explained by a lower amount of hydrates.

Chapter 4. The impact of alkalis on the properites of limestone calcined clay cement (LC³)

4.1	Introduction	41
4.2	Formulations.....	42
4.3	Compressive strength	43
4.4	Kinetics.....	44
4.5	Degree of reactions	46
4.6	Phase assemblage	47
4.7	C-A-S-H composition	50
4.8	Porosity	52
4.9	Discussion	55
4.10	Summary.....	57

4.1 Introduction

The replacement of clinker with supplementary cementitious materials (SCMs) is the most viable option to reduce the CO₂ emissions from cement production, [2-4]. However, the use of any SCMs, especially for high clinker replacement levels, may cause a reduction of the early age strength of the blended cement because of the slower reaction of SCMs compared to clinker. One way of improving early-age strength is to increase the alkalinity of cement. Alkalis are known to accelerate the hydration reaction of clinker phases at an early age [60, 61] and they enhance the reactivity of SCMs for blended cements [62-66]. Nevertheless, this early-age strength increase is accompanied by a reduction of the mechanical properties at later ages, which could be due to a higher porosity [67] or a change of hydrate morphology and/or composition [68, 69].

Several publications showed the effect of alkalis on the reactivity of SCMs. For blast furnace slag cement, Frigione and Sersale [62] found a good correlation between the compressive strength and the total soluble alkali content. Fraay et al. [63] showed the enhancement of the pozzolanic reaction of fly ash when the pH of the pore solution increases. Lagier and Kurtis [64] reported that the reaction of metakaolin increased with increasing the equivalent alkali content of cement. Similar observations were found by Cyr et al. [66]. They mentioned that the reduction of pH of pore solution led to reducing the dissolution of metakaolin.

However, the supplies of traditional SCMs such as slags or fly ashes are limited. The use of calcined clay, especially with 40-60% kaolinite content, coupled with limestone to produce limestone calcined clay cement (LC³) is a commercially and technically viable option [7, 12, 28, 30, 70]. There is no work published on the impact of alkalis on the hydration and the properties of LC³ systems. Thus, the aim of this paper is to investigate the impact of alkalis both of potassium (K) and sodium (Na) on the mechanical properties of LC³ systems in order to optimize early-age strength without affecting later-

age strength. The strength results will be correlated to the kinetics of hydration, the phase assemblage and the porosity development of LC³.

4.2 Formulations

LC³-65(2:1) was used in this study. It corresponds to a blended cement in which 35 parts of cement are replaced by 20 parts of calcined clay and 10 parts of limestone (2:1 calcined clay to limestone ratio). This calcined clay to limestone ratio was shown to give the best strength [29]. In order to avoid undersulfation, 0.5% of gypsum was added (>98%, AcrosOrganics). A OPC type I (PC) with 0.52% Na₂O_{eq} (%alkali equivalent, %Na₂O_{eq} = %Na₂O+0.658×%K₂O), was used as the plain cement. Limestone powder used was a commercial product (Durcal 5, Omya). The calcined clay contains approximately 50% of metakaolin (MK) and this clay was calcined at 750°C for 5 sec in fluidized bed combustor. Potassium hydroxide (KOH, >85%, reagent grade, Fisher Scientific) and sodium hydroxide (NaOH, >99%, pellets for analysis, Merck) were used to adjust the percentage of alkali equivalent. The formulations of each batch are given in Table 4.1.

The concentration of KOH and NaOH were determined using an acid–base titration. A standard solution of acid (HCl 1M, Carlo Erba Reagents) was diluted 10 times to get 0.1M of HCl solution and then it was used as a titrant. A pH meter was used to monitor the progress of the acid–base reaction. The pH of the equivalence point was estimated about 7 for a strong acid–base neutralization. After the titration, the results of the amount of KOH and NaOH are 85±1% and 98±1% respectively. Thus, 85% of KOH and 98% of NaOH were used to calculate the percentage of alkali equivalent for each system.

Table 4.1 Formulations and name of LC³-65(2:1) with various alkali contents

Samples	wt.%					Gypsum addition
	PC	Calcined clay	Limestone	KOH	NaOH	
PC	100.00	0	0	0	0	0
LC ³ -65(2:1) 0.44%Na ₂ O _{eq}	69.65	19.90	9.95	0	0	0.50
LC ³ -65(2:1) 0.61%-K	69.30	19.90	9.95	0.35	0	0.50
LC ³ -65(2:1) 0.77%-K	68.95	19.90	9.95	0.70	0	0.50
LC ³ -65(2:1) 0.93%-K	68.61	19.90	9.95	1.04	0	0.50
LC ³ -65(2:1) 1.09%-K	68.25	19.90	9.95	1.40	0	0.50
LC ³ -65(2:1) 0.63%-N	69.41	19.90	9.95	0	0.24	0.50
LC ³ -65(2:1) 0.82%-N	69.16	19.90	9.95	0	0.49	0.50
LC ³ -65(2:1) 1.00%-N	68.95	19.90	9.95	0	0.70	0.50
LC ³ -65(2:1) 1.20%-N	68.65	19.90	9.95	0	1.00	0.50

4.3 Compressive strength

The compressive strength of LC³-65(2:1) systems compared to PC (dash line with pale color) are shown in Figure 4.1. The strength of LC³-65(2:1)-0.44%Na₂O_{eq} without any alkali adjustment, is similar to the PC from 7 days onwards. The increase of alkali content has a significant impact on the strength development of LC³-65(2:1) at early ages. Use of either alkali hydroxide (KOH or NaOH) improves the compressive strength at 1 day with a maximum reached for about 0.80% Na₂O_{eq}, but these higher alkali contents lead to lower strengths at later ages. Additionally, the type of alkali hydroxide influences strength development. KOH shows a more positive impact than NaOH as 0.77% addition KOH gives a strength of LC³-65(2:1), similar to the PC at 3 days, while the NaOH addition does not reach this value. In order to see more clearly the impact of alkali on the strength development of LC³-65(2:1), the relative compressive strengths are shown in Figure 4.2.

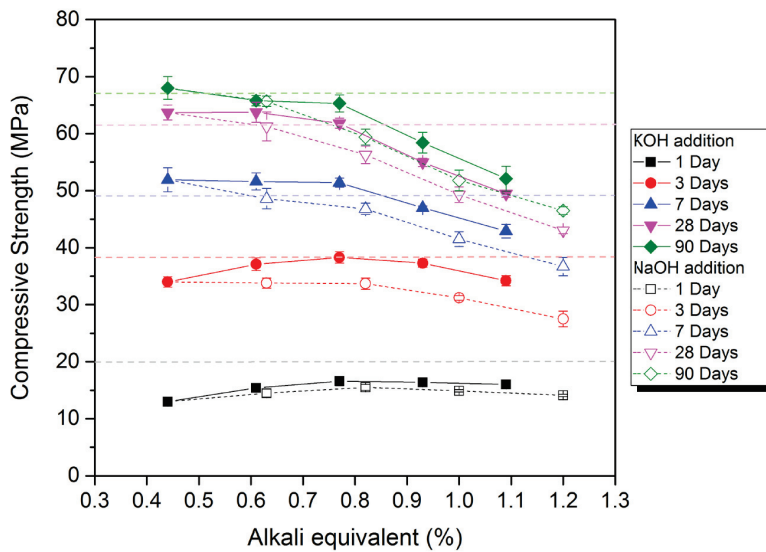


Figure 4.1 Compressive strength of PC and LC³-65(2:1) with various alkali contents

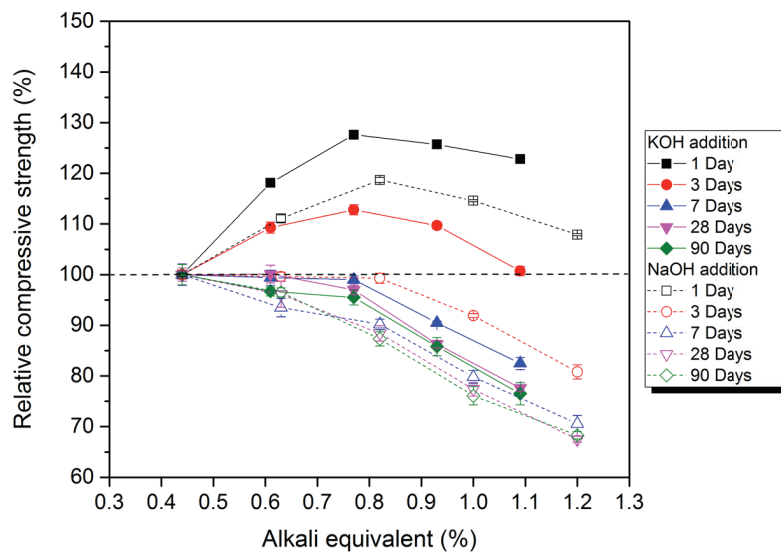


Figure 4.2 Relative compressive strength of LC³-65(2:1) with various alkali contents

Figure 4.2 shows the relative compressive strength of LC³-65(2:1) with various alkali contents to LC³-65(2:1)-0.44%Na₂O_{eq}. The strength increases by 128% at 1 day and 113% at 3 days for KOH addition, while NaOH increases strength up to 119% at 1 day but has no impact at 3 days. At the later ages, higher levels of alkali have an adverse effect on strength. The addition of KOH, at about 0.77% equivalent, is most interesting because of the highest strength of 1 day and 3 days and the same strength value as the reference system from 7 days onwards. For NaOH, there are negative impacts for all levels of addition from 7 days onwards. The maximum alkali content for NaOH should be about 0.63% for this system.

4.4 Kinetics

The increase of alkali content using both KOH and NaOH addition enhances the reaction of the silicate phase and the aluminate phase as seen in Figure 4.3. The main impact is the steeper slope of the main silicate reactions. This suggests that the alkalis speed up the growth of C-S-H. However the mechanism behind this effect and the reason for the stronger impact of sodium compared to potassium is not clear.

Furthermore, an indirect effect of C₃S acceleration is the earlier sulfate depletion due to the higher sulfate adsorption on C-(A)-S-H [71]. NaOH shows a stronger effect on the sulfate depletion than KOH as seen the shift of the aluminate peak towards earlier age with increasing alkalinity.

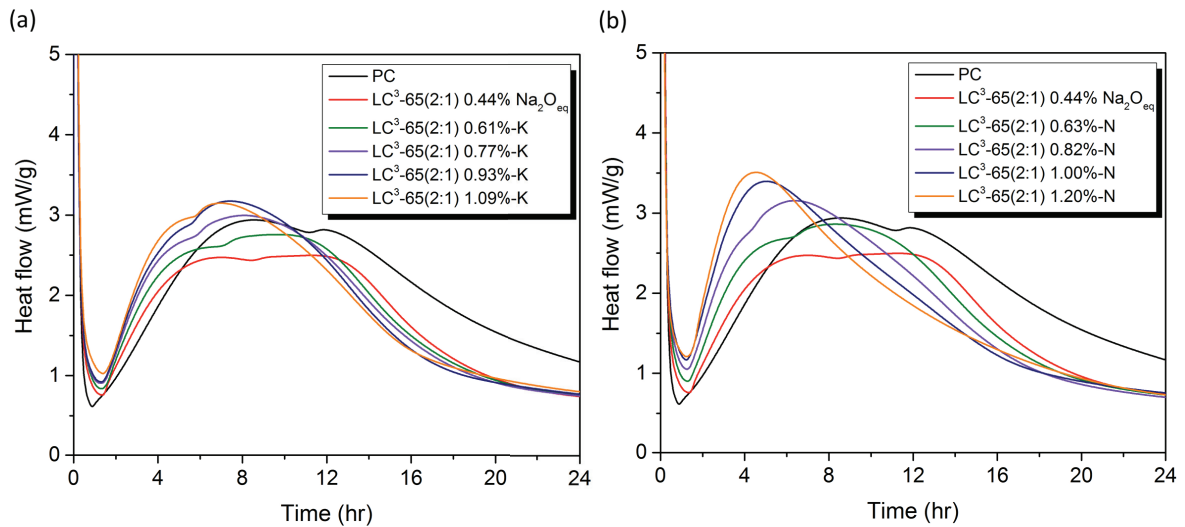
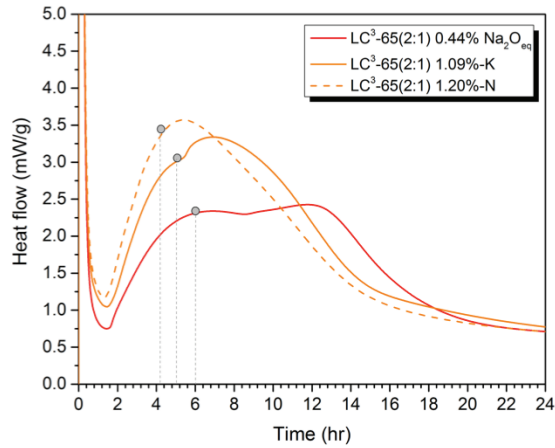
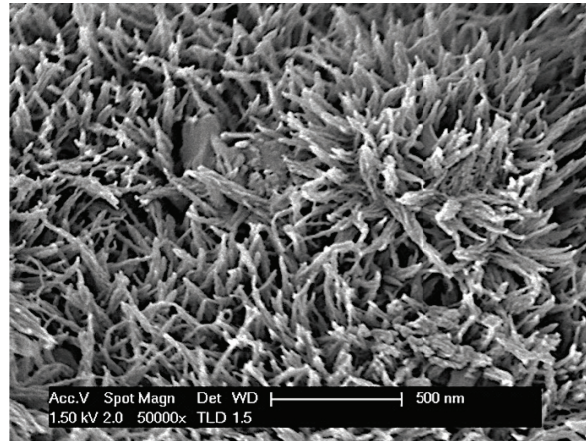


Figure 4.3 Heat flow of PC and LC³-65(2:1) with various alkali contents (a) KOH addition and (b) NaOH addition

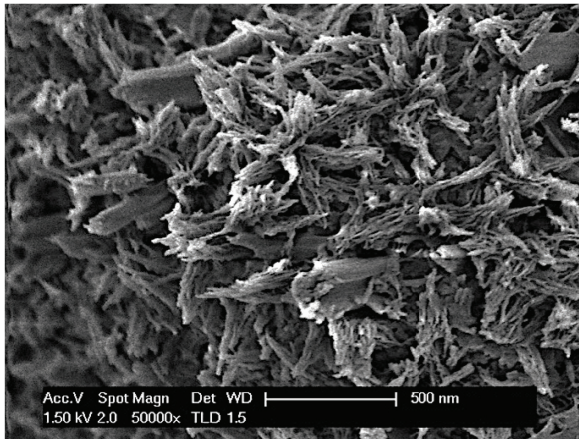
The influence of alkali on the morphology of C-A-S-H at the end of the acceleration period can be observed in Figure 4.4. It is clearly seen that alkalis modify the morphology of C-A-S-H as seen the C-A-S-H structure gradually change from a divergent structure to a foil-like structure when increased the alkalinity. LC³-65(2:1)-1.20%-N shows obviously a foil-like structure due to the complete sulfate depletion as seen the peak corresponding to the aluminate phase hydration is combined with the peak of silicate phase hydration. This result is in agreement with Mota's work [61] discovered a foil-like morphology of C-S-H presenting in the system containing NaOH alone with no sulfate content.



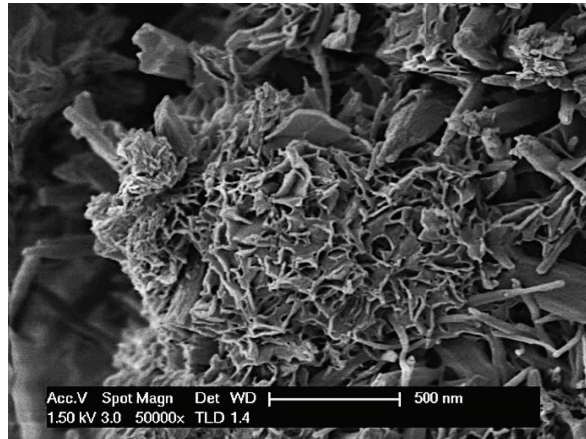
Time to stop the hydration



LC³-65(2:1)-0.44%Na₂O_{eq}



LC³-65(2:1)-1.09%-K



LC³-65(2:1)-1.20%-N

Figure 4.4 Determination of time to stop the hydration at the end of the acceleration period corresponding to the identical DoH of LC³-65(2:1)-0.44%Na₂O_{eq} (top left) and C-A-S-H morphology of LC³-65(2:1)-0.44%Na₂O_{eq}, LC³-65(2:1)-1.09%-K and LC³-65(2:1)-1.20%-N after stopped the hydration

4.5 Degree of reaction

The degree of clinker hydration (DoH) of the LC³-65(2:1) with various alkali contents are shown in Figure 4.5. The acceleration of C₃S phase by alkali (Figure 4.3) is reflected in the increase of degree of clinker hydration at 1 day. For KOH addition, at 1 day the DoH increases by 5% when increased alkali equivalent from 0.44% to 0.61% and the DoH is approximately the same for higher addition levels. For NaOH addition, increasing alkali up to 0.82% increases the DoH but no effect on DoH for the further addition of alkali. At later ages, the DoH decreases with increasing the percentage of alkali content and dramatically decreases for the highest alkali content.

The degree of metakaolin (MK) reaction calculated by mass balance is shown in Figure 4.6. The reaction of metakaolin increases with time but there is no significant effect in the alkali content or the type of addition on the reaction degree of metakaolin at 3 days. However, similarly to the DoH, the higher alkalinity lowers the degree of metakaolin reaction at later ages in both cases of KOH and NaOH.

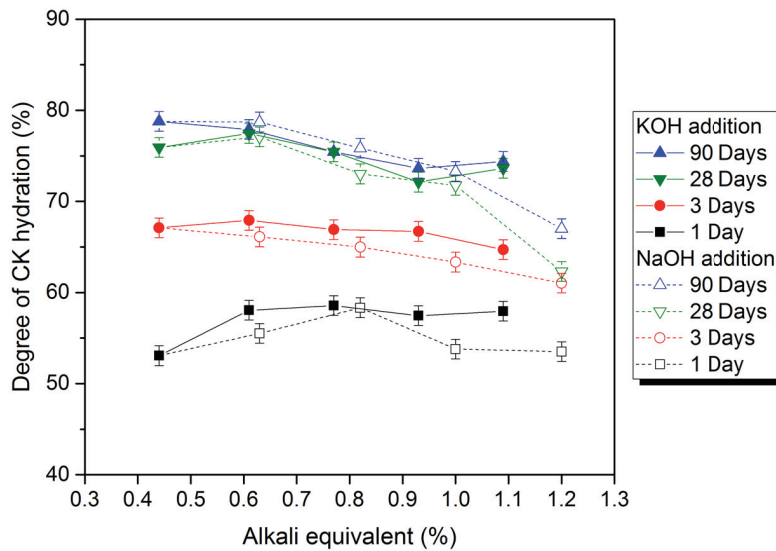


Figure 4.5 Degree of clinker hydration of LC³-65(2:1) with various alkali contents

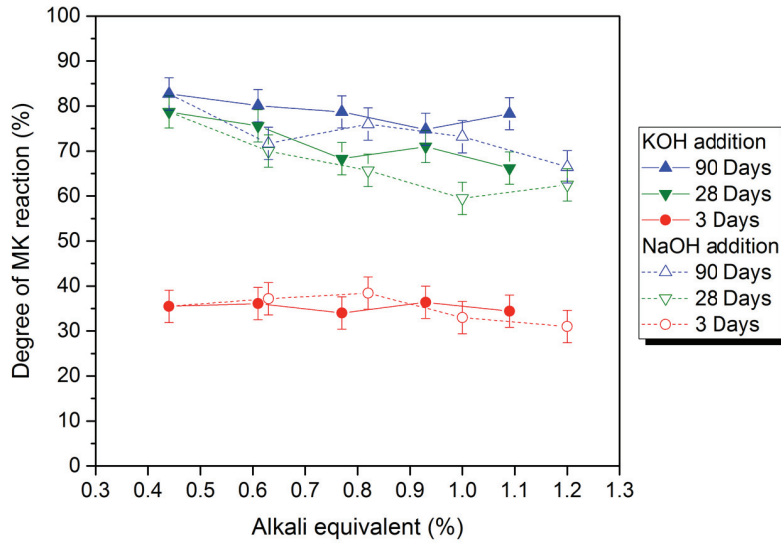


Figure 4.6 Degree of MK reaction of LC³-65(2:1) with various alkali contents

4.6 Phase assemblage

Based on mass balance calculation (section 2.2.9), the overall volume distribution of phases is obtained and is presented in Figure 4.7. It is clearly seen that alkalis lower the total volume of hydrated phases, especially at 28 days. As mentioned previously, increasing alkalinity leads to a decrease of DoH resulting in a lower formation of C-(A)-S-H. Thus, the decrease of volume of C-(A)-S-H (in blue) is observed with increasing alkali content in both cases of alkali addition.

Although, adding either KOH or NaOH to increase the alkalinity does not affect the amount of ettringite formed (in purple), it affects the carboaluminate hydrates (in yellow) formation. The constant quantity of ettringite at high alkali conditions in this study is in contrast with the previous results [72, 73], which indicated that an increase of alkalinity increases the solubility of ettringite. However here, the addition of calcium carbonate ensures that hemicarboaluminate (Hc) and monocarboaluminate (Mc) are the AFm phases present so all sulfate (the same in all systems) is available to form ettringite [24, 26].

However, the increase of alkalinity affects the formation of carboaluminate hydrates (Hc and Mc) independent of the alkali species. Alkalis enhance the formation of carboaluminate hydrates at early ages and the transformation of Hc to Mc is favoured by increasing alkalinity [44]. At later ages, increasing alkalinity results in a lower DoH and less Hc and Mc precipitated but the causal relation between these two observations is not clear yet. Nevertheless, these cause a reduction of the total volume of hydrated phases in the alkali condition as seen in Figure 4.7.

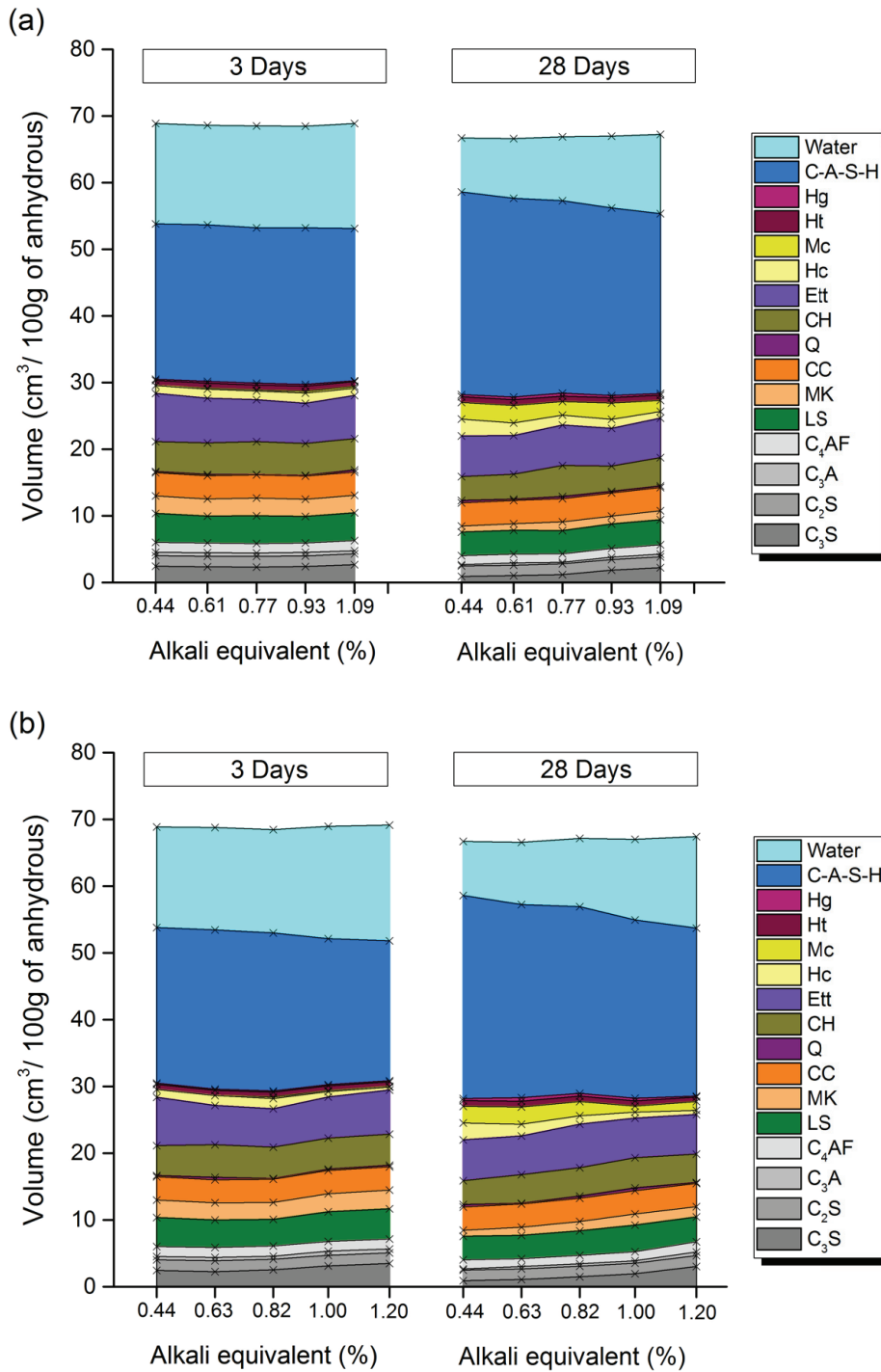


Figure 4.7 Volume of phase assemblage at 3 days and 28 days of LC³-65(2:1) with various alkali contents (a) KOH addition and (b) NaOH addition

LS = limestone, MK = unreacted metakaolin, CC = other components in calcined clay, Q = quartz, CH = portlandite, Ett = ettringite, Hc = hemicarbonate, Mc = monocarbonate, Ht = hydrotalcite, Hg = hydrogarnet

The volume of hydrated products per unit space available called gel-space ratio can explain the compressive strength development. There are several definitions of gel in the previous works [40-42]. In this study, considering only C-A-S-H as a part of gel and also the total of the volume of hydrated products (C-A-S-H, CH, Ett, Hc, Mc, Ht, and Hg) as the gel was examined. In both cases, space was defined as the sum of an initial volume of water and the volume of reacted binders (clinker, metakaolin, limestone). Both these definitions show good correlation with the compressive strength as shown in Figure 4.8. This indicates that the lower DoH and lower amount of hydration products are directly linked to the lower compressive strength and there is no particular influence of hydrate morphology of type on the strength development.

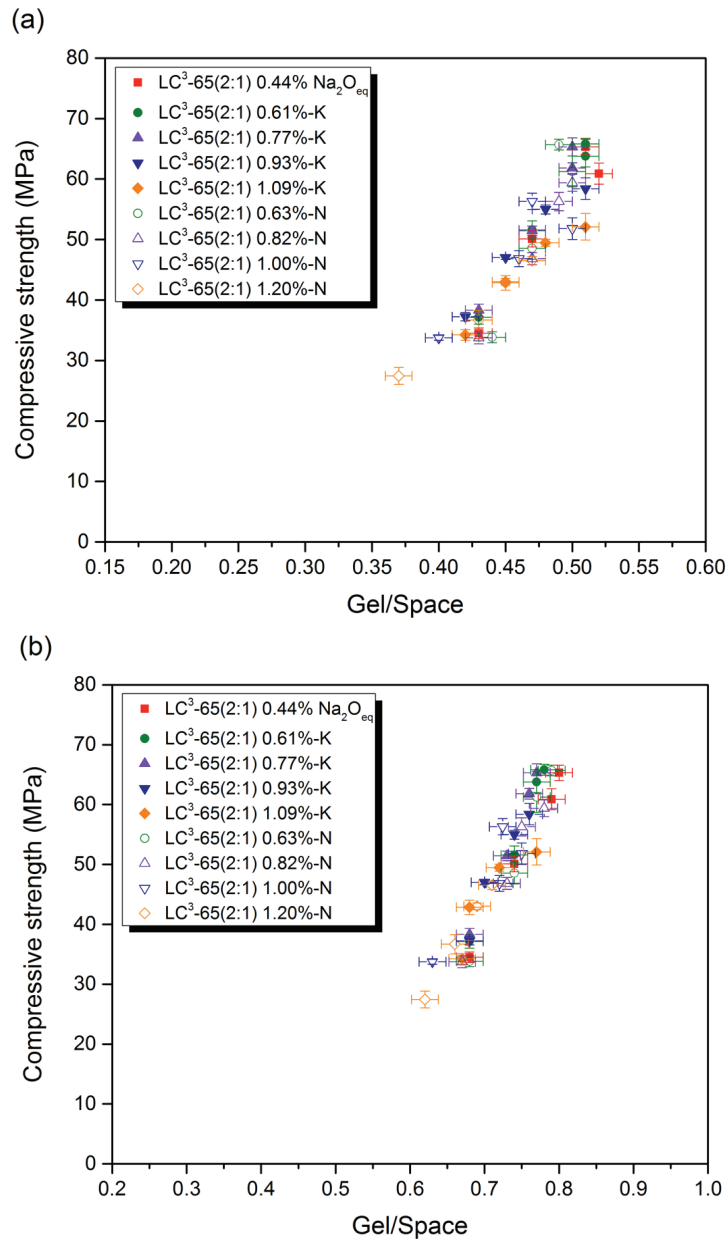


Figure 4.8 Compressive strength vs gel-space ratio of LC³-65(2:1) systems, considering only C-A-S-H as the gel (a) and total volume of hydrated as the gel (b)

4.7 C-A-S-H composition

The C-A-S-H composition of LC³-65(2:1) with various alkali contents determined by SEM-EDX are shown in Figure 4.9 and the results are summarized in Table 4.2. It shows that the Al/Si ratio increases and the Ca/Si decreases from 3 days to 28 days due to the pozzolanic reaction. Increasing alkali shows a higher impact on Al/Si compared to Ca/Si as seen the increase of Al/Si when increased the percentage of alkali at 28 days. Figure 4.10 shows the K/Si and Na/Si ratios, however the state of incorporation of the alkalis in the C-S-H is not known.

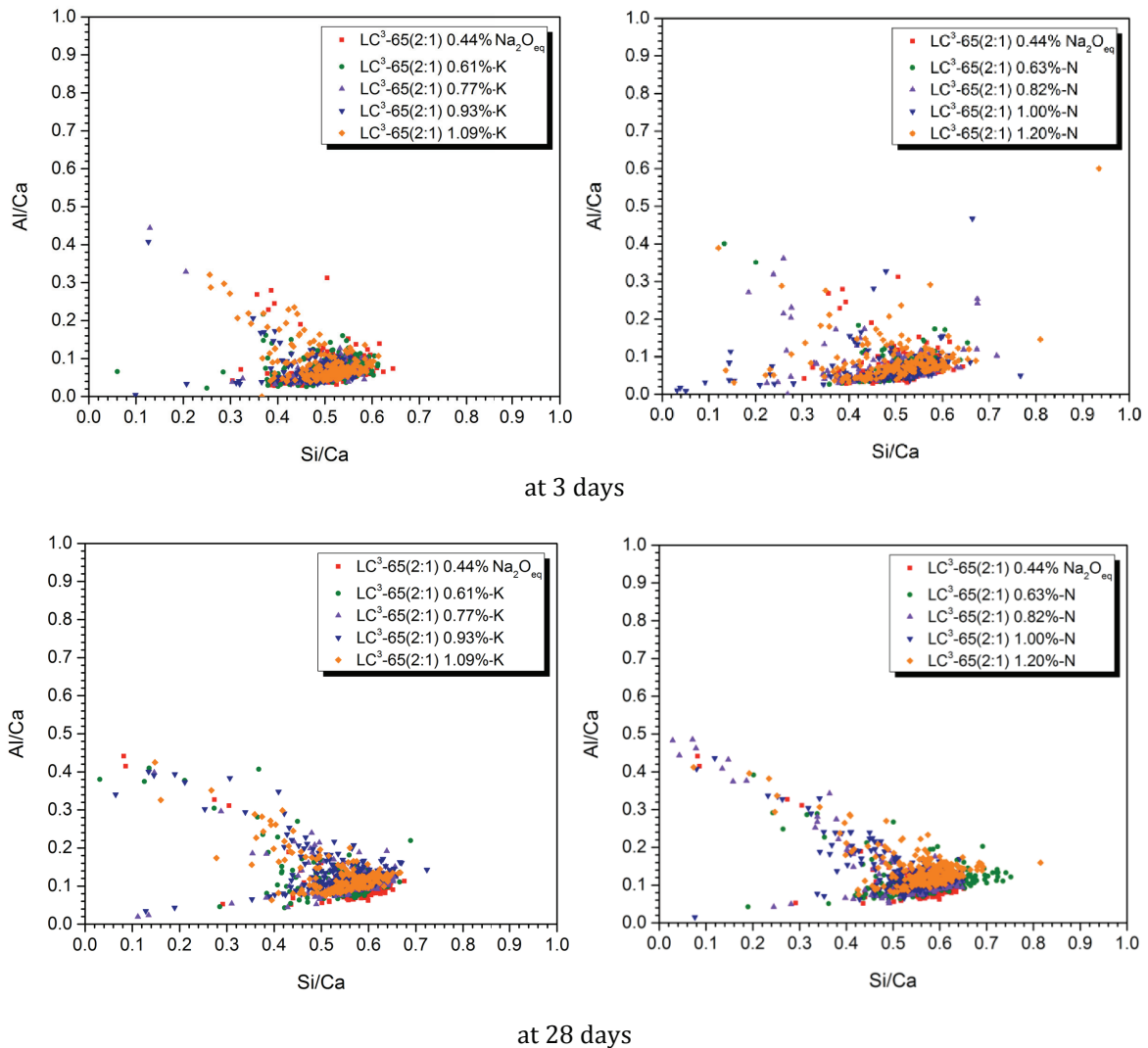


Figure 4.9 EDS analysis of LC³-65(2:1) with various alkali contents at 3 days (top) and 28 days (bottom)

Table 4.2 The C-A-S-H composition of LC³-65 (2:1) with various alkali contents

Samples	3 days		28 days	
	Al/Si	Ca/Si	Al/Si	Ca/Si
LC ³ -65(2:1) 0.44% Na ₂ O _{eq}	0.10	1.75	0.16	1.64
LC ³ -65(2:1) 0.61% - K	0.10	1.75	0.16	1.64
LC ³ -65(2:1) 0.77% - K	0.10	1.75	0.18	1.64
LC ³ -65(2:1) 0.93% - K	0.10	1.75	0.18	1.64
LC ³ -65(2:1) 1.09% - K	0.11	1.75	0.19	1.61
LC ³ -65(2:1) 0.63% - N	0.11	1.75	0.16	1.64
LC ³ -65(2:1) 0.82% - N	0.11	1.75	0.17	1.64
LC ³ -65(2:1) 1.00% - N	0.11	1.72	0.18	1.64
LC ³ -65(2:1) 1.20% - N	0.12	1.69	0.20	1.60

Note: The error of Al/Si is ± 0.005 and Ca/Si ± 0.01

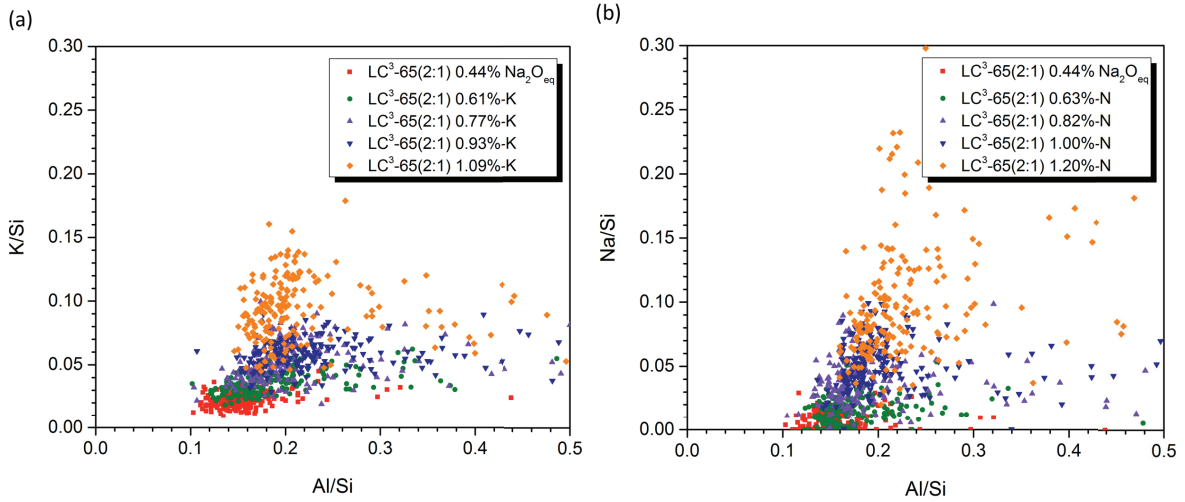


Figure 4.10 K/Si and Al/Si at 28 days of LC³-65(2:1) adjusted alkali content (a) KOH addition and (b) NaOH addition

4.8 Porosity

The impact of alkalis on the pore entry sizes of LC³-65(2:1) are shown in Figure 4.11 and Figure 4.12. At 3 days, the pore refinement is observed in the systems containing high alkali content due to the higher degree of hydration. However, by 90 days the situation is reversed with a coarsening porosity for systems with higher amounts of alkali.

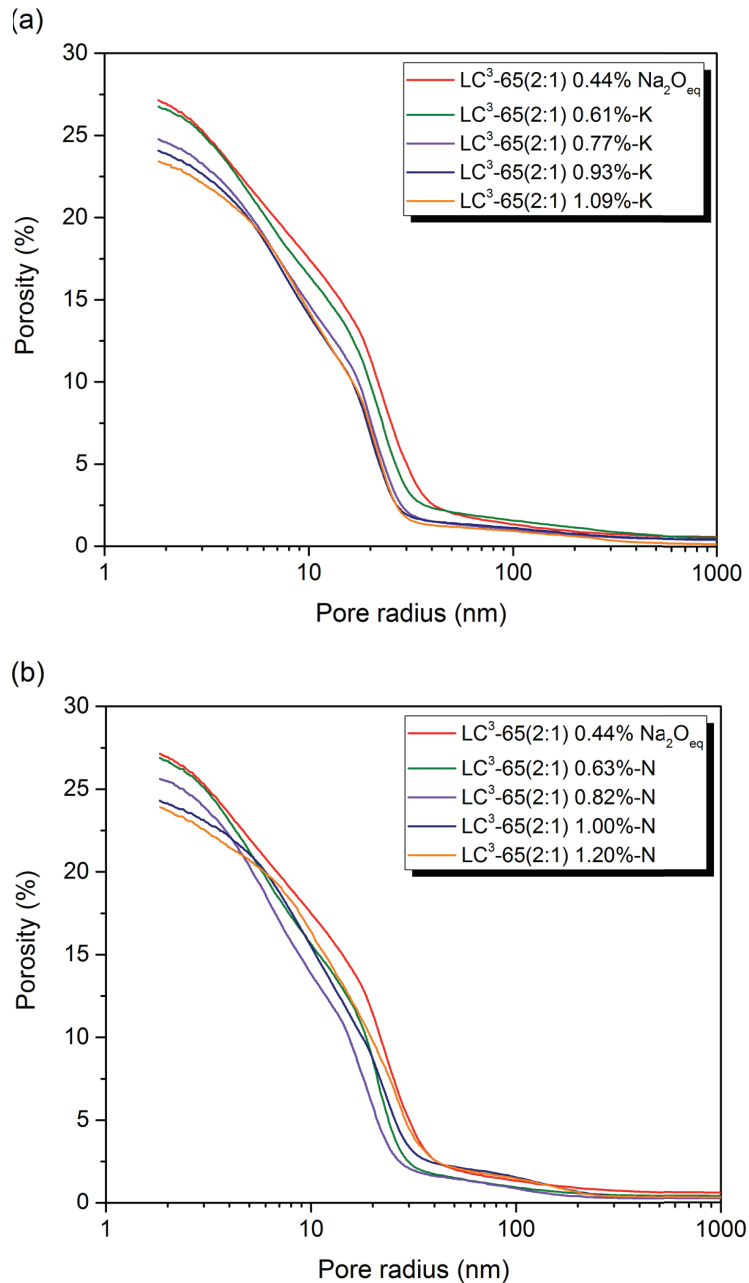


Figure 4.11 Pore entry size distribution of LC³-65(2:1) with various alkali contents at 3 days for KOH addition (a) and NaOH addition (b)

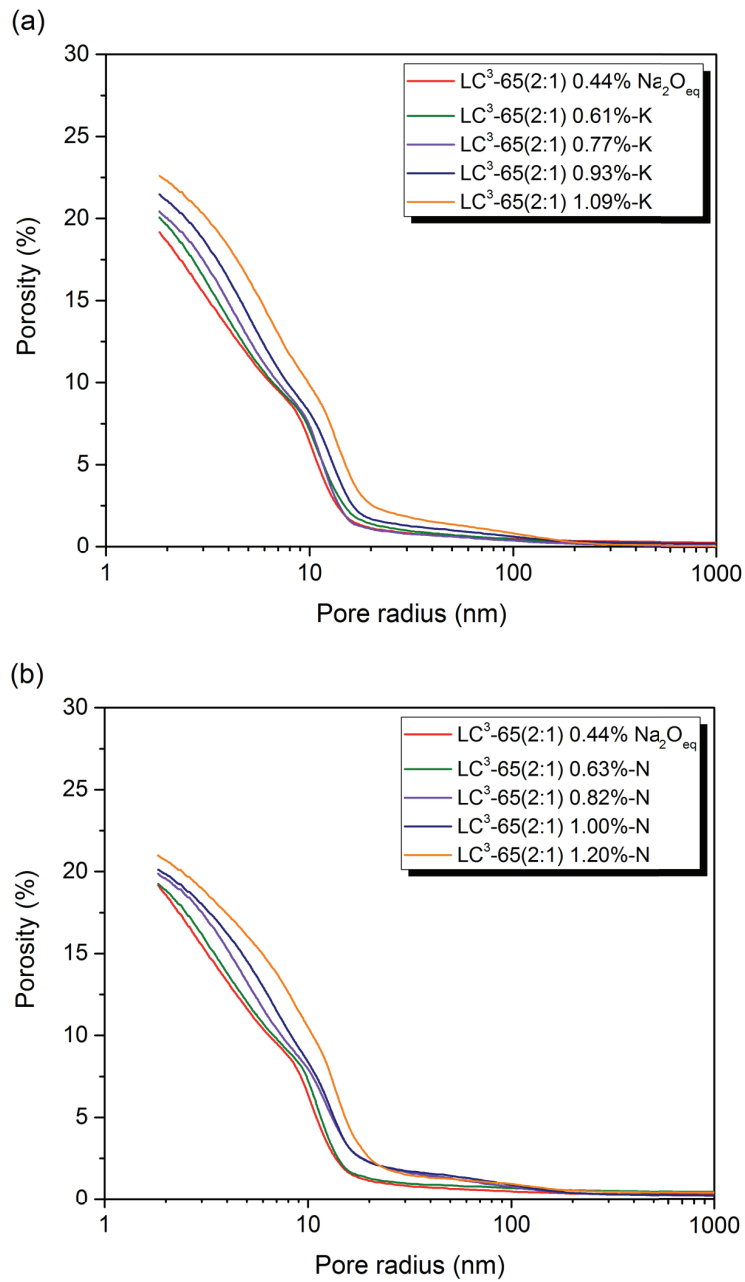


Figure 4.12 Pore entry size distribution of LC³-65(2:1) with various alkali contents at 90 days for KOH addition (a) and NaOH addition (b)

The correlation of porosity with compressive strength of LC³-65(2:1) is shown in Figure 4.13, total porosity Figure 4.13(a) and threshold pore radius Figure 4.13(b). Both types of alkali addition show a similar trend, the bigger the threshold pore radius, the lower the strength. However, the total porosity is fairly related to the compressive strength but a higher scattered data is observed compared to the threshold pore radius. In fact, the total porosity should reflect the relationship with gel/space ratio seen in Figure 4.8. The higher scatter probably reflects that MIP may also detect different amounts of the gel porosity.

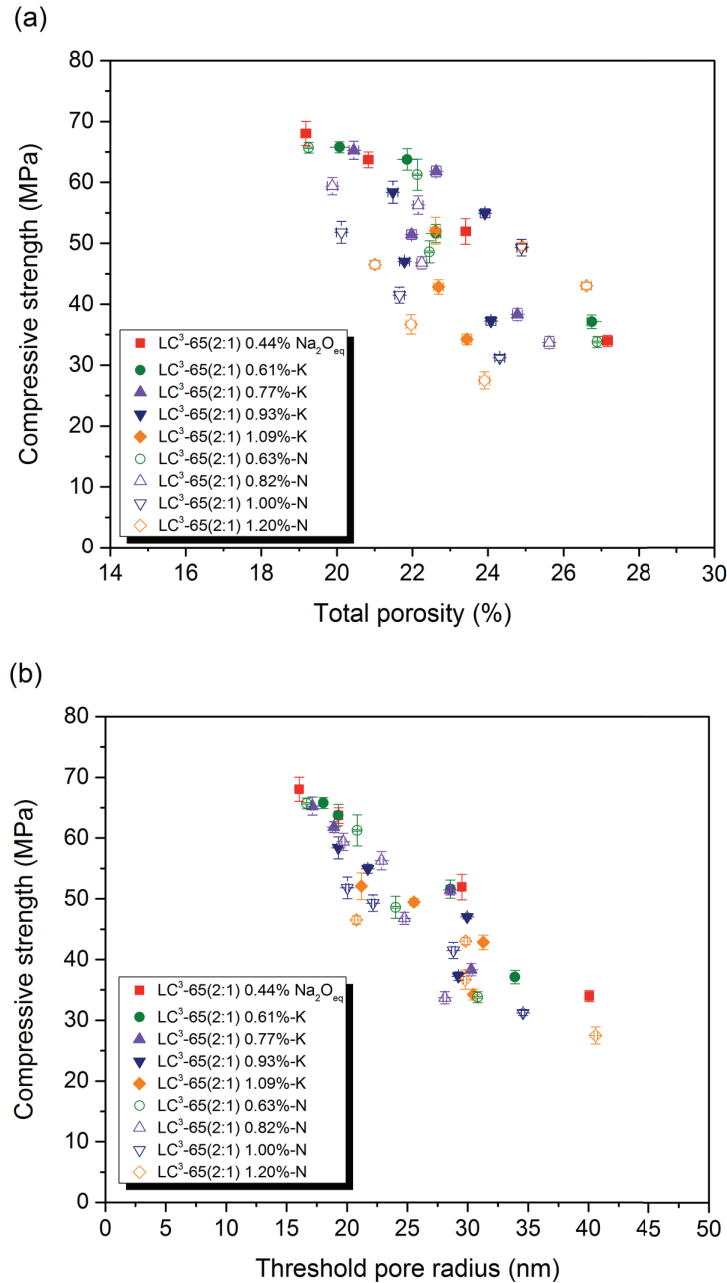


Figure 4.13 Compressive strength of LC³-65(2:1) with various alkali contents plotted as a function of total porosity (a) and threshold pore radius (b)

4.9 Discussion

It is not clear yet why alkalis have a negative effect on the hydration of cement at later ages. One of the possible explanations is that the alkali alters the ionic strength, the chemical equilibrium, and consequently the supersaturation in the pore solution. As seen in Figure 4.14, the saturation index (SI) of C-S-H for LC³-65(2:1) at 28 days calculated using GEMS with Cemdata18 [46] is lower when alkali is added. Although the result of SI calculated from GEMS shows a high error, due to the difficulty of getting accurate measurement of the pore solution, it gives an indication about the minimum pore size required for the growth of hydrates.

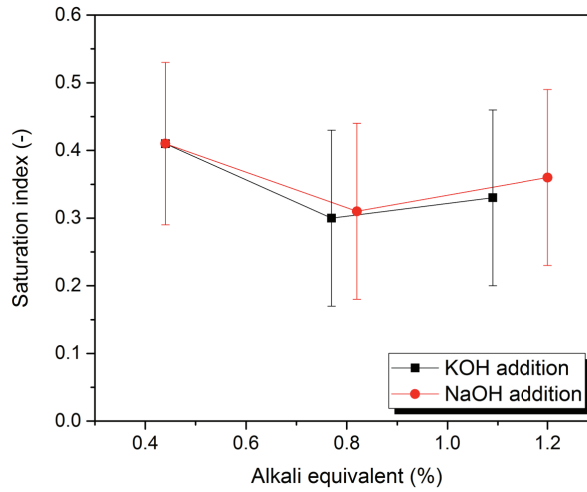


Figure 4.14 Saturation index of C-S-H at 28 days of LC³-65(2:1) with various alkali contents

As hydrates grow into smaller and smaller pores, their curvature must increase. Because of this, a point is reached where the saturation of the pore solution is no longer sufficient to sustain growth in pores below a critical size. This is now believed to be the major factor limiting hydration. This minimum pore radius can be calculated using Equation 4.1.

$$P = \frac{RT}{V_m} \ln(10^{SI}) = \frac{2\gamma}{r} \quad \text{Equation 4.1}$$

where, P is the crystallization pressure (MPa), R is the gas constant (8.314 J/K/mol), T is the temperature (K), V_m is the molar volume (cm³/mol) of the hydration product growing in the pore ($V_m = 81$ cm³/mol for C-S-H [74]). SI is the saturation index (-), γ is the interfacial energy (J/m²) between the hydration product and the solution assumed to be 0.1 J/m² [55, 75, 76] and r is size of pore (nm)

From Equation 4.1, increasing alkali decreases the saturation index of hydrated products, the greater pore size is required for the growth of hydrated in high alkali condition. The minimum pore radiuses for the growth of C-S-H are given in Table 4.3. This is corresponding to a coarsening of porosity of LC³-65(2:1) with high alkali contents at later ages as seen in Figure 4.12.

Table 4.3 The minimum pore radius for the growth of C-S-H at 28 days

Samples	r (nm)
LC ³ -65(2:1) 0.44%Na ₂ O _{eq}	7.4 ± 1.1
LC ³ -65(2:1) 0.77%-K	11.1 ± 2.1
LC ³ -65(2:1) 1.09%-K	10.0 ± 1.8
LC ³ -65(2:1) 0.82%-N	10.7 ± 1.9
LC ³ -65(2:1) 1.20%-N	8.8 ± 1.5

Considering that the interfacial energy is not known precisely, there is good agreement between the minimum critical pore entry radius measured by MIP and the minimum pore radius for the growth of C-S-H calculated from the saturation index by Equation 4.1 at 28 days is shown in Figure 4.15. The critical pore entry radius (MIP) progressively increases with increasing the percentage of alkali while the pore size for C-S-H growth is increased when alkali is added. Thus, a bigger size of pore is required for the growth of the hydrates. Similar effects to this illustration for C-S-H are expected for the other hydrates. The critical pore entry radius of LC³-65(2:1) reaches the maximum pore refinement earlier in high alkali conditions. As described in Chapter 3, once the limit critical pore size is reached, no hydration products can grow. Consequently, a lower formation of carboaluminate phases is observed in high alkali conditions as seen in Figure 4.7.

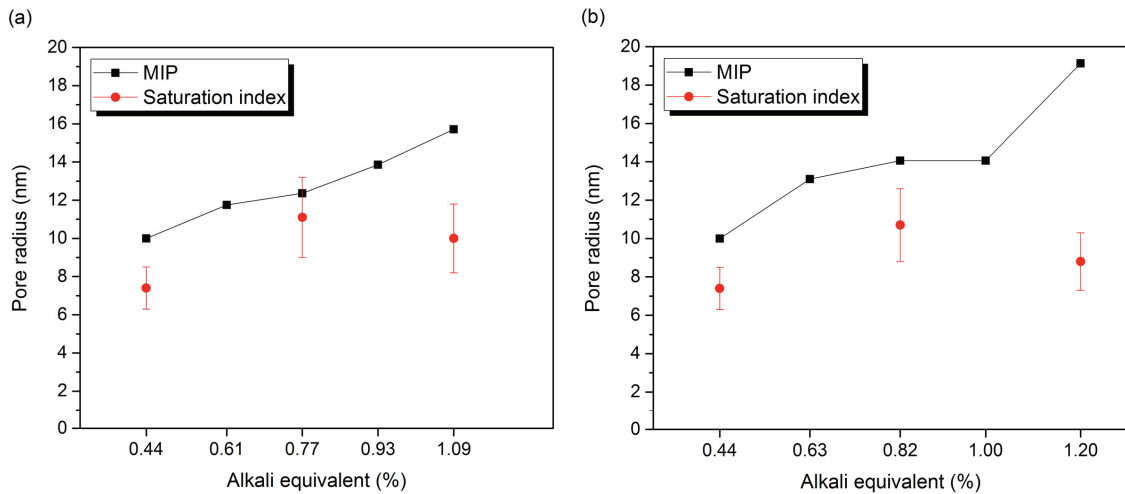


Figure 4.15 Comparison between the critical pore entry radius measured by MIP and the minimum pore radius for the growth of C-S-H calculated from saturation index at 28 days of LC³-65(2:1) with various alkali contents (a) KOH addition (b) NaOH addition

4.10 Summary

Changes in alkali equivalent (0.44%-1.20%) using KOH or NaOH additions impact the properties of LC³-65(2:1) as followed:

- The increase of alkalinity improves the compressive strength at early ages, especially at 1 day, but the excess of alkali reduces the strength from 7 days onwards.
- The optimal alkali content is 0.77% for KOH addition and 0.63% and NaOH addition without a reduction of the strength at later ages
- The increase of alkali significantly enhances the clinker hydration at 1 day but the clinker hydration decreases with the increase of the alkali content at later ages.
- Increasing alkalinity either KOH or NaOH addition does not affect the reaction of MK at 3 days but it does slightly affect at later ages.
- Alkali alters the saturation of the pore solution with respect to the growth of hydrates. So, the minimum critical pore size for growth is larger.
- Due to the lower amount of hydration products precipitation, the decrease of gel-space ratio for the high alkali conditions resulted in the lower compressive strength.

Chapter 5. Influence of calcination process on the reactivity of calcined clay and the properties of LC³

5.1	Introduction	59
5.2	Raw clays	60
5.3	Calcination and grinding process.....	61
5.4	Evaluation of quality of calcination.....	61
5.5	Calcined clay characterization.....	63
5.6	The reactivity of calcined clays	64
	5.6.1 Influence of kaolinite content	64
	5.6.2 Influence of particle size.....	65
	5.6.3 Influence of calcination process.....	65
5.7	Workability of LC ³	67
5.8	Activation energy of calcined clays	70
	5.8.1 Determination of activation energy of calcined clays.....	70
	5.8.2 Results of activation energy of calcined clays.....	73
5.9	Summary.....	76

5.1 Introduction

The abundant availability of clays in Thailand leads to a strong interest in LC³ from Siam Cement Group (SCG). To serve the increasing demand for calcined clay in the near future, SCG has been studying suitable ways to produce calcined clay on a commercial scale. Fortunately, it would be possible to adapt the existing cement plants slightly to calcine clays. In a feasibility study, a rotary kiln and a fluidized bed production techniques were compared. In 2016, SCG already achieved a pilot-scale production as shown in Figure 5.1. The maximum capacities of this pilot-scale production are 150 kg/hr using rotary kiln and 500 kg/hr with fluidized bed.

In order to study and understand the reactivity of calcined clay from the two different calcination processes with various calcined kaolinite contents and particle sizes, the R³ test was applied to obtain information about the reactivity of calcined clays. This was compared to the compressive strength of mortars. The influence of the calcination process on workability was also assessed. Then, an evaluation of the activation energy of calcined clays was made, to predict the chemico-mechanical developments of LC³ with temperature.



Figure 5.1 Pilot scale production for clay calcination (a) Rotary kiln (b) Fluidized bed

5.2 Raw clays

The clays used in this study come from the central part of Thailand and contain 45% and 50% of kaolinite determined using TGA as seen in Table 5.1. The chemical composition of raw clays is shown in Table 5.2 and the mineralogical composition evaluated using XRD shown in Table 5.3.

Table 5.1 Kaolinite and calcite content of raw clays by TGA

Name	Calcination process	Kaolinite(%)	Calcite(%)
RC-RK45	Rotary kiln	45.0	2.3
RC-FB45	Fluidized bed	45.9	4.1
RC-FB50	Fluidized bed	51.2	1.9

Table 5.2 The chemical composition of raw clays by XRF

(%)	RC-RK45	RC-FB45	RC-FB50
SiO ₂	45.6	43.2	35.8
Al ₂ O ₃	26.4	24.7	26.8
Fe ₂ O ₃	10.4	11.5	17.6
CaO	1.5	3.6	2.2
MgO	0.6	0.6	0.5
SO ₃	0.0	0.1	0.0
Na ₂ O	0.4	0.2	0.3
K ₂ O	1.0	0.4	0.1
TiO ₂	1.8	1.7	2.3
P ₂ O ₅	0.1	0.1	0.5
MnO	0.1	0.2	0.1
LOI	11.8	13.3	13.4

Table 5.3 The mineralogical composition of raw clays by XRD

Phase (%)	RC-RK45	RC-FB45	RC-FB50
Anatase	2.4	3.0	3.4
Calcite	1.1	3.8	2.0
Goethite	2.0	2.7	9.4
Hematite	1.1	1.7	2.4
Kaolinite	45.6	46.1	48.6
Quartz	1.3	3.0	1.0
Rutile	3.9	2.5	1.5
Amorphous	42.7	37.3	31.7

5.3 Calcination and grinding process

The sample preparation differed depending on the calcination processes. In case of the rotary kiln, clay with 45% kaolinite (RC-RK45) was crushed to get around 1-2 cm size pieces and then was calcined in the rotary kiln at 800°C soaked in burning zone for 15 minutes. For fluidized bed, clays with 45% (RC-FB45) and 50% kaolinite (RC-FB50) were ground to get a particle size of approximately 30 µm. Calcination was carried out at 750°C for 5 seconds. The raw materials are shown in Figure 5.2. After calcination for both processes, calcined clays were ground to get the particle size between 5 µm and 10 µm using a pilot scale ball mill equipped with separator for rotary kiln and a laboratory ball mill for fluidized bed.



Figure 5.2 Visual observation of the raw clays for (a) rotary kiln and (b) fluidized bed

5.4 Evaluation of quality of calcination

To investigate the calcination efficiency, XRD and TGA were used. Figure 5.3 shows the XRD results of raw clays (RC-RK45, RC-FB45, RC-FB50) and clays after calcining from the different processes (RK45, FB45, FB50). Complete calcination is achieved in both processes as seen by the absence of kaolinite peaks. The peak of goethite also disappears due to the dehydroxylation of goethite leading to the formation of hematite. TGA and DTG results are shown in Figure 5.4. After calcination, there is no mass loss corresponding to kaolinite dehydroxylation, from about 400°C to 600°C. This confirms the complete calcination already observed by XRD. TGA results also confirm the complete dehydroxylation of goethite and the partial decarbonation of calcite.

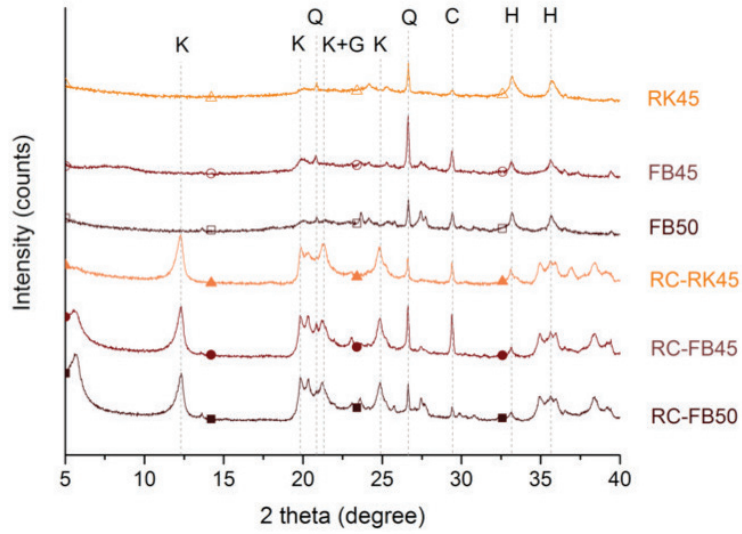


Figure 5.3 XRD of raw clays and calcined clays

K = Kaolinite, Q = Quartz, G = Goethite, C = Calcite, H = Hematite

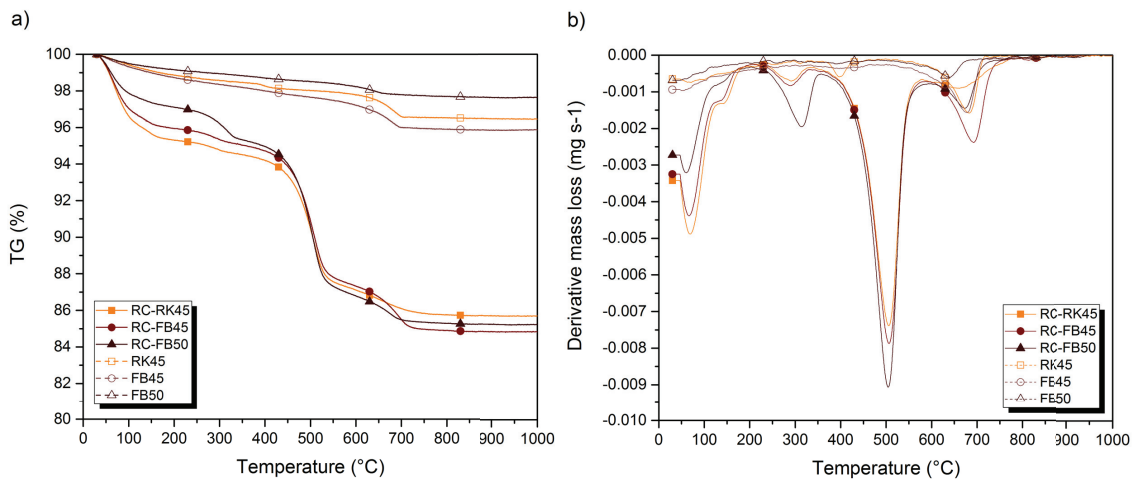


Figure 5.4 TGA (a) and DTG (b) curves of raw clays and calcined clays

5.5 Calcined clay characterization

The physical properties of calcined clays are summarized in Table 5.4. It shows that independent of the calcination process. There is no direct relation between the particle size and the surface area as the clay particles have considerable internal surface area due to the plate-like structure of the clay. Clay particles calcined from rotary kiln process show a coarser pore width, with a smaller surface area.

Table 5.4 The characterization of calcined clay particles

Name	Calcination process	Kaolinite content (%)	Particle size D(v,50) (μm)	BET (m^2/g)	Pore volume (cm^3/g)	Pore width (nm)
RK45	Rotary kiln	45	Crush	N/A	N/A	N/A
RK45-10 μm	Rotary kiln	45	10.1	24.8	0.13	22.4
FB45-30 μm	Fluidized bed	45	33.3	39.6	0.14	15.9
FB45-10 μm	Fluidized bed	45	9.3	29.4	0.12	17.9
FB50-30 μm	Fluidized bed	50	31.6	35.6	0.14	15.8
FB50-10 μm	Fluidized bed	50	7.5	32.3	0.12	15.8
FB50-5 μm	Fluidized bed	50	4.0	31.1	0.12	17.2

The SEM images of the raw clay with 45% kaolinite content and its morphology after calcination and grinding from both processes are shown in Figure 5.5. RC-FB45 (raw clay) and FB45-30 μm (after calcination using fluidized bed) show an angular shape of particles. Moreover, more rounded edges and more agglomerated particles are observed in FB45-10 μm compared with RK45-10 μm . The FB45-10 μm was ground using a laboratory ball mill that is not equipped with the separator. This uncontrolled grinding is likely to be responsible for the overgrinding of the clay, leading to the agglomeration of clay particles observed in Figure 5.5.

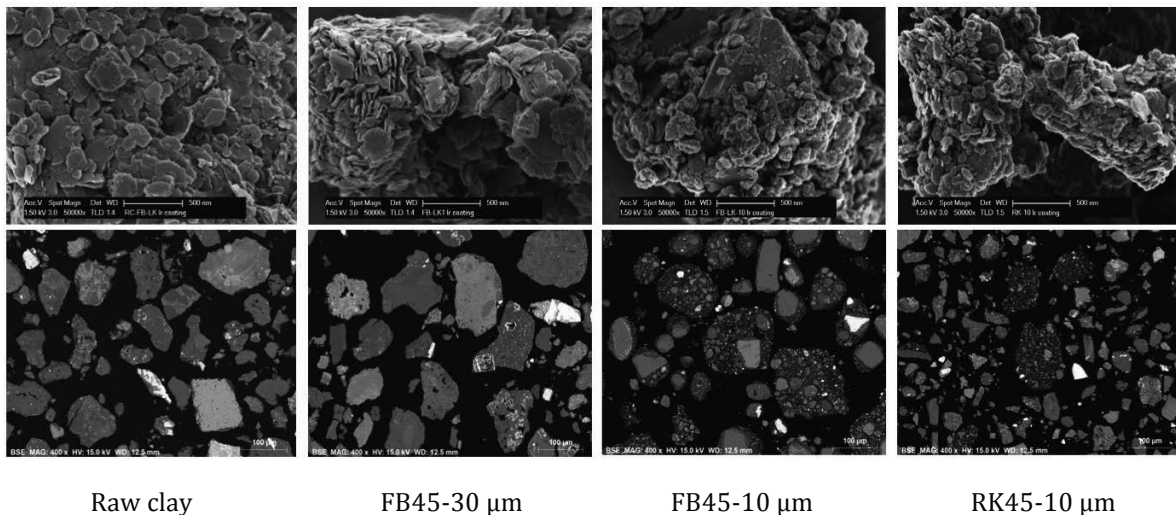


Figure 5.5 SEM images of raw clay with 45% kaolinite content and calcined clay taken by SEM-SE for morphology surface (top) and SEM-BSE for polishing surface (bottom)

5.6 The reactivity of calcined clays

This study focuses on evaluating how the kaolinite content, particle size, and calcination process influence the reactivity of calcined clays. To determine the reactivity of calcined clays, the R³ test was used [70]. The composition of material for the R³ test used in this study is shown in Table 5.5. The mechanical properties were then investigated to determine the influence of each parameter on the development of compressive strength of LC³ cement. From Chapter 3, it was shown that LC³-65(2:1) is the most promising mix design to implement in Thailand, so this system was investigated.

Table 5.5 Composition of materials for R³ test

Composition	(g)
Water	60.00
Calcined clay	11.11
Limestone	5.55
Ca(OH) ₂	33.33
K ₂ SO ₄	1.473
KOH	0.316
CH/SCM	3
water/binder	1.2

5.6.1 Influence of kaolinite content

Clays with 45% and 50% of kaolinite calcined by fluidized bed were used in this study. The reactivity determined by the R³ test of the calcined clays and the compressive strength result of LC³-65(2:1) is shown in Figure 5.6. The highest calcined kaolinite content shows the highest reactivity as indicated by the greater heat release for FB50-10 μm compared with FB45-10 μm. LC³-65(2:1) containing FB50-10 μm also gives the higher compressive strength and shows similar strength to the plain PC from 7 days onwards.

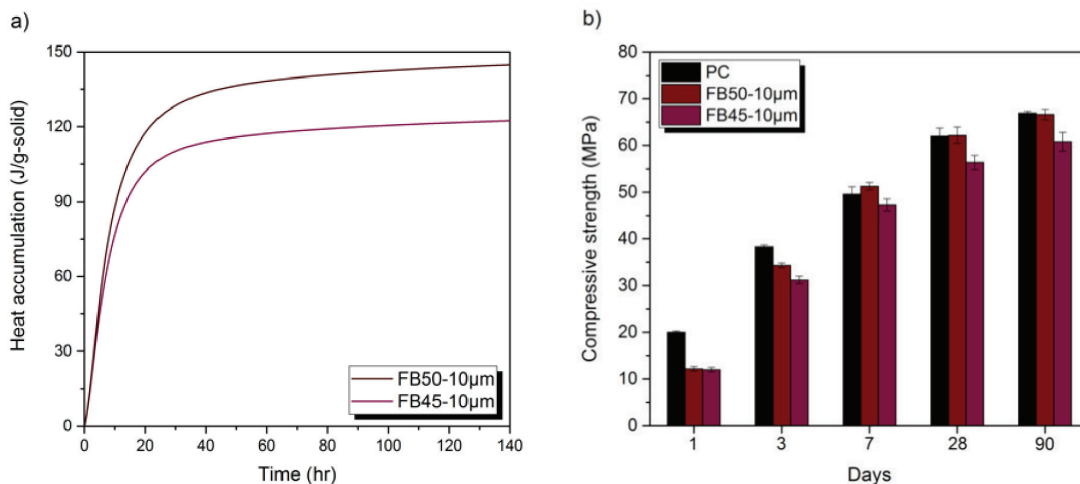


Figure 5.6 The R³ test (a) and compressive strength (b) of LC³-65(2:1) with different kaolinite content

5.6.2 Influence of particle size

The influence of the particle size was investigated. Particle sizes of approximately 30 μm , 10 μm and 5 μm were studied. Clay with 50% of kaolinite content and calcined by the fluidized bed were ground in order to reach the targeted size of particles. The influence of particle size on the reactivity of calcined clay characterized by the R³ test and compressive strength of LC³-65(2:1) is shown in Figure 5.7. FB50-30 μm shows the lowest reactivity and the lowest compressive strength. However, there is no significant difference in reactivity between FB50-10 μm and FB50-5 μm neither in the R³ test nor in the compressive strength measurements. Thus, it is not necessary to grind clay too fine in LC³, below 10 μm is sufficient.

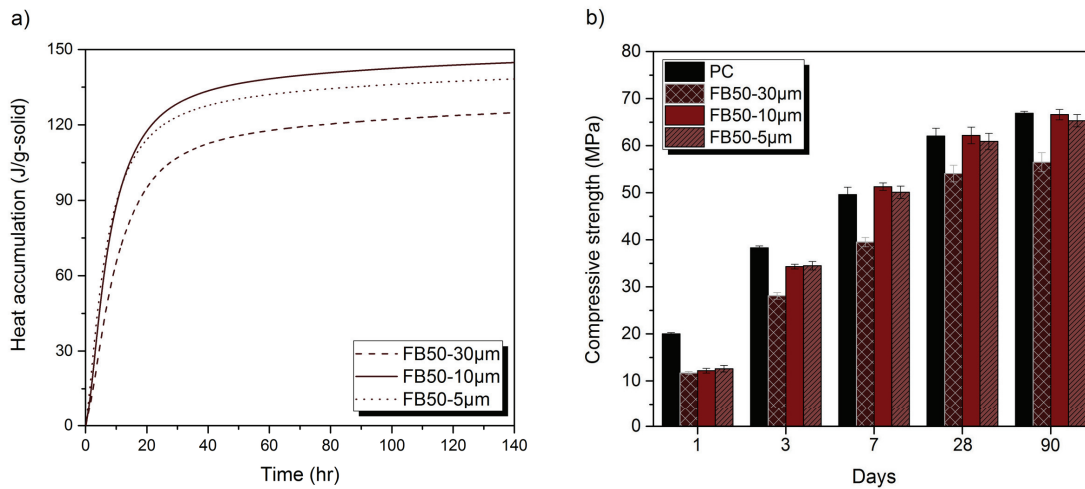


Figure 5.7 R³ test (a) and compressive strength of LC³-65(2:1) (b) with different size of calcined clay

5.6.3 Influence of calcination process

In this study, clay with 45% kaolinite content calcined using the rotary kiln and the fluidized bed was studied. The reactivity of the calcined clays and compressive strength of LC³-65(2:1) are shown in Figure 5.8. The raw clay (RC-FB45) shows some reactivity compared to sand that is been widely considered as an inert material. The reactivity of the raw clay cannot be explained by the crystalline phases identified by XRD. Thus, it is expected that some amorphous components of the clay are responsible for the reactivity. The reactivity of calcined clays is promoted significantly after calcination as seen from the higher heat release of calcined clays compared with the raw clay. Moreover, FB45-10 μm reacts faster as observed by the R³ test but there is no significant difference in terms of compressive strength of LC³-65(2:1) at any age. This slightly reactivity difference could be explained by the higher surface area for FB45-10 μm compared with RK45-10 μm as seen in Table 5.4.

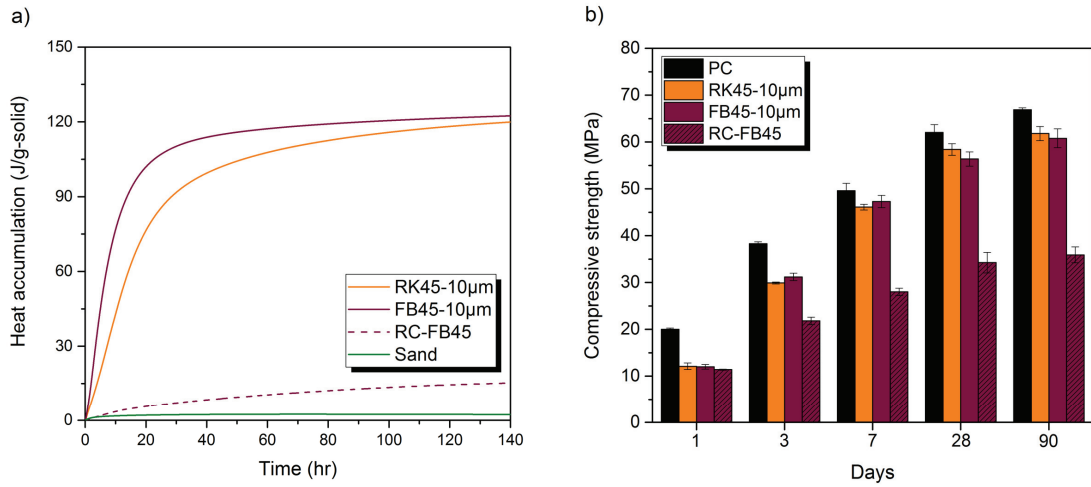


Figure 5.8 R³ test (a) and compressive strength of LC³-65(2:1) (b) with different calcination process

The correlation of the heat release by R³ test at 24 hr to the compressive strength of mortar of all calcined clays used in this study is shown in Figure 5.9. The higher the heat, the higher the strength. Thus, R³ test is reliable to determine the reactivity of calcined clays.

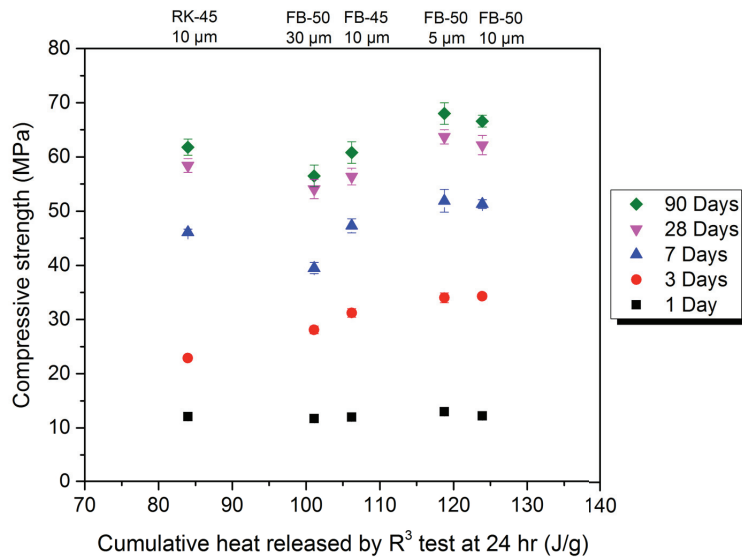


Figure 5.9 The correlation between heat release by R³ test at 24 hr and the compressive strength of LC³-65(2:1) of all calcined clays used in this study

5.7 Workability of LC³

The workability of LC³-65(2:1) containing various calcined clays was tested and compared to PC. It was characterized on mortar and paste. The mortar was cast following EN 197-1 with fixing a water to binder ratio at 0.5 without any superplasticizer. The flow test was carried out following ASTM C1437 – 15. The diameter of the mortar flow was measured after tapping 25 times in 15 seconds on a flow table.

The workability of the pastes was evaluated using the mini-slump cone test developed by Construction Technology Laboratories (CTL), Inc. The paste was mixed with a high speed mixer (1,600 rpm) for 2 min using a water to binder ratio at 0.4 and a polycarboxylate superplasticizer (Mapei, SP490) was added at 0 wt%, 0.25 wt%, and 0.5 wt% of binder. The fresh paste was immediately poured into the mini cone (H = 5.7 cm, ϕ_{top} = 2 cm, ϕ_{bottom} = 3.8 cm) after mixing and then gently lifting the cone to prevent inertial effects. The diameter of the spread was measured to evaluate the workability of paste samples.

The results of the mortar are shown in Figure 5.10. The flow of the PC is about 19.5 cm and the flows of all LC³ are in the range of 17.1-18.5 cm which is close to the value of the PC. This result is very promising for LC³, showing that despite using water-adsorbing calcined clays, similar workability to PC is reached, without the use of superplasticizer. The impact of calcined clays obtained from the different process cannot be seen clearly in the case of mortar.

However, some influence of calcination process on the workability can be observed on the paste samples as seen in Figure 5.11. The results reflect the amount of superplasticizer required for improving the workability of the paste. Obviously, the workability of PC is more sensitive to the addition of superplasticizer over LC³-65(2:1). For LC³ blended using calcined clay from the fluidized bed (FB), the need of superplasticizer to improve the workability of LC³ is independent on the kaolinite content (45%-50%) and the particle size of calcined clay (30 μ m, 10 μ m, 5 μ m) as seen in Figure 5.11(a) and Figure 5.11(b) but it depends on the calcination process as seen in Figure 5.11(c). Using calcined clay from different calcination process leads to a difference in the spread of LC³ paste. The fluidized bed calcined clay shows a higher spread compared to the rotary kiln when superplasticizer was added.

It is interesting that calcined clay from fluidized bed process containing a higher surface area, as given in Table 5.4, shows a better workability than that from the rotary kiln. Thus, it seems that there is no obvious impact of the surface area of clay particles in the range used in this study on the superplasticizer requirement to improve the workability of LC³.

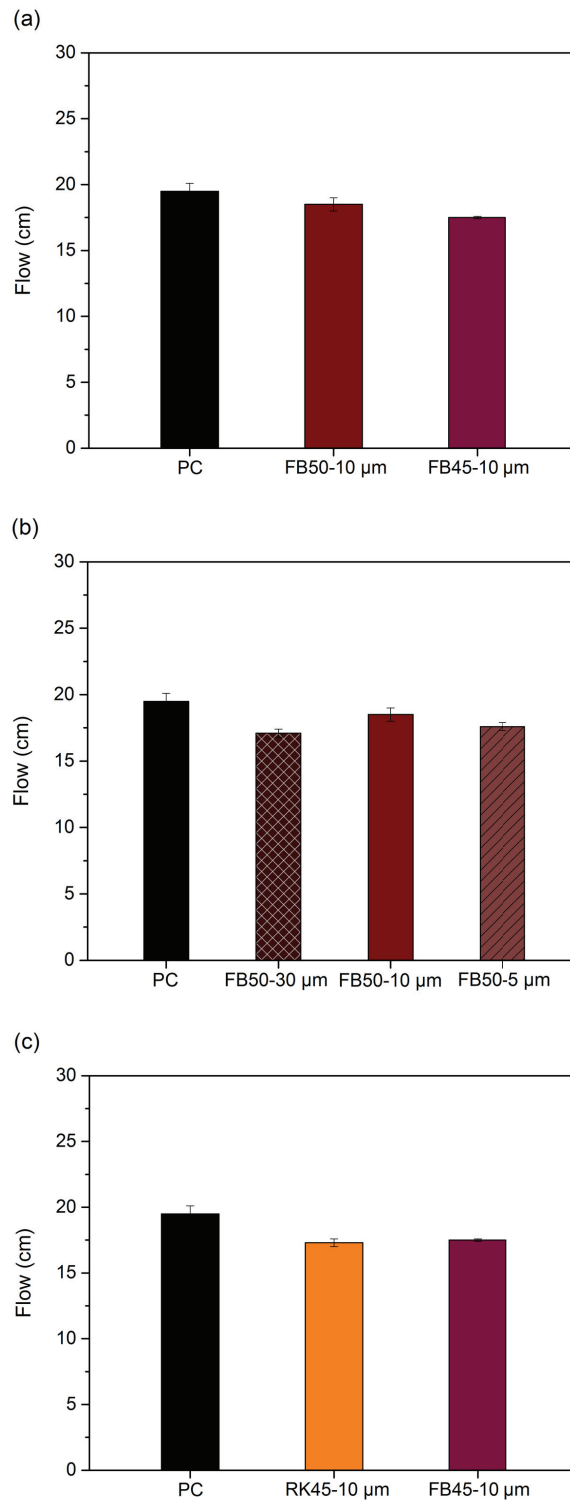


Figure 5.10 Flows of the mortar of PC and LC³-65(2:1) with the different condition of calcined clays (a) kaolinite content (b) particle size, and (c) calcination process

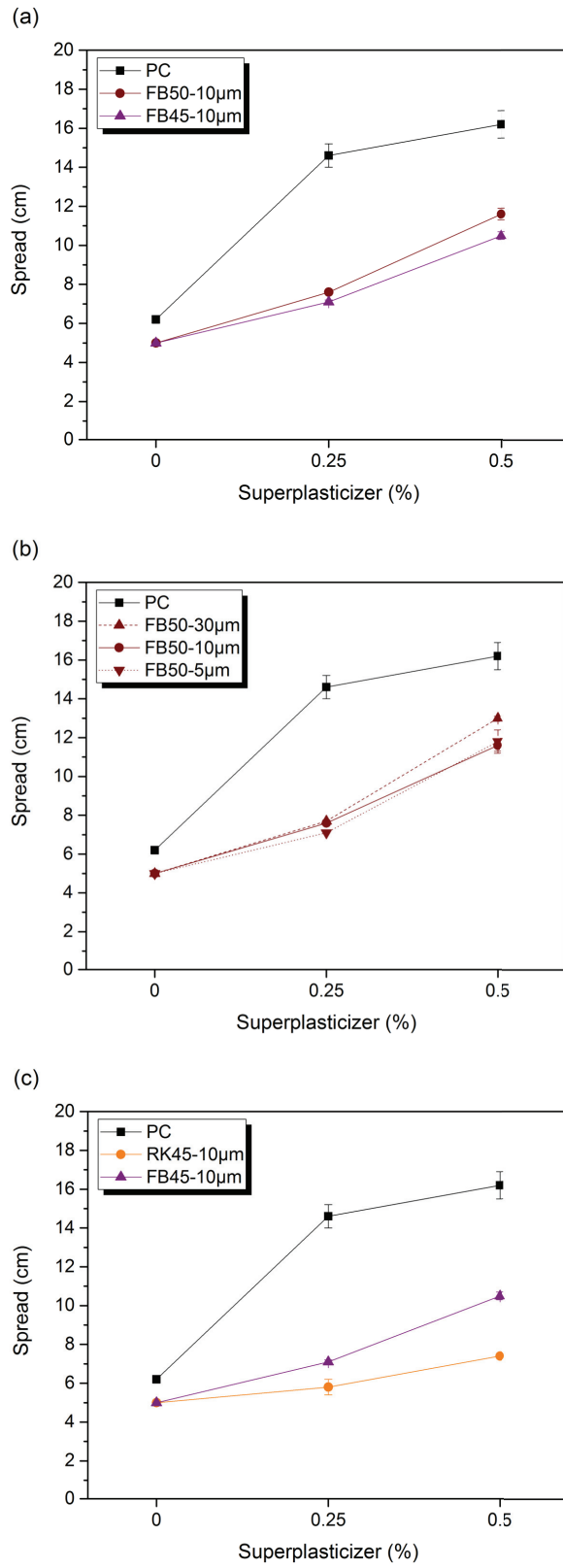


Figure 5.11 Spreads of PC and LC³-65(2:1) with the different condition of calcined clays (a) kaolinite content (b) particle size, and (c) calcination process

5.8 Activation energy of calcined clays

Cement hydration is temperature dependent and the activation energy indicated how sensitive hydration is to temperature. As described in Chapter 3, using calcined clay to produce Limestone Calcined Clay Cement (LC³) is becoming more attractive to decrease the carbon footprint of the cement industry. Thanks to the synergic effect between calcined clay and limestone, clinker is usually replaced up to 30% and can go up to 45% of replacements while the properties of LC³ are comparable or better than PC. This study is examining how sensitive of calcined clay is to temperature. As a first step, the R³ test developed by Avet et al. [70], which was designed to obtain information about the reactivity of calcined clays, was applied to evaluate the activation energy of calcined clays.

5.8.1 Determination of activation energy of calcined clays

To define the sensitivity of hydration reaction to the temperature, the Arrhenius theory was applied. The activation energy is the minimum energy needed for a chemical reaction to start. As seen in Equation 5.1, a higher activation energy means that the reaction rates are more sensitive to changing temperature.

$$k = A \times e^{\frac{-E_a}{RT}} \quad \text{Equation 5.1}$$

where k is the rate of heat evolution (W), A is a constant same unit as k , E_a is the activation energy (J/mol), R is the natural gas constant (8.314 J/mol/K) and T is the temperature in K at which reaction occurs.

In this work, the data from isothermal calorimeter was collected at three different temperatures: 20°C, 30°C, and 40°C for 28 days. The rate of heat evolution of calcined clays obtained from the R³ test. Three calcined clays were used to investigate the activation energy, one clay from the rotary kiln and two clays from the fluidized bed process. The composition of the R³ test and the list of calcined clays are given in Table 5.6.

Table 5.6 The composition of R³ test and the list of investigated calcined clays

Composition	(g)	Calcined clays
Water	60.00	RK45-10 μm
Calcined clay	12.50	FB45-10 μm
Ca(OH) ₂	37.50	FB50-10 μm
K ₂ SO ₄	1.473	
KOH	0.316	
CH/SCM	3	
water/binder	1.2	

There are several methods to determine the activation energy as described in [77, 78], in this study two methods were used for calculating the activation energy of calcined clays including the superposition method and the rate method.

The superposition method

This method uses the concept of an equivalent time to fit the curves of the heat accumulation obtained from the R³ test at different temperatures as seen in Figure 5.12. This method is modified from ASTM C1074-04, by using the isothermal calorimetry data instead of the compressive strength data. Because the calorimetry provides the continuous measurement and is more reliable to measure the rate of chemical reaction compared to strength [79].

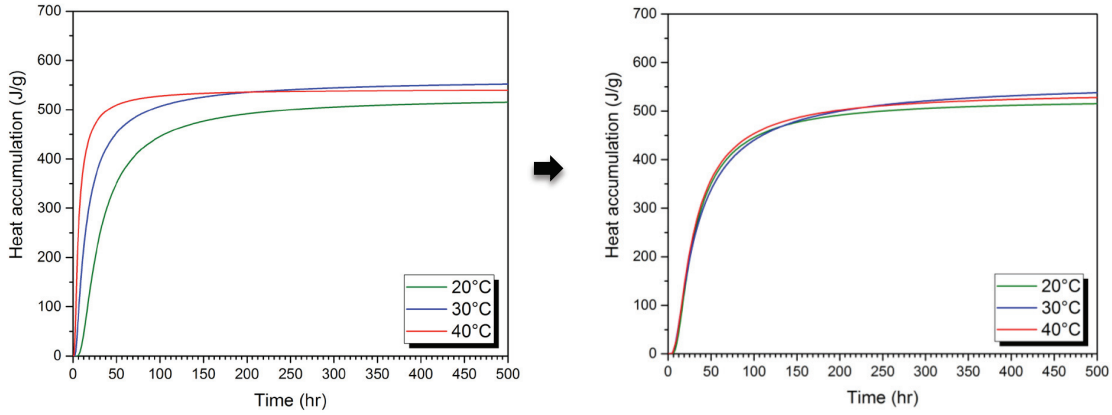


Figure 5.12 Fitting three heat accumulative curves for the superposition method

The equation to compute the equivalent time is given in Equation 5.2. The exponential function used for fitting the heat accumulation curve is Equation 5.3 [77, 79, 80].

$$t_e = \sum_0^t e^{\left[\frac{-E_a}{R} \left(\frac{1}{T} - \frac{1}{T_r}\right)\right]} \Delta t \quad \text{Equation 5.2}$$

where t_e refers to the equivalent time (hr or day) at a reference temperature (T_r), T and Δt are the testing temperature (K) and time interval (hr), E_a and R are defined previously

$$H(t_e) = H_u \times e^{-[\tau/t_e]^\beta} \quad \text{Equation 5.3}$$

where $H(t_e)$ equals the heat accumulation at the equivalent time (J/g), H_u is the ultimate heat evolved (J/g), τ is the reaction (hydration) time parameter (hr or day), β is the reaction (hydration) shape parameter

To determine the E_a , the data from the isothermal calorimeter was collected at 20°C, 30°C, and 40°C. Fitting the accumulative heat curve using Equation 5.3 to solve H_u , τ , and β was performed at each temperature using MATLAB software. Only τ was assumed to be a temperature dependent parameter [81], thus, H_u and β were presumed independent of the given temperature. The average value from three temperatures of H_u and β were used to calculate τ for each temperature. The E_a was calculated by plotting $\ln k(\tau)$ versus $1/T$ and the data were fit to Equation 5.4 using a least squares fit as seen in Figure 5.13.

$$E_a = -\frac{\ln(\tau_r/\tau)}{\left(\frac{1}{T_r} - \frac{1}{T}\right)} \times R \quad \text{Equation 5.4}$$

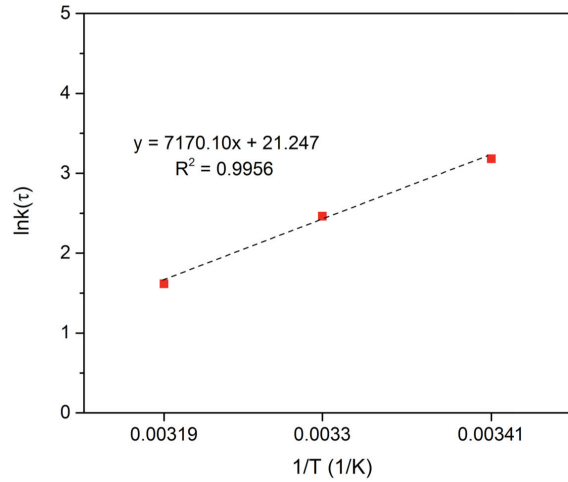


Figure 5.13 Detemination of E_a from the plot of $\ln k(\tau)$ versus $1/T$ for the superposition method

The rate method

This method considers the data from the heat flow and then it was integrated to get the total heat of evolution. The determination of the reaction rate for two different testing temperatures is given in Equation 5.5. At the same heat of evolution value, the activation energy for the two temperatures can be calculated as shown in Equation 5.6.

$$\left(\frac{dH}{dt}\right)_{T_1} = k(T_1)f(H)$$

$$\left(\frac{dH}{dt}\right)_{T_2} = k(T_2)f(H) \quad \text{Equation 5.5}$$

where $f(H)$ refers to a function depending on the degree of reaction

$$E_a(H) = R \left[\frac{T_1 \cdot T_2}{T_1 - T_2} \ln \left(\frac{\frac{dH_1}{dt}}{\frac{dH_2}{dt}} \right) \right] \quad \text{Equation 5.6}$$

5.8.2 Results of activation energy of calcined clays

The superposition method

The isothermal calorimetry curves of each calcined clay before and after fitting are shown in Figure 5.14. FB50-10 μm has a slightly higher heat compared to the other two calcined clays due to the higher calcined kaolinite content. According to Equation 5.3 and Equation 5.4, the parameters for fitting these curves and the activation energy of calcined clays are given in Table 5.7. It shows that the activation energies of three calcined clays calculated using the superposition method are similar. The values are between 58 kJ/mol and 63 kJ/mol which are in the range of the deviation calculated from each pair of temperature (20-30°C, 30-40°C, and 20-40°C).

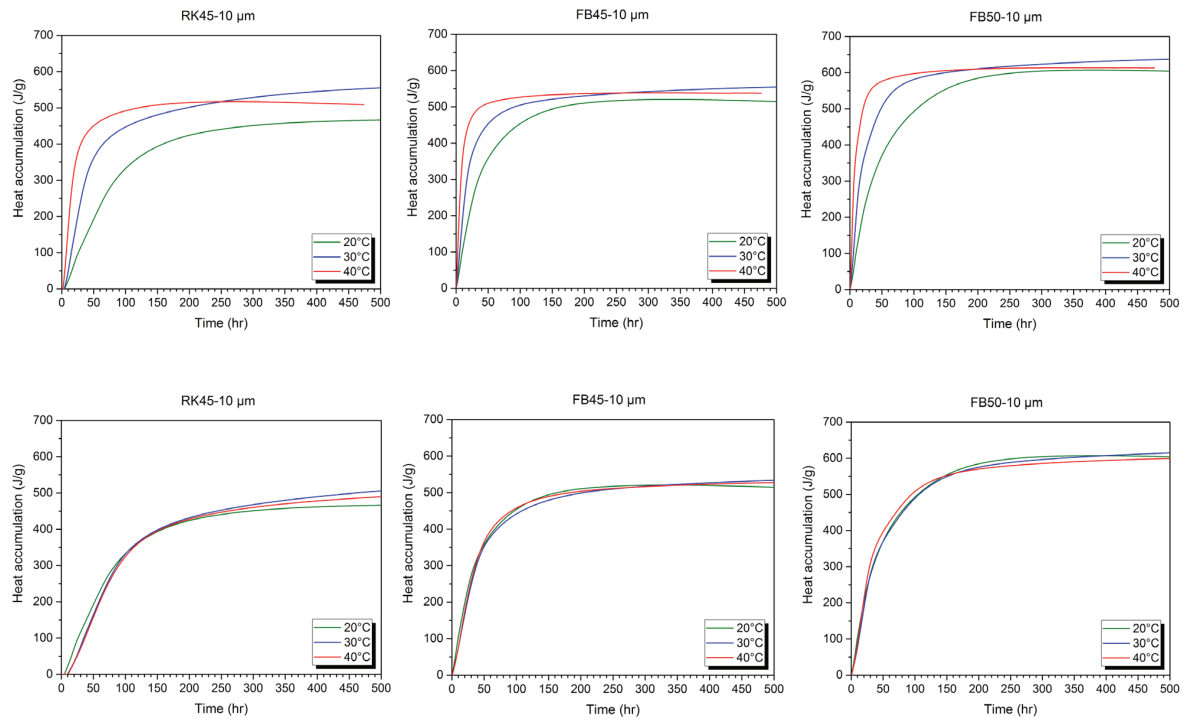


Figure 5.14 Heat accumulative curve of R³ test for the superposition method, before curve fitting (top) and after curve fitting (bottom)

Table 5.7 The parameters for curve fitting and evaluated E_a using the superposition method

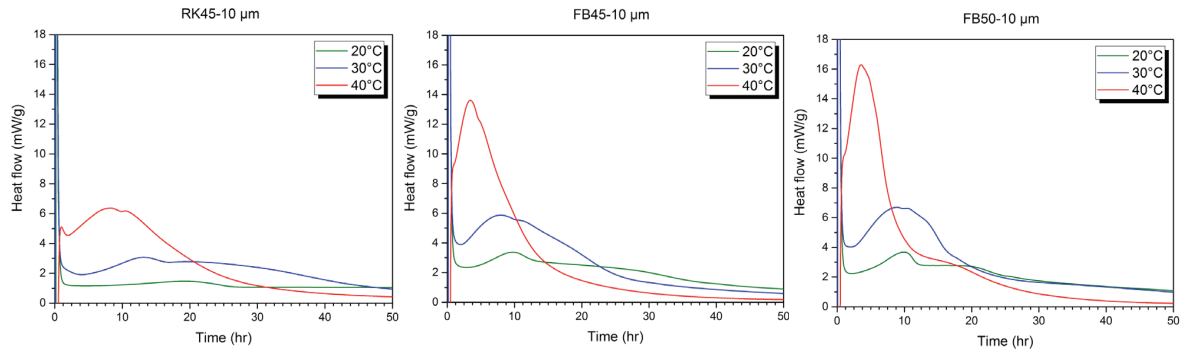
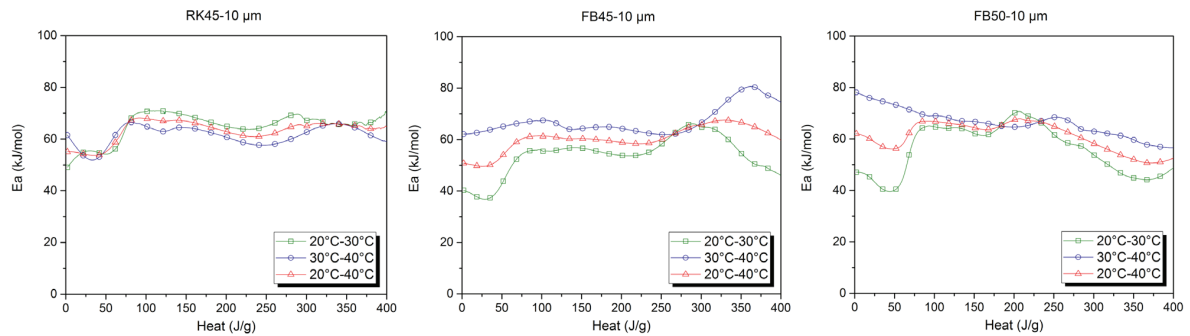
Sample	H_u (J/g)	β	τ			E_a (kJ/mol)
			20°C	30°C	40°C	
RK45-10 μm	532.7	1.14	55.9 (R ² =0.95)	21.0 (R ² =0.95)	10.8 (R ² =0.99)	63.0 \pm 9.9 (R ² =0.99)
FB45-10 μm	546.4	1.09	21.5 (R ² =0.96)	10.0 (R ² =0.98)	4.5 (R ² =0.99)	59.6 \pm 6.9 (R ² =0.99)
FB50-10 μm	633.6	1.09	26.6 (R ² =0.98)	12.6 (R ² =0.99)	5.8 (R ² =0.97)	58.0 \pm 3.6 (R ² =0.99)

*R² (τ) of least squares best-fit line of three parameters exponential model vs measured heat flow

**R² (E_a) of least squares best-fit line of $\ln(\tau)$ vs $1/T$

The rate method

The heat flow curves are shown in Figure 5.15 and Equation 5.6 was applied to determine the sensitivity to the temperature of calcined clays. The plots of E_a as a function of the heat released are presented in Figure 5.16 and the average of E_a for each pair of temperature over the range of the constant heat value (100-300 J/g) are illustrated in Table 5.8.

Figure 5.15 Heat flow curve of R³ test for the rate methodFigure 5.16 The E_a of calcined clays plotted as a function of heat releases for the rate methodTable 5.8 The E_a results using the rate method over the heat releases of 100 – 300 J/g

Calcined clays	The average E_a (kJ/mol)		
	20°C – 30°C	30°C – 40°C	20°C – 40°C
RK45-10 μ m	67.4 \pm 2.5	61.2 \pm 2.4	64.4 \pm 2.3
FB45-10 μ m	57.4 \pm 3.8	64.1 \pm 1.5	60.6 \pm 2.0
FB50-10 μ m	63.3 \pm 4.1	66.3 \pm 1.6	64.6 \pm 2.3

The variations of the E_a value at the beginning of the reaction ($H < 100$ J/g) and also at the long term of the reaction ($H > 300$ J/g) can be explained that the reactions during those periods are not governed by chemical reactions (it can be a diffusion process as mentioned in [78, 82]) resulted in the different in the sensitivity to the temperature. Therefore, the Arrhenius equation cannot be used in these cases.

Comparison of the activation energy of calcined clay from the different methods

The determination of the sensitivity to the temperature of calcined clays from different calcination processes using the superposition method and the rate method is shown in Figure 5.17. The E_a values obtained from the superposition method and the rate method show no significant difference in E_a between the two different calcination processes. Thus, the physical properties of calcined clay do not play any role in E_a , i.e. the sensitivity to temperature. This is in agreement with the results [79], showing that the main factor influencing the sensitivity to temperature of calcined clay reaction is the chemical composition of the calcined clay. In this study, the same clay was used but using different calcination process. Moreover, the variation of kaolinite content in the range of 45-50% is too low to impact the E_a .

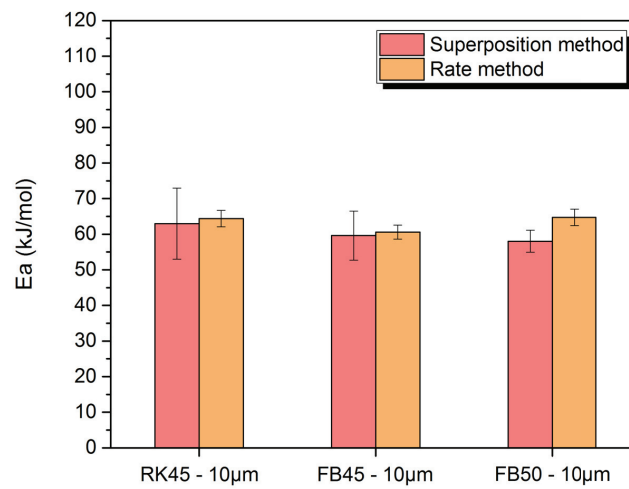


Figure 5.17 The comparison of E_a using the different methods

In addition, the investigation of the effect of calcined clays on the temperature sensitivity of LC³ systems is shown in Appendix G. It was found that the apparent activation energy of all LC³ blended cements calculated using the superposition method is about 40-45 kJ/mol, which is similar to the value of reference PC.

5.9 Summary

- Complete calcination was observed using either a rotary kiln or a fluidized bed. Kaolinite was not detected in calcined clays, shown by XRD and TGA.
- Calcined clay obtained from the rotary kiln process shows a coarser pore width, accordingly, a lower surface area is measured compared to the clay calcined by the fluidized bed.
- Due to a higher surface area of calcined clay from fluidized bed calcination, the faster reaction of calcined clay is observed by the R³ test but there is no significant difference in terms of compressive strength of LC³-65(2:1).
- For the reactivity of calcined clays, a higher calcined kaolinite content shows higher reactivity. Moreover, it is not necessary to over-grind calcined clay. There is no increase of reactivity for calcined clay finer than 10 μm.
- The activation energy of calcined clays from different calcination processes determined using the superposition method and the rate method is similar, about 58 – 65 kJ/mol. The variation of kaolinite content (45-50%) does not impact the E_a either.

Chapter 6. Durability properites of LC³

6.1	Introduction	77
6.2	Carbonation	78
6.3	Chloride ingress.....	82
6.3.1	Migration testing	82
6.3.2	Ponding testing.....	83
6.4	Alkali silicate reaction (ASR)	86
6.5	Summary.....	88

6.1 Introduction

Once the optimization of the mix design was completed, and the rheology and mechanical properties assessed, the durability properties were then characterized. Carbonation, chloride ingress and alkali silica reaction were considered in this study. Thus, the aim of this study is to investigate the durability properties of LC³ in order to clarify the robustness properties of LC³. The durability properties and the systems used of each study are shown in Figure 6.1.

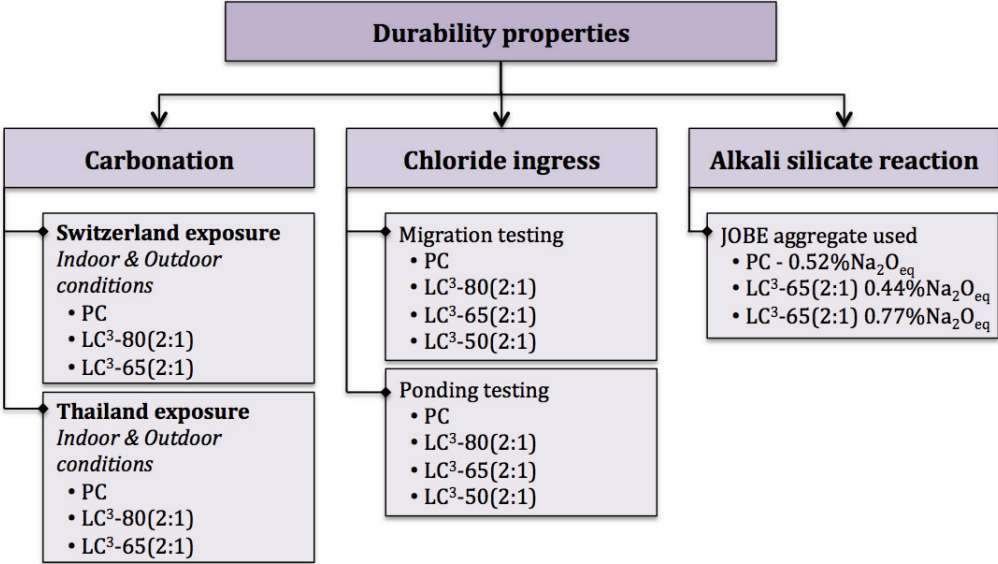


Figure 6.1 The diagram showing the durability properties investigated in this study

6.2 Carbonation

Carbonation occurs due to the attack of carbon dioxide (CO₂) with the calcium hydroxide (CH) or hydrated silicates (C-S-H) in the cement paste to form CaCO₃. As a result of the lower amount of CH in blended cements compared to the normal PC, in most cases SCM blended cements have the lower carbonation resistance [83] due to their lower amount of carbonatable phases. Carbonation lowers the pH of pore solution, which is harmful to the protective passivation layer of reinforced steel bars in concrete and results in the corrosion. The carbonation rate depends on the relative humidity (RH) of the environment as shown in Figure 6.2. The carbonation process needs sufficient moisture to dissolve CO₂ to form H₂CO₃. In case RH < 50%, CO₂ cannot dissolve due to the lack of water. On the contrary at RH > 80%, CO₂ enters the pore network slowly due to water filling. In both cases, carbonation rates are much reduced [84].

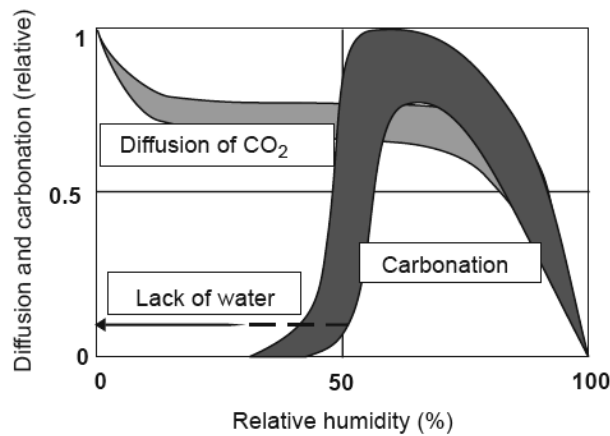


Figure 6.2 The relative rate of carbonation as a function of the relative humidity of environment [84]

The results of natural carbonation for 6 months, 1 year and 2 years for PC, LC³-80(2:1), and LC³-65(2:1) mortar samples exposed to both indoor and outdoor conditions in Switzerland and Thailand are presented from Figure 6.3 to Figure 6.5. For all exposure times, LC³ systems have a lower resistance to carbonation compared to PC both under Switzerland and Thailand conditions. Moreover, a slightly higher carbonation depth can be observed on the samples exposed in Thailand. It is related to the higher relative humidity and the higher CO₂ concentration in Thailand, which can promote the carbonation reaction. However, a proper curing time can significantly improve the carbonation resistance of LC³ blended cements.

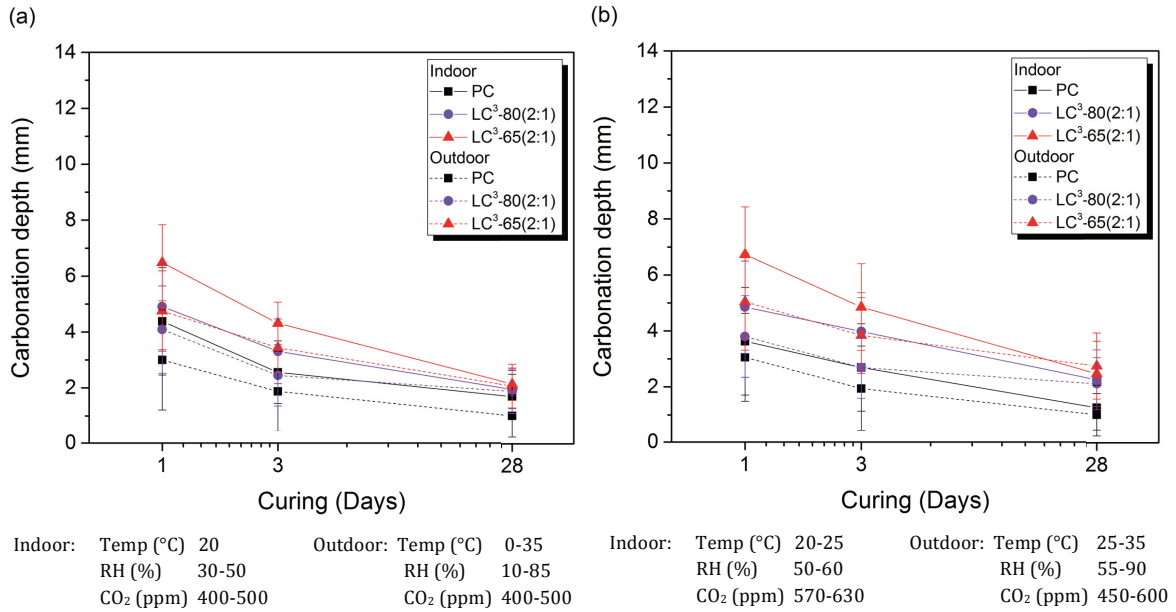


Figure 6.3 Carbonation depth of PC, LC³-80(2:1), and LC³-65(2:1) for 6 months of exposure both indoor and outdoor conditions in (a) Switzerland and (b) Thailand

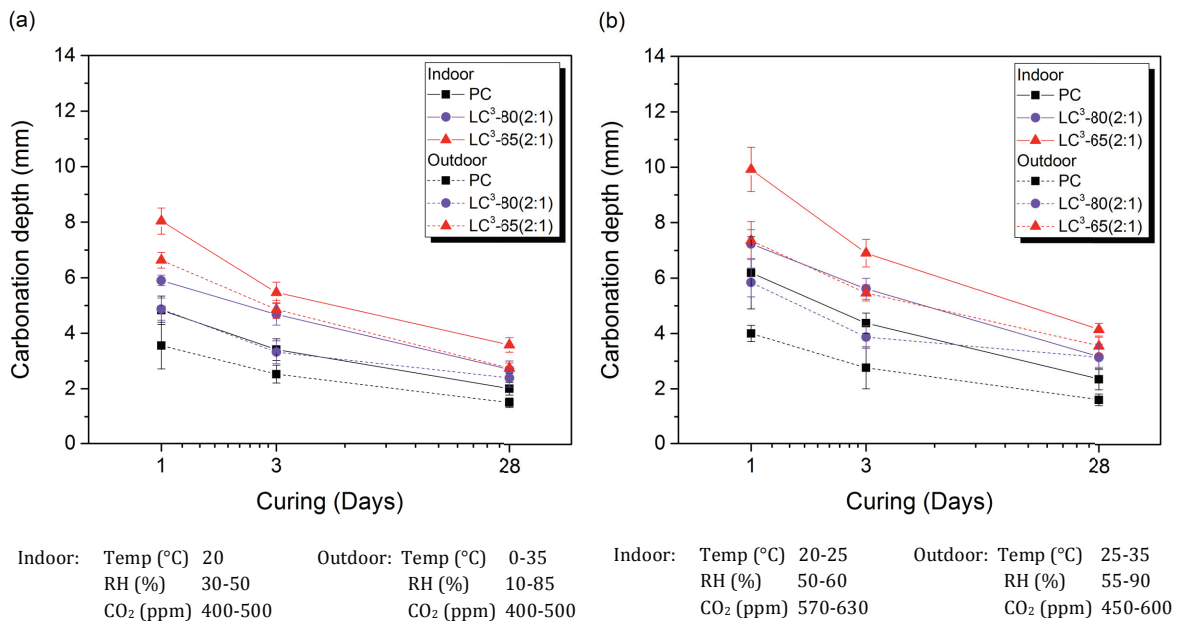


Figure 6.4 Carbonation depth of PC, LC³-80(2:1), and LC³-65(2:1) for 1 year of exposure both indoor and outdoor conditions in (a) Switzerland and (b) Thailand

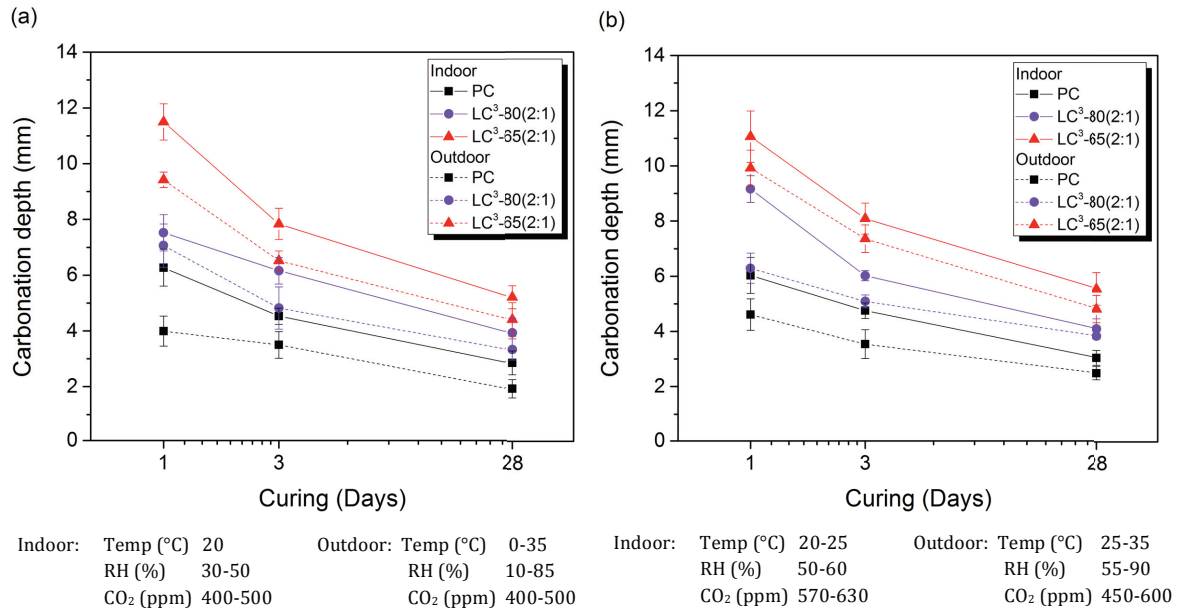


Figure 6.5 Carbonation depth of PC, LC³-80(2:1), and LC³-65(2:1) for 2 years of exposure both indoor and outdoor conditions in (a) Switzerland and (b) Thailand

The carbonation depths of all systems curing for 28 days before exposure plotted as a function of square root of time are shown in Figure 6.6. It is clearly seen that the carbonation depths of all mortars are lower than 6 mm after 2 years of exposure. PC shows the smallest carbonation depth followed by LC³-80(2:1) and LC³-65(2:1). A higher carbonation depth is found in indoor exposure condition. The carbonation coefficient determined from the slope of the linear regression between carbonation depth and exposure time are summarized in Table 6.1.

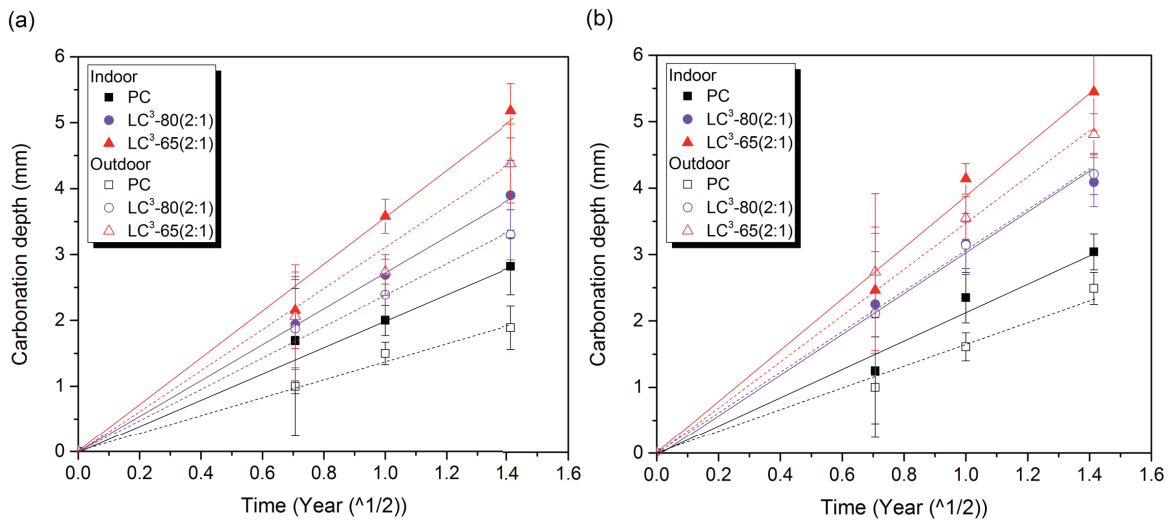


Figure 6.6 Carbonation depth plotted as a function of square root of time for samples cured for 28 days before exposure both indoor and outdoor conditions in (a) Switzerland and (b) Thailand

Table 6.1 Carbonation coefficient of PC, LC³-80(2:1) and LC³-65(2:1)

Samples	Carbonation coefficient (mm/year ^{1/2})	
	Indoor	Outdoor
<i>Switzerland exposure</i>		
PC	2.05	1.38
LC ³ -80(2:1)	2.74	3.78
LC ³ -65(2:1)	3.55	2.97
<i>Thailand exposure</i>		
PC	2.15	1.67
LC ³ -80(2:1)	3.01	3.02
LC ³ -65(2:1)	3.92	3.51

The coefficients of carbonation are in the range of 1.38-2.97 mm/year^{1/2} for Switzerland exposure condition and 1.67-3.92 mm/year^{1/2} for Thailand exposure condition. Higher carbonation rate is found in Thailand exposure condition. It is because of a higher relative humidity in Thailand.

Although LC³ systems show the higher rate of carbonation compared to PC, it is similar to the other blended cements and is below the limit of design working life of 100 years for moderate humidity (XC3) exposure class as seen in Figure 6.7.

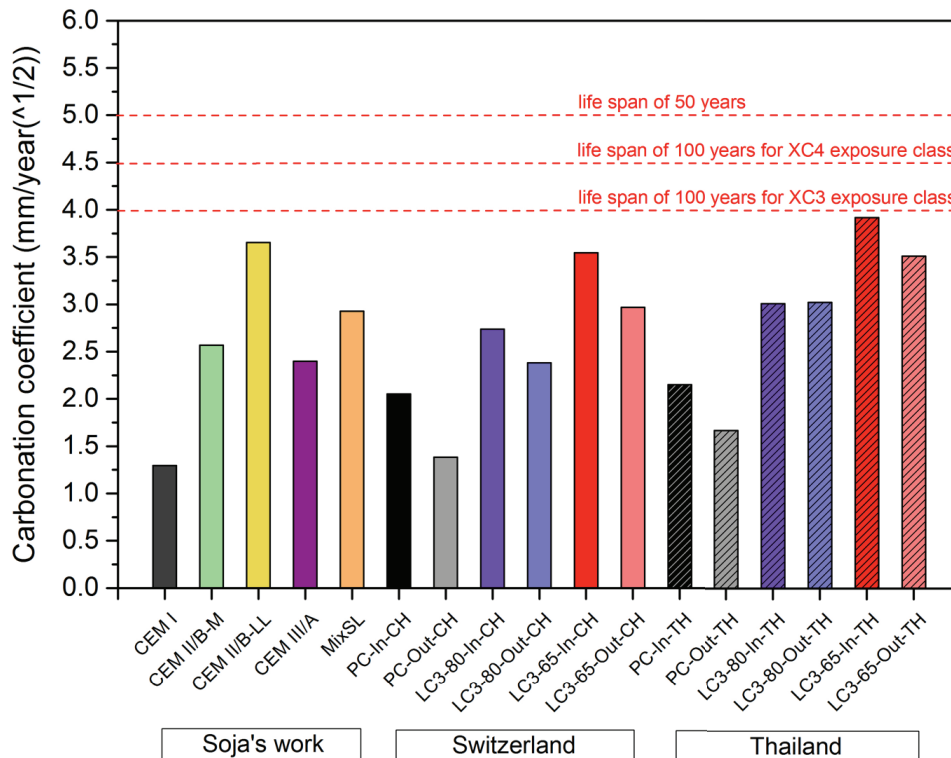


Figure 6.7 Carbonation coefficient of natural carbonation tested on mortars cured for 28 days before exposure

MixSL corresponding to a blended cement containing 50% of clinker and 50% of the mix of burn oil shell and limestone
 In-CH = Indoor in Switzerland, Out-CH = Outdoor in Switzerland, In-TH = Indoor in Thailand, Out-TH = Outdoor in Thailand

6.3 Chloride ingress

Due to the high alkalinity of the concrete ($\text{pH} > 12$), a protective oxide layer is formed on the surface of the steel used as reinforcement in concrete. The intrusion of chloride ions into reinforced concrete can induce steel corrosion. When oxygen and moisture are available, chloride ions (Cl^-) can penetrate through concrete and attack the iron oxide film leading to corrosion. As long as the protective layer is still present, the steel remains in a non-corroding state. Once chloride ions reach the steel, they will break down the passivating layer and the process of corrosion begins. The rust formed can take up to 5-10X more volume than the original steel leading to cracking, spalling, and delamination of the concrete. The risk of corrosion increases as the chloride content of concrete increases. The primary rate-controlling factors are the availability of oxygen, the electrical resistivity and relative humidity of the concrete, and the pH and temperature [85].

6.3.1 Migration testing

Figure 6.8 shows the result of chloride migration test of PC and LC³ systems. The detected current relates to the ionic migration through the hardened sample. Table 6.2 shows the concentrations of ions in the pore solution of all samples cured for 28 days before testing. The higher the levels of substitution, the lower the ions concentration in pore solution. Moreover, the porosity refinement of LC³ as seen in Figure 6.9 reduces ion mobility. These result in a lower current detected of LC³, especially at a higher substitution. The lower current also reflects the fewer chloride ions passed through [86]. The increase of substitution levels strongly decreases the current.

Table 6.2 The ions concentration in the pore solution of PC and LC³ systems cured at 20°C for 28 days before exposure

Samples	Ions concentration (mmol/l)		
	Na ⁺	K ⁺	OH ⁻
PC	105.6	227.1	227.8
LC ³ -80(2:1)	80.8	133.5	188.9
LC ³ -65(2:1)	38.9	63.5	95.6
LC ³ -50(2:1)	20.1	38.4	58.2

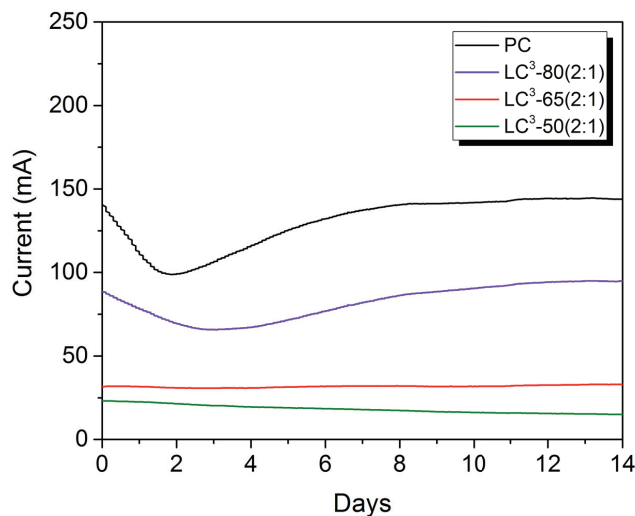


Figure 6.8 Chloride migration test results of PC and LC³ systems (applied voltage = 20V)

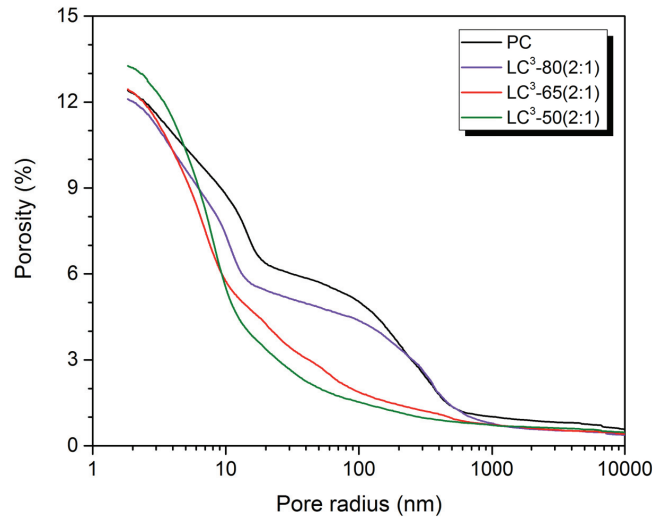


Figure 6.9 MIP results of PC and LC³ systems mortars cured at 20°C for 28 days before testing

6.3.2 Ponding testing

The chloride penetration profiles of the samples ponded in 3% NaCl solution after 6 months and 1 year of exposure are shown in Figure 6.10. The penetration depth decreases with increasing the level of SCMs substitution thanks to the porosity refinement in LC³ systems. LC³-50(2:1) shows the best resistance to chloride penetration. The chloride penetration depth for this system is less than 10 mm after ponding for 1 year. The chloride content at the surface of LC³-80(2:1) and LC³-65(2:1) is higher than that of PC and LC³-50(2:1). This indicates a higher binding capacity [87] for these two blends, which could be correlated with the higher formation of carboaluminate hydrates [88], as seen in Figure 6.11. However, the surface concentration is lower for the LC³-50(2:1) system, clearly demonstrating the porosity refinement is of greater importance with respect to the impact of limestone and calcined clay on the transport of ions.

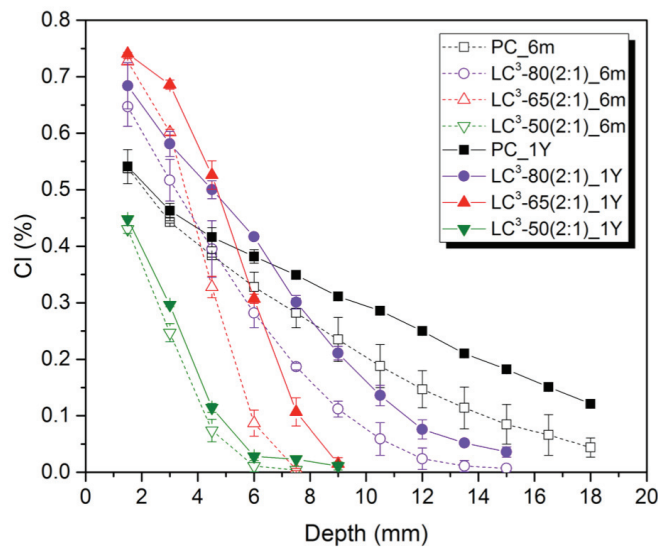


Figure 6.10 The total chloride content as a function of depth of PC and LC³ systems at 6 months and 1 year of exposure

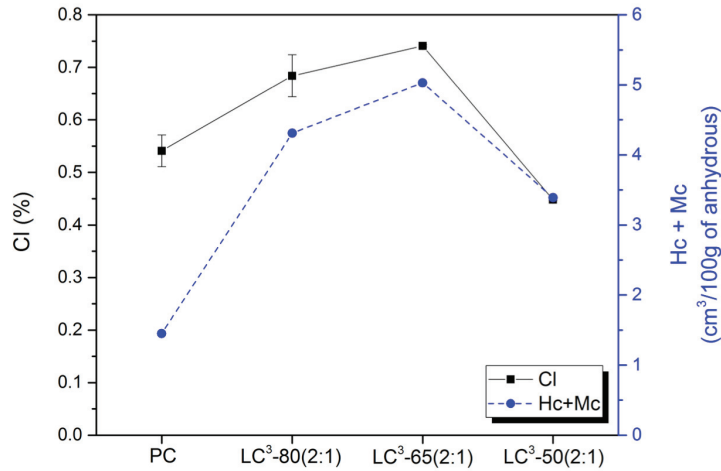


Figure 6.11 The relation between chloride content at the top surface of mortars after 1 year of exposure in 3%NaCl solution and volume of AFm phases (Hc+Mc) analyzed on pastes cured for 28 days

The apparent chloride diffusion coefficient, D_{eff} (m²/s) can be evaluated by fitting chloride penetration profiles with a least squares fit of the solution of Fick's second law as given in Equation 6.1.

$$C_x = C_s \left(1 - \operatorname{erf} \frac{x}{2\sqrt{D_{eff}t}} \right) \quad \text{Equation 6.1}$$

Where C_x is chloride concentration at depth x (m) after exposure at time t (s), C_s is surface concentration calculated in this regression analysis

Figure 6.12 shows the results of the apparent chloride diffusion coefficient of PC and LC³ systems. It is clearly seen that the replacement of clinker with limestone and calcined clay improve the resistance of chloride diffusion. This improvement can be explained from the decrease of the threshold pore radius of LC³ as seen in Figure 6.13. The threshold pore radius defined from MIP curves of mortars in Figure 6.9 shows a good relationship with the apparent chloride diffusion coefficient. The smaller the threshold pore radius, the lower the diffusion coefficient. Therefore, the smaller threshold pore radius can be used to explain the improvement of the resistance of chloride diffusion.

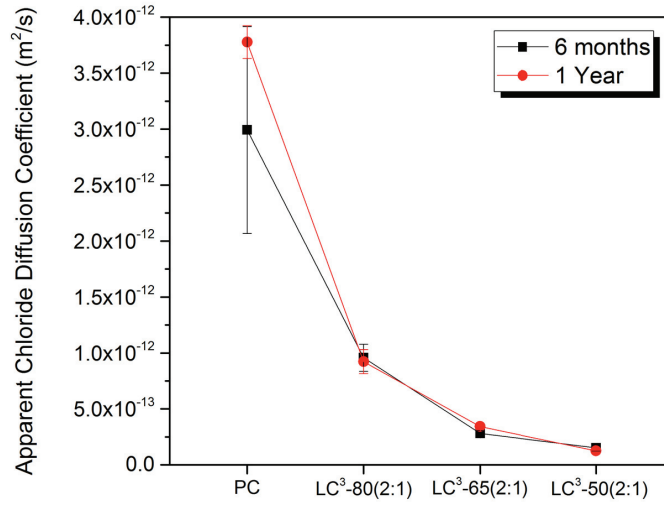


Figure 6.12 Apparent chloride diffusion coefficient of PC and LC³ systems

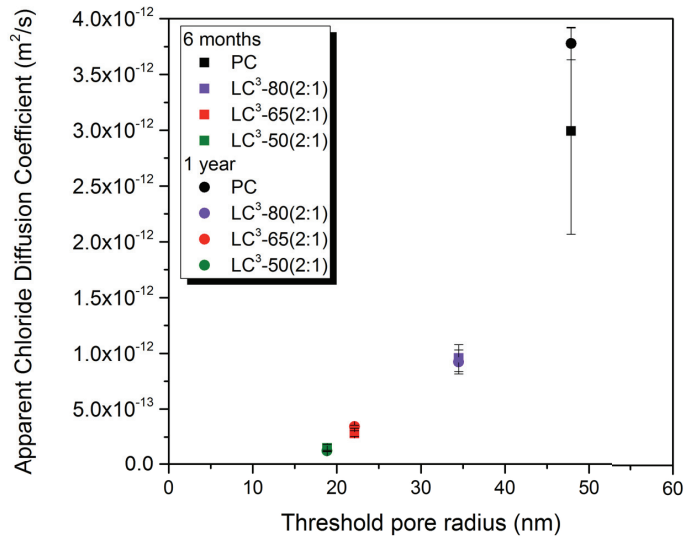


Figure 6.13 Apparent chloride diffusion coefficient of PC and LC³ systems plotted as a function of threshold pore radius of mortars cured for 28 days before exposure

6.4 Alkali silicate reaction (ASR)

Alkali-silica reaction (ASR) is caused by a reaction between the hydroxyl ions in the alkaline cement pore solution in the concrete and reactive forms of silica in the aggregate [89] to form a gel that swells as it absorbs water from the surrounding cement paste or the environment as seen in Figure 6.14. These gels can induce enough expansive pressure resulting in failure of the concrete.

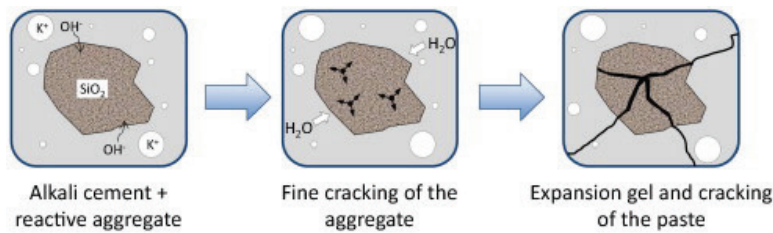


Figure 6.14 Mechanism of ASR damage in concrete [90]

In this study, alkali silicate reaction (ASR) was carried on in the system of PC with 0.52%Na₂O_{eq} and LC³-65(2:1) with two different alkali contents including 0.44%Na₂O_{eq} and 0.77%Na₂O_{eq}. The highly reactive aggregate from North America called JOBE was used. As seen in Figure 6.15, both LC³-65(2:1) mortars show an excellent result compared to PC even though LC³-65(2:1)- 0.77%Na₂O_{eq} has an alkali content higher than that of PC. The expansion of LC³-65(2:1) mortars are lower than 0.04% (expansion limit) after exposure for more than 1 year. The indirect improvement of ASR mitigation of LC³-65(2:1) over the PC is possible due to the porosity refinement of LC³-65(2:1) as seen in Figure 6.16 which can reduce the permeability of reactive ions to form ASR gel. The key parameter for the improvement of ASR mitigation is the chemical compositions in pore solution which lead to prevention of the expansion in mortar bar [91, 92]. The pH and the composition of pore solution extracted from hardened cement paste samples containing the same amount of cementitious materials with the tested mortars are given in Table 6.3 and Figure 6.17. They give information on ions concentration in pore solution before exposure that LC³-65(2:1) has a lower OH⁻ ions, which could lead to a lower attraction of the reactive silica toward the pore solution. Moreover, LC³-65(2:1) has a higher content of Al ions provided by the calcined clay which can reduce silica dissolution to form the ASR gel as also observed in Chappex's works [93, 94]. Furthermore, lower alkalis (Na, K) ions are measured not only the less clinker content but also the presence of calcined clay which enhances the formation of C-(A)-S-H with a high alkali-binding capacity [95] as seen in Chapter 4.

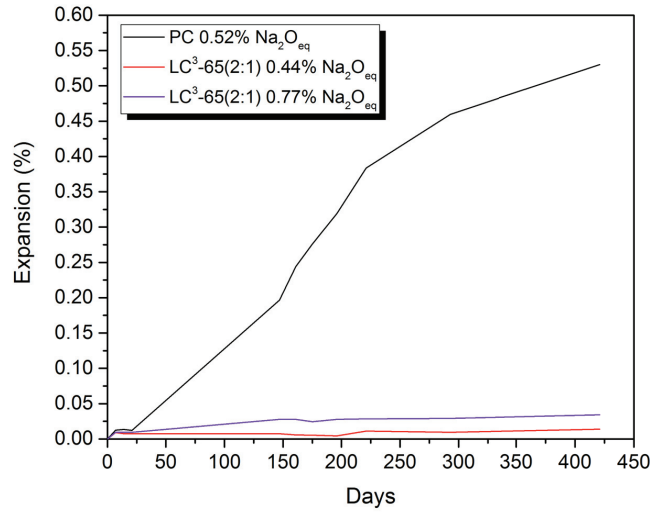


Figure 6.15 Expansion of PC and LC³-65(2 :1) soaked in 0.32 mol/L of NaOH at 38°C

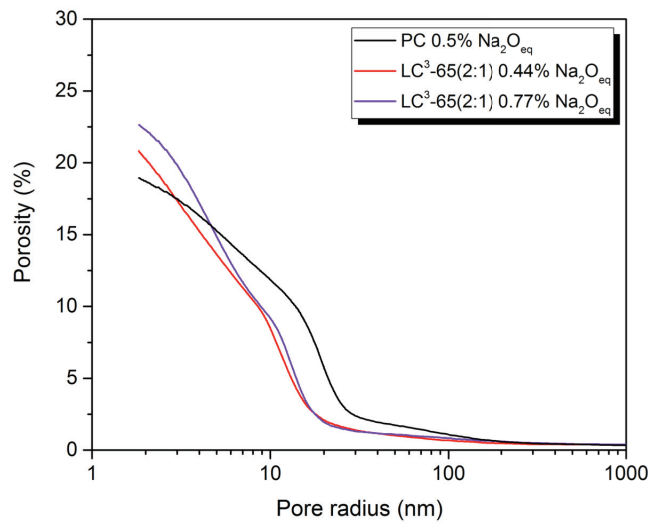


Figure 6.16 MIP results at 28 days of cement pastes containing the same amount of cementitious materials with the tested mortars of PC and LC³-65(2:1) systems

Table 6.3 The pH of pore solution of cement pastes containing the same amount of cementitious materials with the tested mortars of PC and LC³-65(2 :1) systems cured for 28 days (before exposure)

Sample	pH
PC	13.35 ± 0.07
LC ³ -65(2:1)-0.44%Na ₂ O _{eq}	12.98 ± 0.04
LC ³ -65(2:1)-0.77% Na ₂ O _{eq}	13.29 ± 0.05

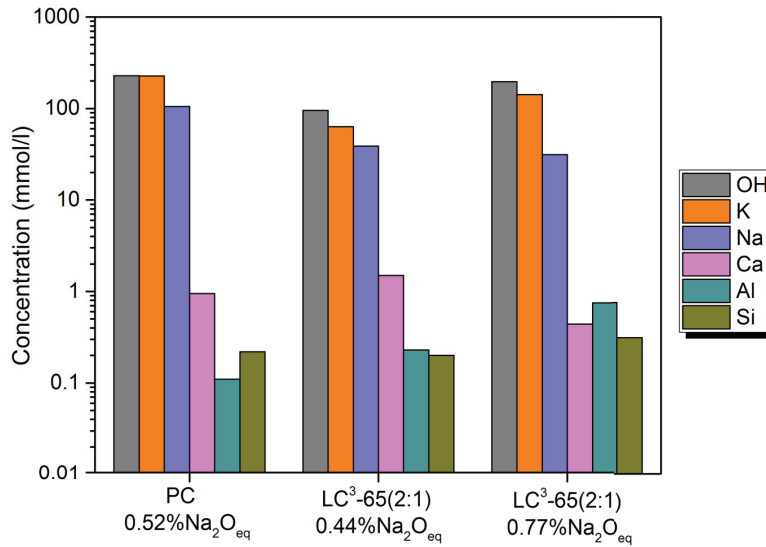


Figure 6.17 The ions concentration of pore solution of cement pastes containing the same amount of cementitious materials with the tested mortars of PC and LC³-65(2:1) systems cured for 28 days (before exposure)

6.5 Summary

The durability properties of LC³ systems compared to PC were monitored.

- The natural carbonation of PC, LC³-80(2:1) and LC³-65(2:1) were tested both indoor and outdoor conditions in Switzerland and Thailand. Although LC³ systems show a lower resistance to carbonation compared to PC, it can be improved by curing for a longer time. A higher carbonation rate was found in the samples exposed in Thailand due to the higher relative humidity and the higher CO₂ concentration of the environment in Thailand.
- Due to the significant porosity refinement of LC³ systems, the resistance of chloride migration and the chloride penetration are improved. The apparent chloride diffusion coefficient determined by fitting the chloride penetration profile with the solution of Fick's second law is shown in the following order: LC³-50(2:1) < LC³-65(2:1) < LC³-80(2:1) < PC.
- LC³-65(2:1) shows an excellent ASR mitigation compared to PC even though LC³-65(2:1)-0.77%Na₂O_{eq} has an alkali content higher than that of PC (0.52%Na₂O_{eq}). It is due to the higher presence of Al ions which can inhibit the silica dissolution from the reactive aggregate and the lower reactive ions in pore solution of LC³-65(2:1) over PC resulted in the lower ASR gel to form.

Chapter 7. Conclusions and Perspectives

The work in this thesis was aimed to explore the potential of using calcined clays with low kaolinite content (approximately 50%) which are widely available in Thailand, for LC³ production. Accordingly, the level of SCMs substitution, the influence of cement composition and the reactivity of calcined clay from different calcination process were investigated.

7.1 Conclusions

7.1.1 Substitution levels

Limestone and calcined clay can replace clinker up to 45% to produce LC³ blended cement. The compressive strength of all LC³ blended systems meets the standard value of OPC type I and CEM I 42.5N. LC³-65(2:1) shows similar strength to PC from 7 days onwards but LC³-50(2:1) does not reach the strength of the plain PC in this study. For all blends, the strengths show a good correlation to the gel-space ratio, so the lower strength of LC³-50(2:1) can be linked to the formation of a lower amount of hydrates.

Increasing temperature from 20°C to 30°C, which is the average temperature in Thailand, stimulates the hydration of clinker and the pozzolanic reaction resulting in the enhancement of strength development at early ages. Although raising the temperature up to 30°C leads to a coarser threshold pore radius at 28 days, it does not affect the strength of PC and LC³.

The progressive replacement of clinker with limestone and calcined clay promotes the porosity refinement, which is beneficial for the resistance of chloride ingress and the improvement of ASR mitigation.

LC³-65(2:1) looks the most promising at a commercial scale in Thailand in term of the maximum substitution level coupled with the satisfactory results of durability properties and similar strength to the reference PC.

7.1.2 Cement composition

Increasing alkalinity accelerates the clinker hydration and enhances the precipitation of hydration products at early ages but opposite effect is observed at later ages. The lower degree of clinker hydration and the lower precipitation of carboaluminate phases in a high alkali condition at late ages lead to the decrease of the gel-space ratio and the increase of total porosity. This causes the decrease of strength at later ages.

The optimum alkali equivalent of LC³-65(2:1) is 0.77% Na₂O_{eq} (or 0.99% Na₂O_{eq} in PC) for KOH addition and 0.63% Na₂O_{eq} (or 0.79% Na₂O_{eq} in PC) for NaOH addition. For these levels, strength is increased at 1 day without negatively impacting the results at later ages, as seen in Figure 7.1.

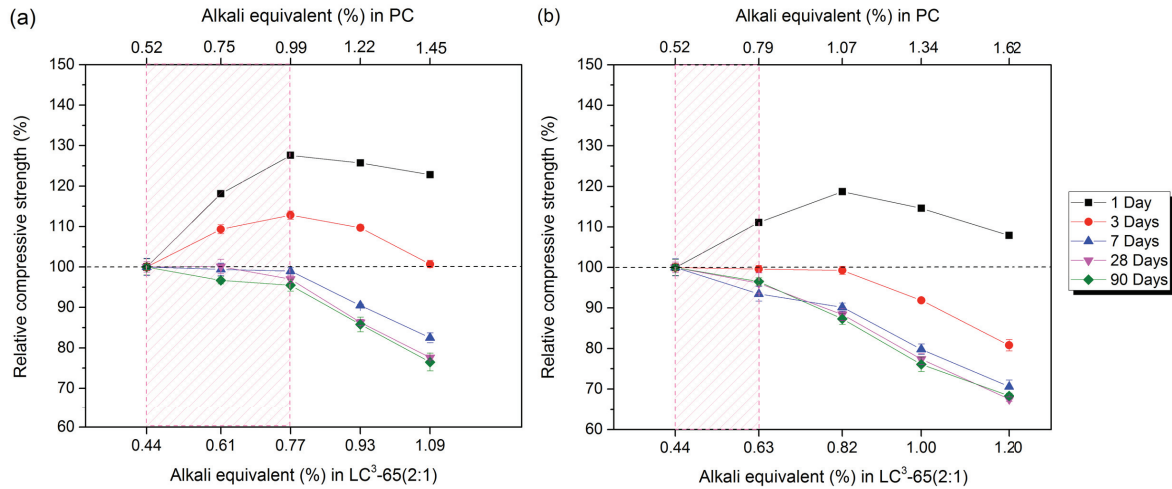


Figure 7.1 The optimal amount of alkali equivalent in PC and LC³-65(2:1) for KOH addition (a) and NaOH addition (b)

7.1.3 Calcination process

Calcined clay obtained from the rotary kiln process has a lower surface area compared to the clay calcined from the fluidized bed because of a coarser pore width of calcined clay particles. Independent of the calcination process, a higher surface area of coarse particles results from the presence of fine pore width and a large internal pore volume.

For the same metakaolin content, the calcined clay produced by fluidized bed has a slightly higher reactivity at the beginning due to a higher surface area. However, similar reactivity of calcined clay is observed later on. The increase of the metakaolin content in calcined clay leads to an increase of reactivity. Moreover, in terms of grinding, there is no gain of reactivity if clay is ground below 10 μm .

The activation energy (E_a) of calcined clays between the two different calcination processes is similar and the variation of kaolinite content (45-50%) does not impact the E_a either. The activation energy of calcined clays determined using the superposition method and the rate method is about 58 – 65 kJ/mol. Compared to the activation energy of about 40-45 kJ/mol for PC, this indicates that the reaction of the calcined clay will be more accelerated by higher temperatures.

7.1.4 Durability properties

LC³ systems show excellent results in terms of durability properties. LC³-80(2:1) and LC³-65(2:1) show a higher carbonation rate compared to PC but it is below the limit of design working life of 100 years for moderate humidity exposure class XC3.

The porosity refinement of LC³ systems significantly improves the chloride resistance. The apparent chloride diffusion coefficient is in the order of LC³-50(2:1) < LC³-65(2:1) < LC³-80(2:1) < PC.

LC³-65(2:1) shows an excellent ASR mitigation compared to PC despite the higher alkali content of LC³-65(2:1). It is due to the higher Al ions measured in the pore solution and the lower amount of reactive ions in the pore solution of LC³-65(2:1). This prevents the formation of the ASR gel.

7.2 Perspectives

7.2.1 Studying the durability properties

As discussed previously, LC³ systems show excellent durability results. In this study, the durability properties with respect to carbonation resistance, chloride ingress, and alkali silicate reaction were investigated. However, there are still other properties needed to be run to validate the feasibility of using limestone and calcined clay with low kaolinite content to substitute clinker. The interesting features include the resistance to high humidity and rain condition, typical in Thailand, the resistance to sulfate attack, the corrosion resistance of chemicals and the resistance to abrasion.

7.2.2 Understanding the workability of LC³

The mortar flow of LC³ systems in this study is similar to PC even for high levels of substitution. The result looks very promising for LC³, showing that despite using water-adsorbing calcined clays, similar workability to PC can be reached, without the use of superplasticizer. These results need to be better understood to determine why in this study, plasticizer was not required whereas several previous studies clearly showed the negative impact of calcined clay on workability [30, 96, 97].

For paste samples, the pore width of calcined clay particles plays an important role in the requirement of superplasticizer to improve the workability of LC³ instead of surface area. As seen in Figure 7.2, when superplasticizer is added, calcined clays containing a higher surface area show a better workability over calcined clays with a lower surface area. On the other hand, the greater the width of pore, the lower the spread of paste. Therefore, it is interesting to more deeply study the parameters which affect the workability for LC³.

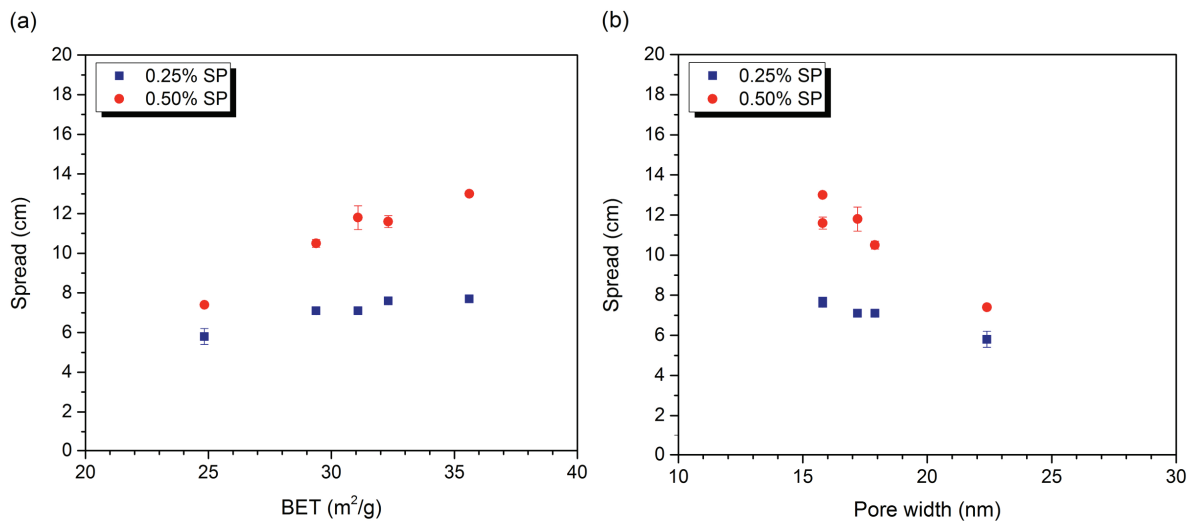


Figure 7.2 Spread of LC³-65(2:1) paste after adding 0.25% and 0.5% of superplasticizer plotted as a function of BET surface area (a) and pore width (b) of the particle of calcined clay

Appendix

Appendix A. Sulfate adjustment for LC³

Appendix B. Influence of substitution levels on the strength development of LC³

Appendix C. Comparison of the degree of metakaolin reaction determined using mass balance and GEMS

Appendix D. Influence of alkalis on the strength development of PC and LC³-50(2:1)

Appendix E. Influence of alkali on the setting time and the workability of LC³

Appendix F. The effect of alkali on the microstructure of LC³

Appendix G. Calculation the apparent activation energy (E_a) of LC³

Appendix A. Sulfate adjustment for LC³

The undersulfation of LC³ can be observed from the heat flow curve showing the higher intensity of the aluminate peak or the shift of the aluminate peak combined with the main peak when increased the amount of calcined clay as seen in Figure A.1. In order to prevent the undersulfation of LC³, the sulfate content was adjusted by adding gypsum. The sulfate adjustment of LC³ systems is shown in Figure A.2 to Figure A.4. The optimum sulfate of LC³ systems depends on the amount of calcined clay content in the blends. It can be determined when the heat flow curve of the aluminate peak does not overlap with the peak of the silicate phase hydration. Generally, the optimum sulfate for cement would be sufficient to delay the aluminate hydration peak not less than 2 hours after the maximum of the main silicate hydration peak (like the optimum sulfate of PC). Thus, the optimal amount of gypsum addition was defined when the beginning of the aluminate peak was shifted for 2 hours from the silicate peak. All the sulfate additions are given in Table A.1.

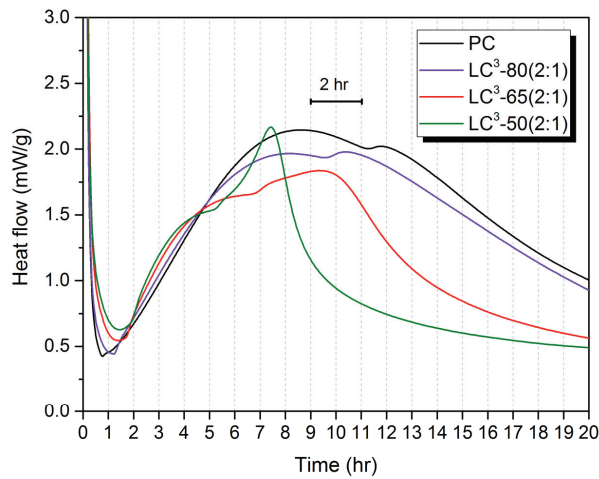


Figure A.1 The heat flow curves of PC and LC³ systems before sulfate adjustment

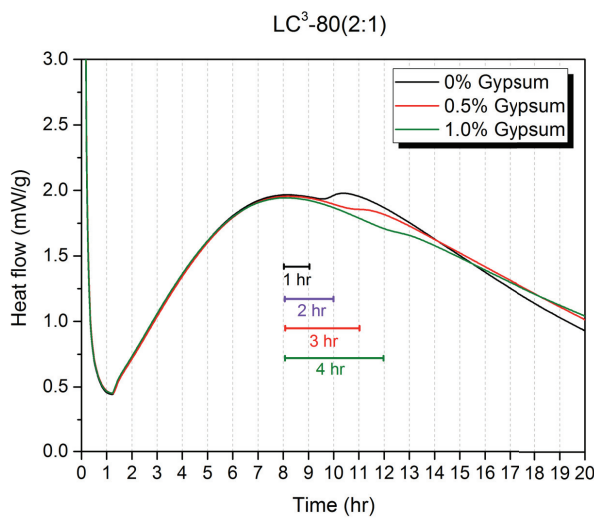


Figure A.2 Sulfate adjustment for LC³-80(2:1)

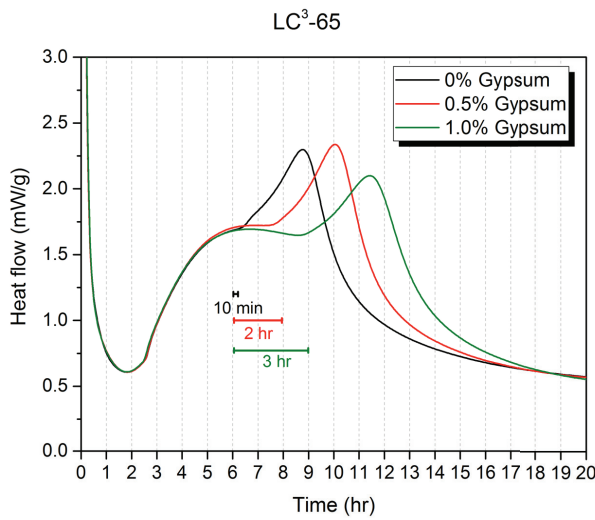
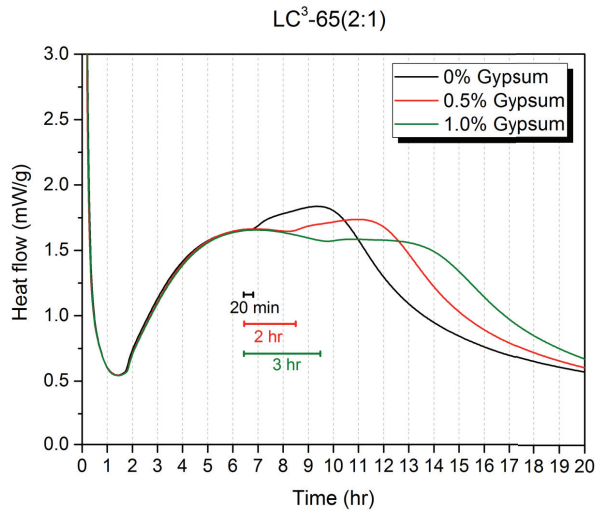
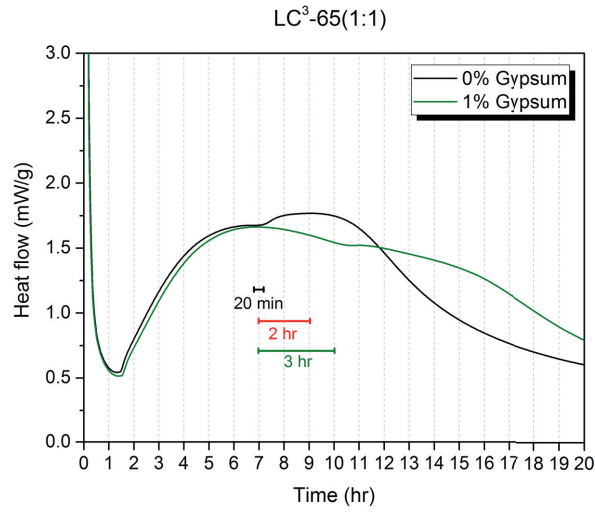


Figure A.3 Sulfate adjustment for LC³-65(1:1), LC³-65(2:1) and LC³-65

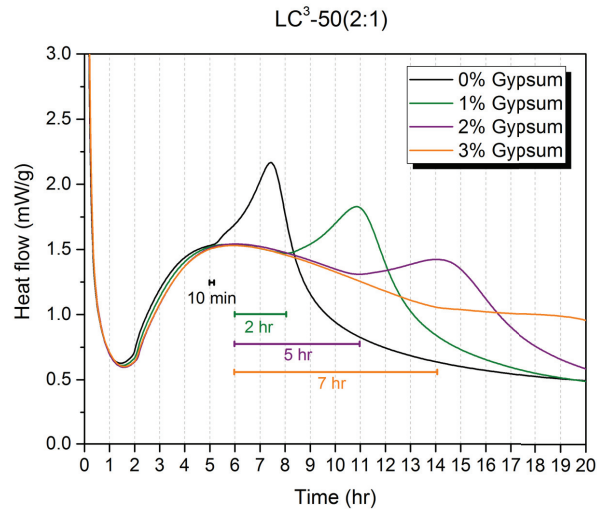


Figure A.4 Sulfate adjustment for LC³-50(2:1)

Table A.1 The composition and the amount of gypsum used for adjusting sulfate of LC³ systems

Name	wt.%				
	Clinker	Calcined clay	Limestone	Gypsum	Gypsum addition
LC ³ -80(2:1)	80	10	5	5	0.25
LC ³ -65(1:1)	65	15	15	5	0.50
LC ³ -65(2:1)	65	20	10	5	0.50
LC ³ -65	65	30	0	5	0.75
LC ³ -50(2:1)	50	30	15	5	1.00

Appendix B. Influence of substitution levels on the strength development of LC³

B.1 Influence of calcined clay to limestone ratio

Various calcined clay to limestone ratios were used in order to define the best combination. Figure B.1 shows the strength results for LC³-65 using either calcined clay only, or 2:1 or 1:1 calcined clay to limestone ratio. Better or equal strengths than the reference PC from 7 days onwards are observed for LC³-65(2:1). It also shows that significant differences are obtained by changing the calcined clay to limestone ratio. These results are in agreement with the work of Antoni [29], who reported that the ratio of 2:1 is the most promising in term of mechanical properties and cost of production. The lower strength of LC³-65(1:1) compared to LC³-65(2:1) can be explained by a coarser pore size distribution of LC³-65(1:1) as seen in Figure B.2.

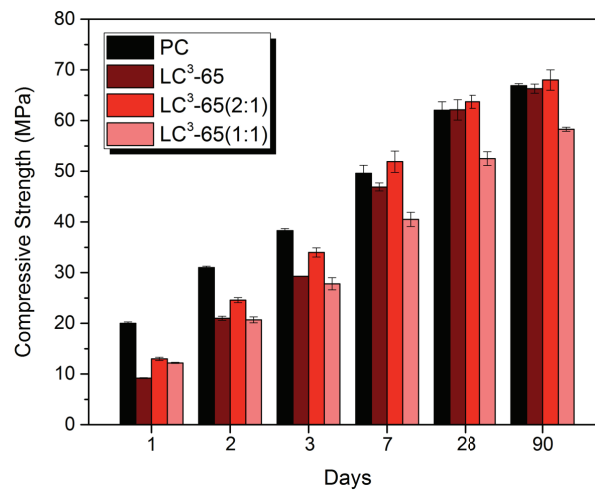


Figure B.1 Compressive strength of PC and LC³-65 varying calcined clay: limestone ratios

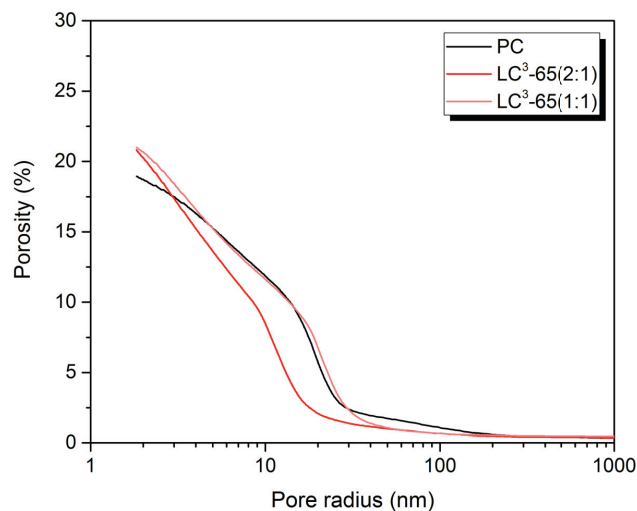


Figure B.2 MIP results of PC, LC³-65(2:1) and LC³-65(1:1) cured at 28 days

B.2 Influence of metakaolin content

The result from Chapter 3 shows the compressive strength of LC³-50(2:1) in this study cannot reach the strength value of the reference PC. This contradicts previous works [29, 31, 98] which showed similar compressive strength of LC³-50(2:1) to plain PC from 7 days onwards. Increasing the amount of metakaolin content does not increase the strength of LC³-50(2:1) at 28 days but it is able to improve the strength at early ages as seen in Figure B.3. Thus, the different results are not explained by the calcined clay source, but by the cement characteristics.

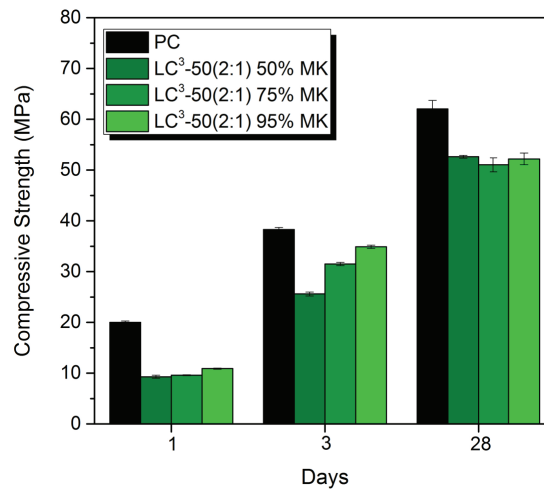


Figure B.3 Impact of metakaolin content of calcined clay to the strength development of LC³-50(2:1)

Appendix C. Comparison of the degree of metakaolin reaction determined using mass balance and GEMS

For the reaction of metakaolin (MK), it was determined using 2 different techniques including mass balance calculation (MB) and GEMS. The step of mass balance calculation was explained in Chapter 2. The input for both calculations can see from Figure C.1. At the interested ages, the result of reacted phase got from XRD were converted to be the fixed available oxides and the free available SiO₂ and Al₂O₃ were obtained from the variation of metakaolin reaction from 0 to 100%. In case of mass balance calculation, the information of C-A-S-H composition from EDS was taken into account to calculate the phase assemblage. For GEMS, instead of using the reacted limestone, the initial amount of limestone and alkali content were used as the input for GEMS calculation. The output that we got from mass balance and GEMS are the hydration products. Comparing the amount of CH from the calculation with the results from the experiment using TGA and XRD we will get the information of reacted metakaolin.

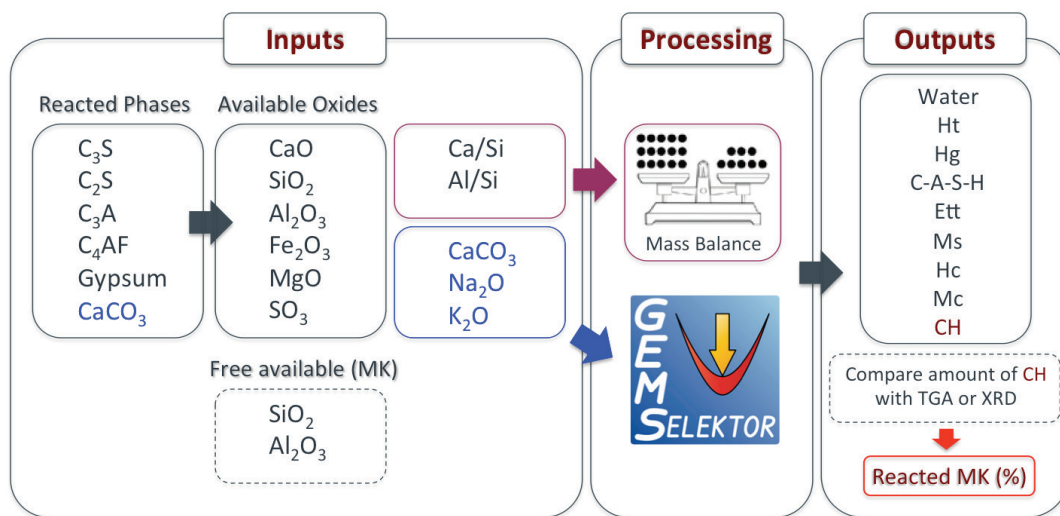


Figure C.1 The step to determine the degree of metakaolin reaction using mass balance calculation and GEMS

The comparisons of reacted metakaolin results from mass balance and GEMS calculation are shown in Figure C.2. In LC³-50(2:1) and LC³-65(2:1) systems, the reacted MK from mass balance and GEMS shows quite similar results. For LC³-80(2:1) system, GEMS shows the overestimation at all ages.

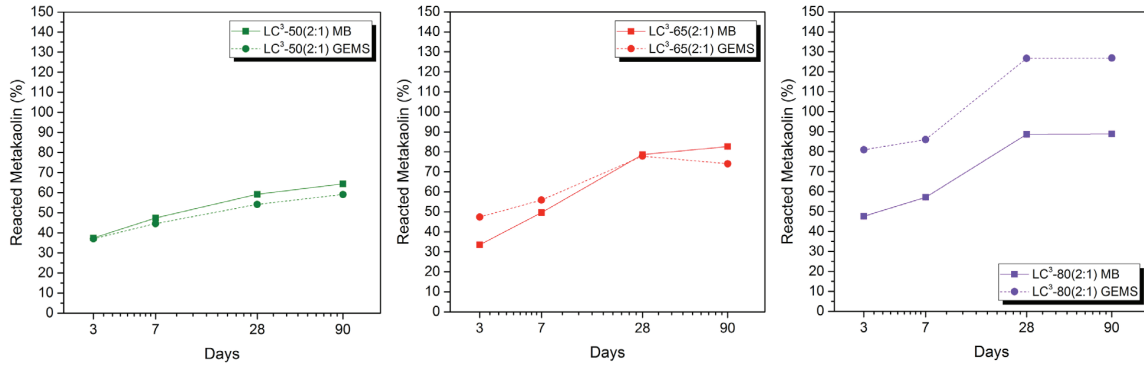


Figure C.2 The comparison of reacted metakaolin results calculated from mass balance and GEMS

The difference of reacted MK from mass balance and GEMS is possible due to the different Ca/Si in C-(A)-S-H used. As seen in Figure C.3, the ratio of Ca/Si used in GEMS is about 1.60 in all systems but from the experiment (SEM-EDS) it shows the variation of Ca/Si depending on the composition and the hydration time. The lower Ca/Si reflects the higher pozzolanic reaction. Thus, the higher estimation of reacted MK for LC³-80(2:1) from GEMS observed is due to the lower Ca/Si used for GEMS. Accordingly, the reaction of metakaolin predicted by mass balance looks promising more than the results obtained from GEMS due to the real Ca/Si used in mass balance calculation.

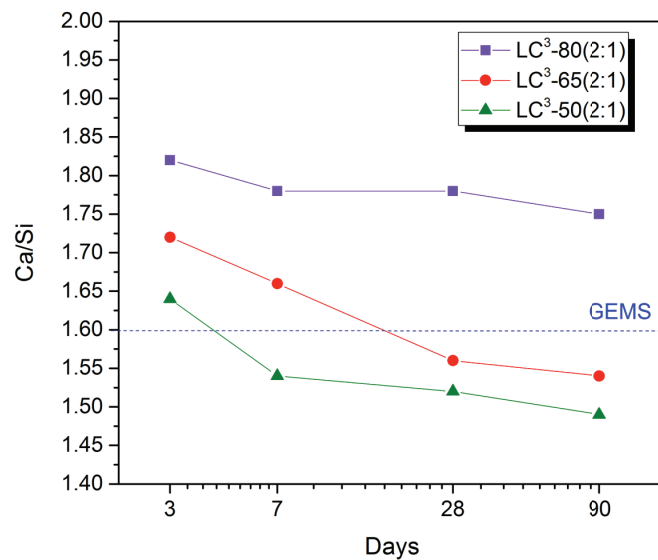


Figure C.3 Ca/Si of LC³ systems analyzed by SEM-EDS and predicted by GEMS

Appendix D. Influence of alkalis on the strength development of PC and LC³-50(2:1)

D.1 PC

The results in Chapter 3 show the compressive strength of LC³-50(2:1) is lower than that of the reference PC which is in contrast with the previous works [28, 29, 31]. One of the reasons is the difference of the alkali content in PC. The PC used in Avet's study [31] has alkali content about 0.97%Na₂O_{eq} while PC used in this study has the percentage of alkali only 0.52%Na₂O_{eq}. The different alkali content directly impacts the strength development of PC as seen in Figure D.1. PC with high alkali content shows higher strength value at 1 day but lower at later ages.

To get more understanding, the alkali content of the PC used in this study was adjusted from 0.52%Na₂O_{eq} to 0.99%Na₂O_{eq} using KOH. The compressive strength results are shown in Figure D.2. The strength of PC after adjustment is increased at 1 day and is reduced at 28 days. Similar values to Avet's work are obtained. Using this adjusted PC to formulate LC³ cements, LC³-65(2:1) gives a higher strength and LC³-50(2:1) shows the comparable strength to the reference PC, as shown in Figure D.3.

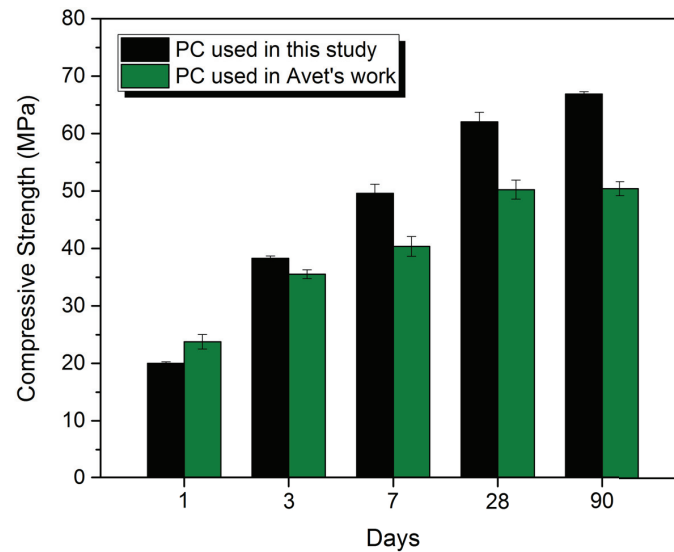


Figure D.1 Compressive strength of PC (0.52%Na₂O_{eq}) used in this study and PC (0.97%Na₂O_{eq}) used in Avet's work [31]

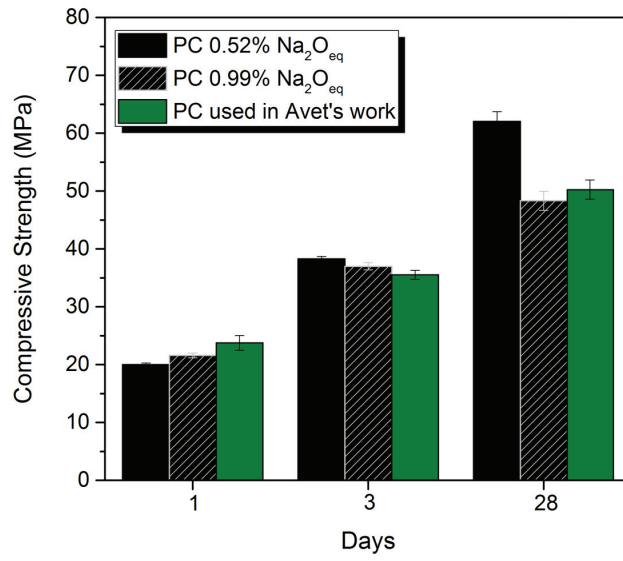


Figure D.2 The compressive strength of PC-0.52%Na₂O_{eq} and PC-0.99%Na₂O_{eq} used in this study compared to PC containing 0.97%Na₂O_{eq} used in Avet's work [31]

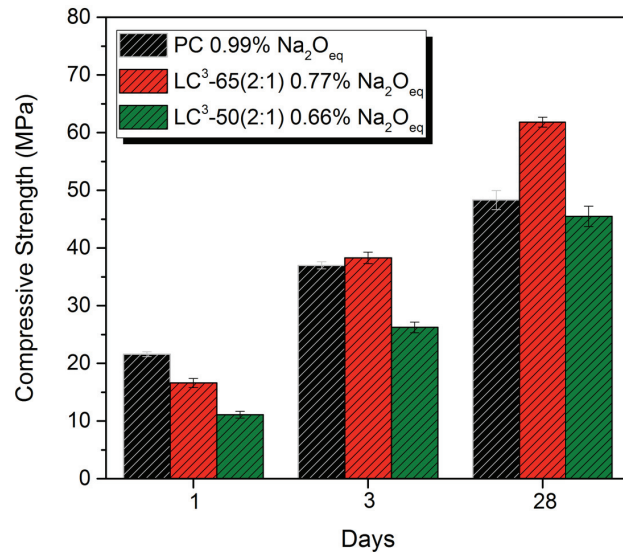


Figure D.3 Compressive strength of PC-0.99%Na₂O_{eq} and LC³ formulated using PC-0.99%Na₂O_{eq}

D.2 LC³-50(2:1)

The study of the impact of alkalis on the mechanical properties of LC³ was also investigated on LC³-50(2:1). The formulation of LC³-50(2:1) with various alkali contents using KOH addition is given in Table D.1 and the compressive strength results show in Figure D.4. Increasing the alkali content of LC³-50(2:1) from 0.40%Na₂O_{eq} to 0.66%Na₂O_{eq} increases the early strength but it negatively influences the strength at later ages.

Table D.1 The composition of LC³-50(2:1) with various alkali contents

Name	wt.%				
	PC	Calcined clay	Limestone	Gypsum addition	KOH
LC ³ -50(2:1) 0.40%Na ₂ O _{eq}	54.5	29.7	14.8	1.0	0.0
LC ³ -50(2:1) 0.50%Na ₂ O _{eq}	54.2	29.6	14.8	1.0	0.4
LC ³ -50(2:1) 0.58%Na ₂ O _{eq}	54.1	29.5	14.7	1.0	0.7
LC ³ -50(2:1) 0.66%Na ₂ O _{eq}	53.9	29.4	14.7	1.0	1.0

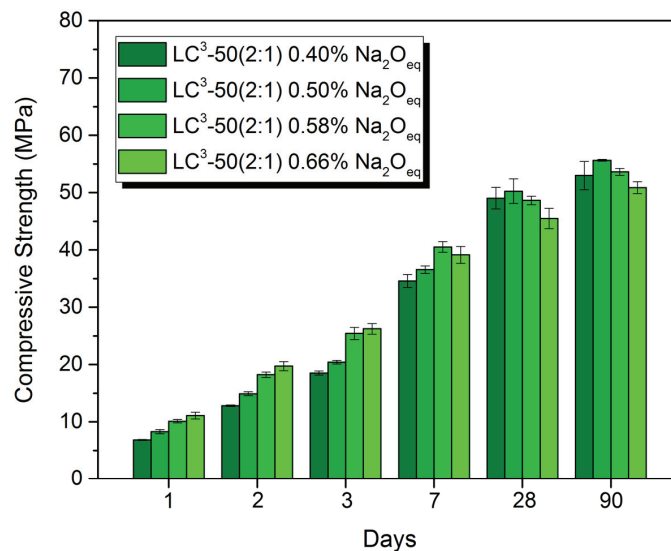


Figure D.4 Compressive strength of LC³-50(2:1) with various alkali contents

The percentages of alkali equivalent (%Na₂O_{eq}) of PC and LC³ systems are shown in Table D.2. It should be emphasized that the influence of alkalis on the strength development of LC³ depends on the amount and species of alkali containing in the plain PC. For the system containing high K₂O, the maximum alkali content in PC for LC³ formulation is about 0.99%Na₂O_{eq}. For the system containing high Na₂O, the alkali content in PC is lower compared to K₂O. It should be less than 0.79 %Na₂O_{eq} to prevent the loss strength at the later ages as discussed in Chapter 4.

Table D.2 The percentage of alkali equivalent (% Na₂O_{eq}) of PC used for LC³ formulation and the amount of alkali equivalent of LC³

Target of % Na ₂ O _{eq}	* Na ₂ O _{eq} (%)	
	PC (clinker)	LC ³ (clinker+clay+limestone)
<i>KOH addition</i>		
LC ³ -50(2:1) 0.40%Na ₂ O _{eq}	0.52	0.40
LC ³ -50(2:1) 0.50%Na ₂ O _{eq}	0.71	0.50
LC ³ -50(2:1) 0.58%Na ₂ O _{eq}	0.85	0.58
LC ³ -50(2:1) 0.66%Na ₂ O _{eq}	0.99	0.66
<i>KOH addition</i>		
LC ³ -65(2:1) 0.44%Na ₂ O _{eq}	0.52	0.44
LC ³ -65(2:1) 0.61%-K	0.75	0.61
LC ³ -65(2:1) 0.77%-K	0.99	0.77
LC ³ -65(2:1) 0.93%-K	1.22	0.93
LC ³ -65(2:1) 1.09%-K	1.45	1.09
<i>NaOH addition</i>		
LC ³ -65(2:1) 0.63%-N	0.79	0.63
LC ³ -65(2:1) 0.82%-N	1.07	0.82
LC ³ -65(2:1) 1.00%-N	1.34	1.00
LC ³ -65(2:1) 1.20%-N	1.62	1.20

* % Na₂O_{eq} = % Na₂O + (0.658 x % K₂O)

** % Na₂O_{eq} of PC and calcined clay equal to 0.52 and 0.39, respectively

Appendix E. Influence of alkali on the setting time and the workability of LC³

E.1 Setting time

The influence of alkalis on the setting time of LC³-65(2:1) was determined using an automatic Vicat needle apparatus and was carried out on the fresh paste samples with fixed the water to binder ratio of 0.4. Automatic recording of the penetration was done every 15 min and each penetration was performed at least 5 mm away from the previous penetration. The time of setting was determined following EN 196-3. The initial setting time is defined at the time for which the distance between the needle and the base-plate is 6 ± 3 mm. The final setting time is the time at which the needle first penetrated into the paste 0.5 mm. The influence of KOH and NaOH on the setting time of LC³-65(2:1) and compared to PC is shown in Figure E.1 and Figure E.2. The presence of calcined clay affects the final setting time of LC³ and increasing alkalinity using KOH slightly decreases the final setting time of LC³-65(2:1). NaOH presents a more noticeable effect than KOH. This can be explained by the acceleration of hydration at the early age using alkali.

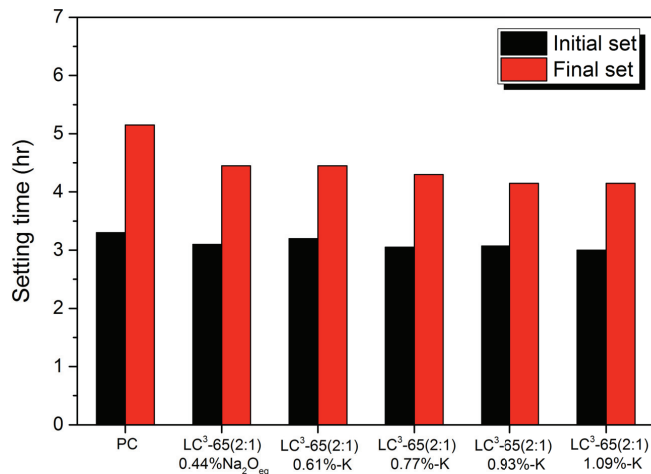


Figure E.1 The setting time of PC and LC³-65(2:1) with various alkali contents using KOH addition

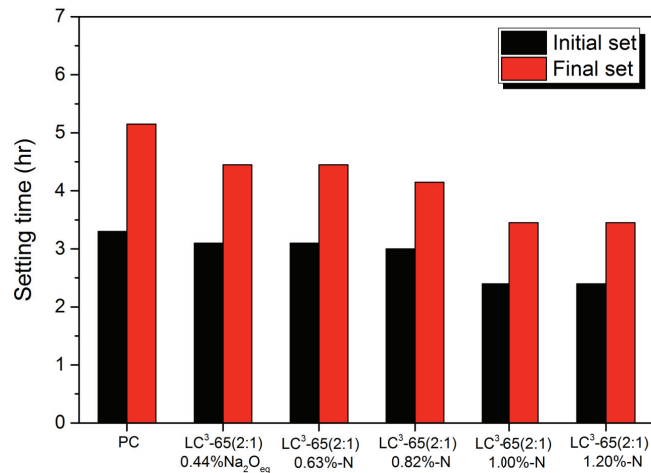


Figure E.2 The setting time of PC and LC³-65(2:1) with various alkali contents using NaOH addition

E.2 Workability

The impact of alkalis on the workability of LC³-65(2:1) was observed by measuring the flow of mortar with no superplasticizer used. The results are shown in Figure E.3. The method for flow testing was described in Chapter 5. The increase of alkalinity improves the workability of LC³ and the maximum flow obtained from the system containing about 0.80%Na₂O_{eq} in both cases of alkali addition. Improved workability of LC³ is possible due to a higher entrained air generated by alkalis. However, after 30 min there is no influence of alkali on the flow of LC³-65(2:1) as seen in Figure E.4.

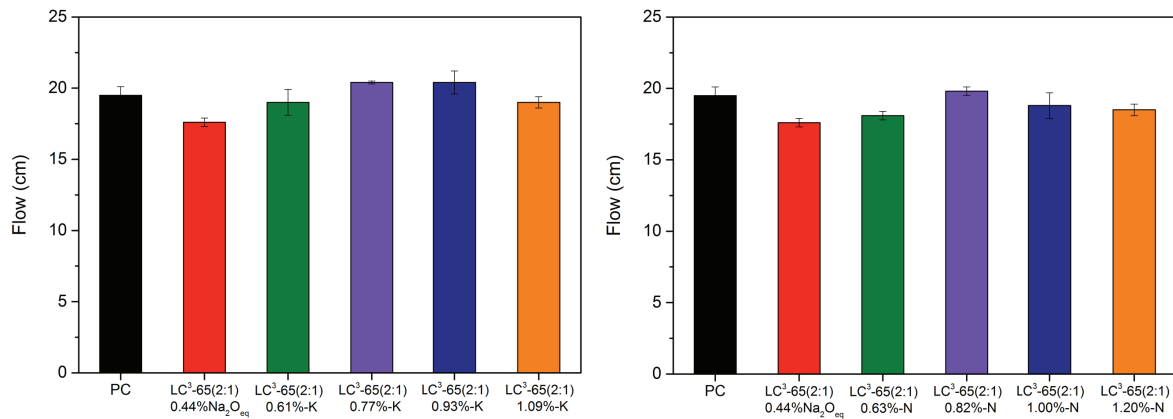


Figure E.3 The mortar flow of PC and LC³-65(2:1) with various alkali contents using KOH addition (left) and NaOH addition (right)

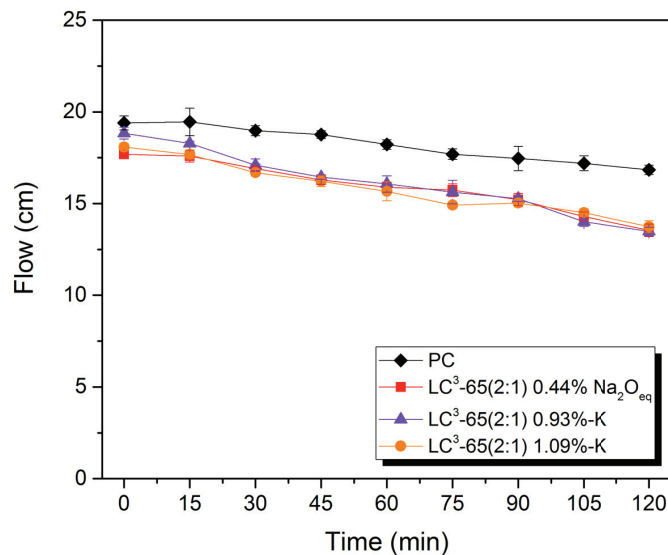


Figure E.4 The mortar flow of PC and LC³-65(2:1) with various alkali contents using KOH addition plotted as a function of time

Appendix F. The effect of alkali on the microstructure of LC³

From Chapter 4, the degree of clinker hydration is increased at 1 day when increased the alkali content up to 1.09%Na₂O_{eq} using KOH, but it is in contrast with the later ages. As a result of the higher degree of clinker hydration by adding KOH at 1 day, the microstructure observed using BSE-SEM shows a thicker layer of C-A-S-H surrounded the alite grains in the pastes with a higher alkali content as seen in Figure F.1. At 28 days, the microstructure of LC³-65(2:1)-1.09%Na₂O_{eq} shows a higher unreacted clinker remaining in the paste as seen in Figure F.2 which is in agreement with the lower degree of clinker hydration compared to LC³-65(2:1)-0.44%Na₂O_{eq}.

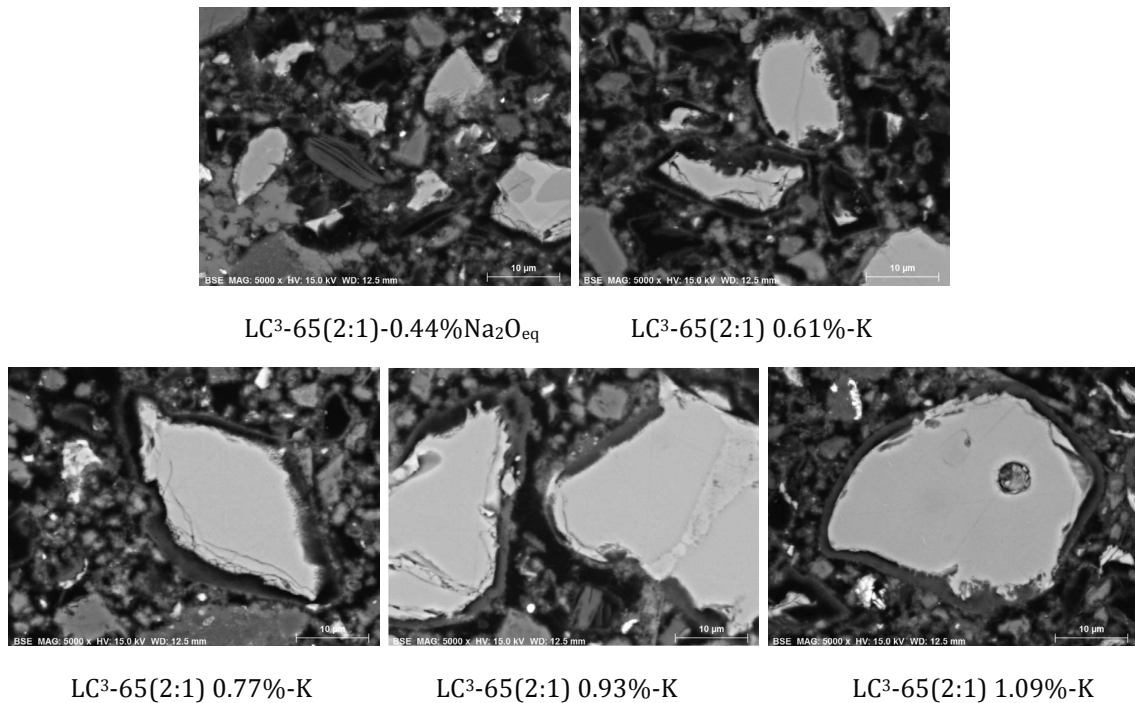


Figure F.1 The microstructure at 1 day of LC³-65(2:1) with various alkali contents

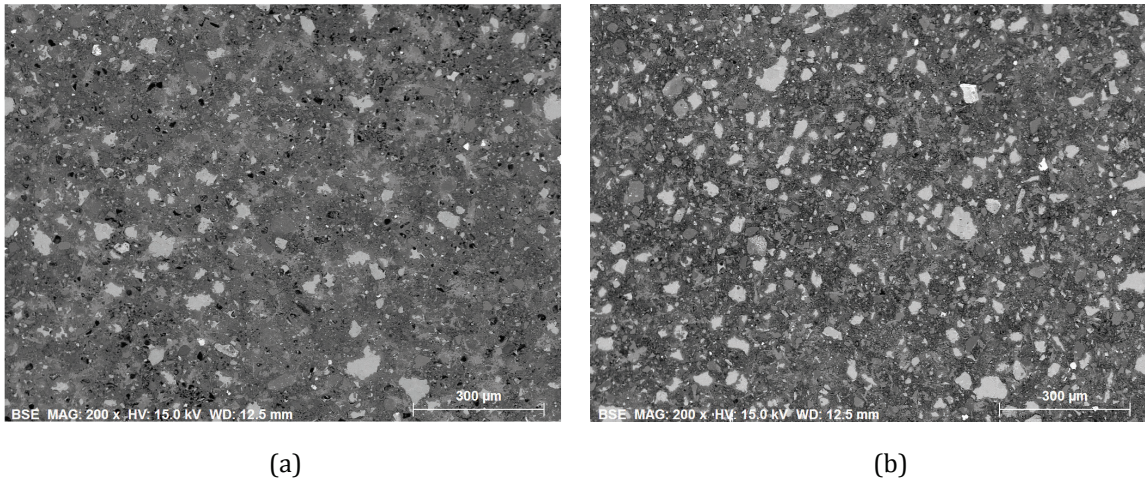


Figure F.2 The microstructure at 28 days of LC³-65(2:1)-0.44%Na₂O_{eq} (a) and LC³-65(2:1) 1.09%-K (b)

The addition of alkali hydroxide to LC³ blended cement results in the increase of pH in the system. The higher pH accelerates the calcium hydroxide (CH) precipitation and results the formation of the smaller size of CH crystals [60, 99]. The morphology of CH in LC³-65(2:1) systems show in Figure F.3, the cluster of CH can be observed in the paste containing low alkali content and the smaller and more number particles of CH in the paste with high alkali content.

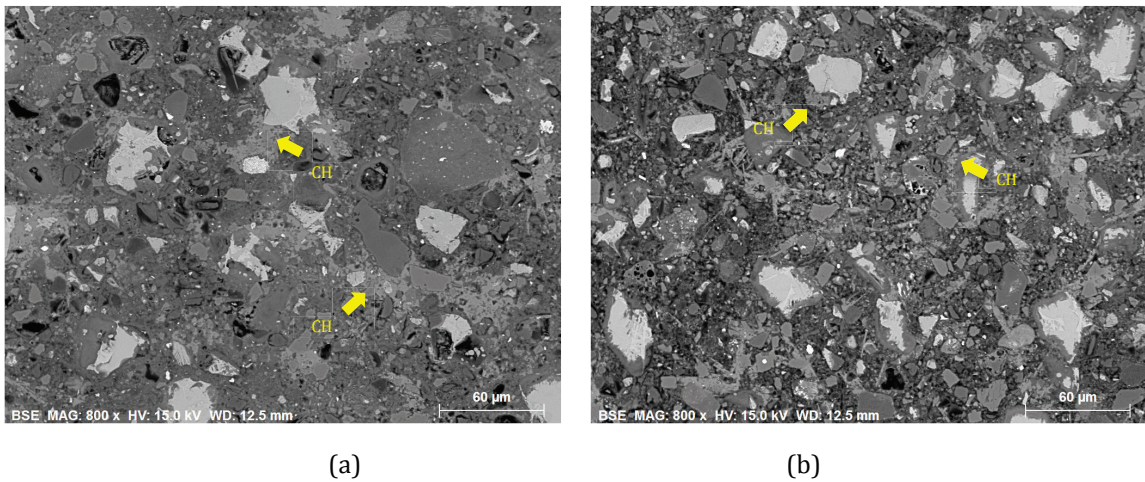


Figure F.3 The morphology of CH at 28 days of LC³-65(2:1)-0.44%Na₂O_{eq} (a) and LC³-65(2:1) 1.09%-K%

Appendix G. Calculation the apparent activation energy (E_a) of LC³

G.1 Apparent activation energy of LC³

To investigate the effect of calcined clays on the temperature sensitivity when the calcined clay was used in the LC³ systems, the isothermal calorimeter was employed to measure the heat of hydration of cement pastes. The term “apparent activation energy” is used due to the several chemical reactions taking place during cement hydration. This study focused on how the replacement level of calcined clay and the calcination process affect the apparent activation energy of LC³.

The method for determining apparent activation energy (E_a) in this study was the superposition method. Because it is the most used in the E_a determination of the cement hydration and the results are accurate and more practical to get compared with the rate method [77, 78].

The method for the preparation of the pastes was explained in Chapter 2 and the calorimeter was operated at 20°C, 30°C, and 40°C for 14 days. The samples used in this study are given in Table G.1. The procedure of the superposition method for determining the apparent activation energy (E_a) was described in Chapter 5. In this study, the data up to 50% of the ultimate heat release (H_u) for each system was used to calculate the sensitivity of the reaction rate as suggested in [78] and it was in the range the useful information (first few days of hydration) for determining E_a as recommended in [77].

Table G.1 The list and composition of samples for studying the apparent activation energy of LC³

Name	Calcination process	Kaolinite (%)	Clinker (%)	Calcined clay (%)	Limestone (%)	Gypsum (%)
PC	-	-	91	0	4	5
LC ³ -80(2:1)	Fluidized bed	50	80	10	5	5
LC ³ -65(2:1)	Fluidized bed	50	65	20	10	5
LC ³ -50(2:1)	Fluidized bed	50	50	30	15	5

The degree of hydration can be estimated from the heat released collected by the isothermal calorimeter. Schindler and Folliard [100] proposed the degree of hydration as a proportion of the heat released to the ultimate heat available as given in Equation G.1.

$$\alpha(t) = \frac{H(t)}{H_u} \quad \text{Equation G.1}$$

where $\alpha(t)$ is the degree of hydration, $H(t)$ is the cumulative heat released (J/g) from time 0 to time t , and H_u is the ultimate heat available (J/g) as calculated based on the composition of cementitious materials.

Zaribaf et al. [101] proposed the empirical models modified from [102] to determine H_u for the blended cement containing MK shown in Equation G.2.

$$H_u = H_{cem} \cdot \rho_{cement} + 461 \cdot \rho_{slag} + 1800 \cdot \rho_{FA-CaO} \cdot \rho_{FA} + 876.5 \cdot \rho_{MK} \quad \text{Equation G.2}$$

where, H_{cem} is total heat of hydration of the cement (J/g) defined as given in Equation G.3 and ρ_x is weight ratio of the x compound in terms of total cement content.

$$H_{cem} = 500\rho_{C_3S} + 260\rho_{C_2S} + 866\rho_{C_3A} + 420\rho_{C_4AF} + 624\rho_{SO_3} + 1186\rho_{FreeCaO} + 850\rho_{MgO}$$

Equation G.3

The calculation of H_{cem} and H_u of PC and LC³ systems are given in Table G.2 and the degree of hydration calculated using Equation G.1 are shown in Figure G.1.

Table G.2 The calculation of H_{cem} and H_u of PC and LC³ systems

XRD	Factor	PC	Calcined Clay	LC ³ -80(2 :1)	LC ³ -65(2 :1)	LC ³ -50(2 :1)
C ₃ S	500	0.67	0	0.57	0.47	0.37
C ₂ S	260	0.08	0	0.07	0.06	0.04
C ₃ A	866	0.07	0	0.06	0.05	0.04
C ₄ AF	420	0.09	0	0.08	0.06	0.05
SO ₃	624	0.02	0	0.03	0.03	0.03
Free CaO	1,186	0	0	0	0	0
MgO	850	0.01	0.06	0.02	0.02	0.02
MK	876.5	0	0.52	0.05	0.10	0.15
H_{cem} (J/g)		477.6		414.1	350.5	290.3
H_u (J/g)		477.6		459.3	441.0	426.0

Figure G.1 shows the degree of hydration decreases with increasing the substitution level due to the lower amount of reactive clinker phases. Moreover, it can be observed that the increase of temperature increases the hydration rate at the beginning but it tends to decrease the degree of hydration, especially at a higher level of substitution. This slowdown of the degree of clinker hydration was explained in Chapter 3.

The superposition method [77, 79, 103] was used to determine the apparent activation energy (E_a) of PC and LC³. The parameters for fitting the curves and the activation energy of PC and LC³ blended cements are given in Table G.3. The E_a of PC is about 41.6 kJ/mol which is in the range of OPC type I concrete suggested in ASTM C1074-04 (40-45 kJ/mol) and the E_a of LC³ systems is about 41.7-44.6 kJ/mol which are very close to the value of the PC as seen clearly in Figure G.2.

Table G.3 The parameter for fitting cumulative heat curve and E_a results of PC and LC³ pastes

Sample	H_u (J/g)	β	τ			E_a (kJ/mol)
			20°C	30°C	40°C	
PC	0.60	0.88	17.2 (R ² =0.99)	9.4 (R ² =0.99)	5.8 (R ² =0.99)	41.6 ± 3.1 (R ² =0.99)
LC ³ -80(2:1)	0.44	0.98	12.5 (R ² =0.99)	7.2 (R ² =0.99)	4.2 (R ² =0.99)	41.8 ± 1.0 (R ² =0.99)
LC ³ -65(2:1)	0.43	0.84	13.0 (R ² =0.99)	7.3 (R ² =0.99)	4.4 (R ² =0.99)	41.7 ± 0.9 (R ² =0.99)
LC ³ -50(2:1)	0.48	0.68	18.4 (R ² =0.98)	9.8 (R ² =0.99)	5.7 (R ² =0.99)	44.6 ± 2.4 (R ² =0.99)

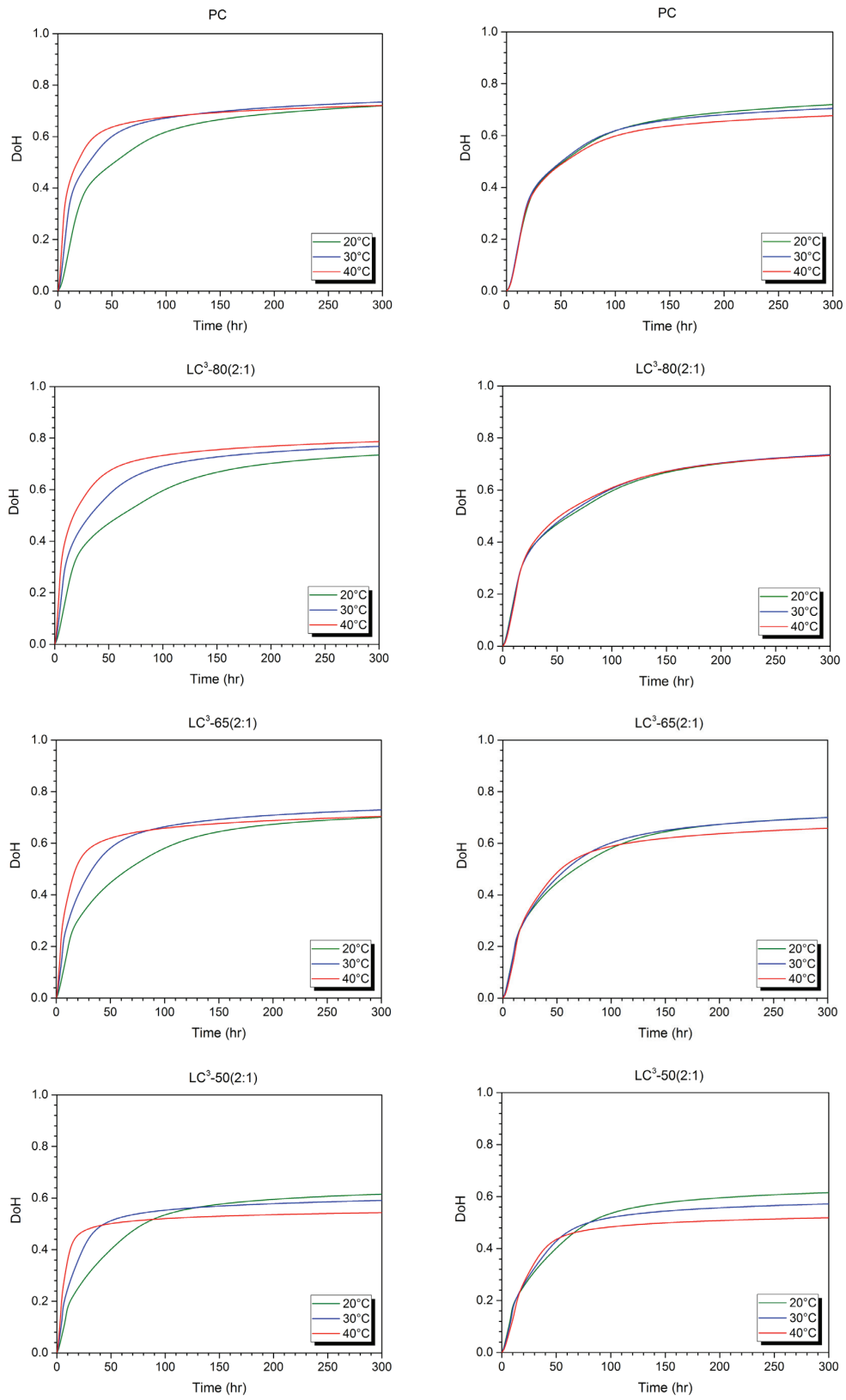


Figure G.1 Degree of hydration curves of PC and LC³ systems with various substitution levels, before curve fitting (left) and after curve fitting (right)

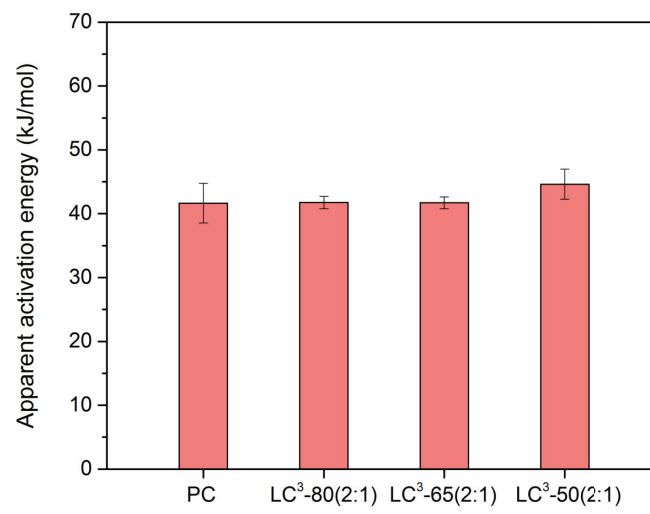


Figure G.2 The apparent activation energy (E_a) of PC and LC³ systems

References

- [1] WBCSD, Technology Roadmap Low-Carbon Transition in the Cement Industry, 2018.
- [2] H. Toutanji, N. Delatte, S. Aggoun, R. Duval, A. Danson, Effect of supplementary cementitious materials on the compressive strength and durability of short-term cured concrete, *Cement and Concrete Research*, 34 (2004) 311-319.
- [3] M. Thomas, The effect of supplementary cementing materials on alkali-silica reaction: A review, *Cement and Concrete Research*, 41 (2011) 1224-1231.
- [4] M.C.G. Juenger, R. Siddique, Recent advances in understanding the role of supplementary cementitious materials in concrete, *Cement and Concrete Research*, 78, Part A (2015) 71-80.
- [5] M.C.G. Juenger, R. Siddique, Recent advances in understanding the role of supplementary cementitious materials in concrete, *Cement and Concrete Research*, 78 (2015) 71-80.
- [6] K. Scrivener, V. John, E. Gartner, *Eco-efficient cements: Potential economically viable solutions for a low-CO₂ cement-based materials industry*, 2016.
- [7] Karen L. Scrivener, Vanderley M John, E.M. Gartner, *Eco-efficient cements: Potential economically viable solutions for a low-CO₂ cement-based materials industry*, UNEP (United Nations Environment Program), 2016.
- [8] K. Scrivener, F. Martirena, S. Bishnoi, S. Maity, Calcined clay limestone cements (LC3), *Cement and Concrete Research*, (2017).
- [9] SCG, http://www.scg.co.th/en/05sustainability_development/eco-value.html, 21.04.2018.
- [10] H.H. Murray, Chapter 2 Structure and Composition of the Clay Minerals and their Physical and Chemical Properties, in: H.H. Murray (Ed.) *Developments in Clay Science*, Elsevier 2006, pp. 7-31.
- [11] <http://pubs.usgs.gov/of/2001/of01-041/htmldocs/clay.htm>, 20.01.2016.
- [12] R. Fernandez, F. Martirena, K.L. Scrivener, The origin of the pozzolanic activity of calcined clay minerals: A comparison between kaolinite, illite and montmorillonite, *Cement and Concrete Research*, 41 (2011) 113-122.
- [13] [http://www.sptn.dss.go.th/otopinfor/attachments/article/142/CF74\(A10\).pdf](http://www.sptn.dss.go.th/otopinfor/attachments/article/142/CF74(A10).pdf), 09.08.2018.
- [14] DMR, Source of clay in Thailand, http://www.dmr.go.th/download/document/minerals/clays/e_074_081.pdf, 08.08.2018.
- [15] M. Fitos, E.G. Badogiannis, S.G. Tsivilis, M. Perraki, Pozzolanic activity of thermally and mechanically treated kaolins of hydrothermal origin, *Applied Clay Science*, 116-117 (2015) 182-192.
- [16] R. San Nicolas, M. Cyr, G. Escadeillas, Characteristics and applications of flash metakaolins, *Applied Clay Science*, 83-84 (2013) 253-262.
- [17] S. Salvador, Pozzolanic properties of flash-calcined kaolinite: A comparative study with soak-calcined products, *Cement and Concrete Research*, 25 (1995) 102-112.
- [18] K.E. Rasmussen, M. Moesgaard, L.L. K hler, T.T. Tran, J. Skibsted, Comparison of the Pozzolanic Reactivity for Flash and Soak Calcined Clays in Portland Cement Blends, in: K. Scrivener, A. Favier (Eds.) *Calcined Clays for Sustainable Concrete*, Springer Netherlands, Dordrecht, 2015, pp. 151-157.
- [19] M. Arikani, K. Sobolev, T. Ert n, A. Yeđinobali, P. Turker, Properties of blended cements with thermally activated kaolin, *Construction and Building Materials*, 23 (2009) 62-70.
- [20] K.L. Konan, C. Peyratout, A. Smith, J.P. Bonnet, S. Rossignol, S. Oyetola, Comparison of surface properties between kaolin and metakaolin in concentrated lime solutions, *Journal of Colloid and Interface Science*, 339 (2009) 103-109.

- [21] S. Hollanders, R. Adriaens, J. Skibsted, Ö. Cizer, J. Elsen, Pozzolanic reactivity of pure calcined clays, *Applied Clay Science*, 132-133 (2016) 552-560.
- [22] J. Ambroise, M. Murat, J. Pera, Hydration reaction and hardening of calcined clays and related minerals. IV. Experimental conditions for strength improvement on metakaolinite minicylinders, *Cement and Concrete Research*, 15 (1985) 83-88.
- [23] T. Matschei, B. Lothenbach, F.P. Glasser, The role of calcium carbonate in cement hydration, *Cement and Concrete Research*, 37 (2007) 551-558.
- [24] B. Lothenbach, G. Le Saout, E. Gallucci, K. Scrivener, Influence of limestone on the hydration of Portland cements, *Cement and Concrete Research*, 38 (2008) 848-860.
- [25] A. Ipavec, R. Gabrovsek, T. Vuk, V. Kaucic, J. Macek, A. Meden, Carboaluminate Phases Formation During the Hydration of Calcite-Containing Portland Cement, *J. Am. Ceram. Soc.*, 94 (2011) 1238-1242.
- [26] K. De Weerd, M.B. Haha, G. Le Saout, K.O. Kjellsen, H. Justnes, B. Lothenbach, Hydration mechanisms of ternary Portland cements containing limestone powder and fly ash, *Cement and Concrete Research*, 41 (2011) 279-291.
- [27] O. Chowanec, *Limestone Addition in Cement*, EPFL, 2012.
- [28] M. Antoni, J. Rossen, F. Martirena, K. Scrivener, Cement substitution by a combination of metakaolin and limestone, *Cement and Concrete Research*, 42 (2012) 1579-1589.
- [29] M. Antoni, *Investigation of cement substitution by blends of calcined clays and limestone*, EPFL, 2013.
- [30] F. Avet, K. Scrivener, Investigation of the calcined kaolinite content on the hydration of Limestone Calcined Clay Cement (LC3), *Cement and Concrete Research*, 107 (2018) 124-135.
- [31] F.H. Avet, *Investigation of the grade of calcined clays used as clinker substitute in Limestone Calcined Clay Cement (LC3)*, LMC, EPFL, 2017.
- [32] S. Krishnan, S. Bishnoi, Understanding the hydration of dolomite in cementitious systems with reactive aluminosilicates such as calcined clay, *Cement and Concrete Research*, 108 (2018) 116-128.
- [33] H. Maraghechi, F. Avet, H. Wong, H. Kamyab, K. Scrivener, Performance of Limestone Calcined Clay Cement (LC3) with various kaolinite contents with respect to chloride transport, *Materials and Structures*, 51 (2018) 125.
- [34] S. Brunauer, P.H. Emmett, E. Teller, Adsorption of Gases in Multimolecular Layers, *Journal of the American Chemical Society*, 60 (1938) 309-319.
- [35] E.P. Barrett, L.G. Joyner, P.P. Halenda, The Determination of Pore Volume and Area Distributions in Porous Substances. I. Computations from Nitrogen Isotherms, *Journal of the American Chemical Society*, 73 (1951) 373-380.
- [36] R.S. Almenares, L.M. Vizcaíno, S. Damas, A. Mathieu, A. Alujas, F. Martirena, Industrial calcination of kaolinitic clays to make reactive pozzolans, *Case Studies in Construction Materials*, 6 (2017) 225-232.
- [37] J.E. Rossen, K.L. Scrivener, Optimization of SEM-EDS to determine the C-A-S-H composition in matured cement paste samples, *Materials Characterization*, 123 (2017) 294-306.
- [38] P.K. Mehta, and Monteiro, P.J.M., *Concrete: Microstructure, Properties, and Materials*, Fourth Edition, McGraw-Hill Education 2014.
- [39] P.T. Durdziński, Hydration of multi-component cements containing cement clinker, slag, calcareous fly ash and limestone, LMC, EPFL, 2016.
- [40] T.C. Powers, Structure and Physical Properties of Hardened Portland Cement Paste, *Journal of the American Ceramic Society*, 41 (1958) 1-6.

- [41] P. Termkhajornkit, Q.H. Vu, R. Barbarulo, S. Daronnat, G. Chanvillard, Dependence of compressive strength on phase assemblage in cement pastes: Beyond gel–space ratio — Experimental evidence and micromechanical modeling, *Cement and Concrete Research*, 56 (2014) 1-11.
- [42] P.T. Durdziński, M. Ben Haha, M. Zajac, K.L. Scrivener, Phase assemblage of composite cements, *Cement and Concrete Research*, 99 (2017) 172-182.
- [43] E. Berodier, K. Scrivener, Understanding the Filler Effect on the Nucleation and Growth of C-S-H, *Journal of the American Ceramic Society*, 97 (2014) 3764-3773.
- [44] D. Damidot, S. Stronach, A. Kindness, M. Atkins, F.P. Glasser, Thermodynamic investigation of the CaO-Al₂O₃-CaCO₃-H₂O closed system at 25°C and the influence of Na₂O, *Cement and Concrete Research*, 24 (1994) 563-572.
- [45] <http://gems.web.psi.ch>, 2018.
- [46] B. Lothenbach, D.A. Kulik, T. Matschei, M. Balonis, L. Baquerizo, B. Dilnesa, G.D. Miron, R.J. Myers, Cemdata18: A chemical thermodynamic database for hydrated Portland cements and alkali-activated materials, *Cement and Concrete Research*, 115 (2019) 472-506.
- [47] B. Lothenbach, F. Winnefeld, C. Alder, E. Wieland, P. Lunk, Effect of temperature on the pore solution, microstructure and hydration products of Portland cement pastes, *Cement and Concrete Research*, 37 (2007) 483-491.
- [48] J. Komonen, V. Penttala, Effects of High Temperature on the Pore Structure and Strength of Plain and Polypropylene Fiber Reinforced Cement Pastes, *Fire Technology*, 39 (2003) 23-34.
- [49] A.A. Almusallam, Effect of environmental conditions on the properties of fresh and hardened concrete, *Cement and Concrete Composites*, 23 (2001) 353-361.
- [50] I. Elkhadiri, F. Puertas, The effect of curing temperature on sulphate-resistant cement hydration and strength, *Construction and Building Materials*, 22 (2008) 1331-1341.
- [51] K.O. Kjellsen, R.J. Detwiler, O.E. GjØrv, Development of microstructures in plain cement pastes hydrated at different temperatures, *Cement and Concrete Research*, 21 (1991) 179-189.
- [52] E. Berodier, K. Scrivener, Evolution of pore structure in blended systems, *Cement and Concrete Research*, 73 (2015) 25-35.
- [53] L. Lam, Y.L. Wong, C.S. Poon, Degree of hydration and gel/space ratio of high-volume fly ash/cement systems, *Cement and Concrete Research*, 30 (2000) 747-756.
- [54] M. Steiger, Crystal growth in porous materials—II: Influence of crystal size on the crystallization pressure, *Journal of Crystal Growth*, 282 (2005) 470-481.
- [55] J. Bizzozero, Hydration and dimensional stability of calcium aluminate cement based systems, EPFL, 2014.
- [56] A.R. Brough, C.M. Dobson, I.G. Richardson, G.W. Groves, A study of the pozzolanic reaction by solid-state ²⁹Si nuclear magnetic resonance using selective isotopic enrichment, *Journal of Materials Science*, 30 (1995) 1671-1678.
- [57] E. L'Hôpital, B. Lothenbach, G. Le Saout, D. Kulik, K. Scrivener, Incorporation of aluminium in calcium-silicate-hydrates, *Cement and Concrete Research*, 75 (2015) 91-103.
- [58] T.T.H. Bach, C.C.D. Coumes, I. Pochard, C. Mercier, B. Revel, A. Nonat, Influence of temperature on the hydration products of low pH cements, *Cement and Concrete Research*, 42 (2012) 805-817.
- [59] F. Deschner, B. Lothenbach, F. Winnefeld, J. Neubauer, Effect of temperature on the hydration of Portland cement blended with siliceous fly ash, *Cement and Concrete Research*, 52 (2013) 169-181.
- [60] A. Kumar, G. Sant, C. Patapy, C. Gianocca, K.L. Scrivener, The influence of sodium and potassium hydroxide on alite hydration: Experiments and simulations, *Cement and Concrete Research*, 42 (2012) 1513-1523.

- [61] B. Mota, T. Matschei, K. Scrivener, The influence of sodium salts and gypsum on alite hydration, *Cement and Concrete Research*, 75 (2015) 53-65.
- [62] G. Frigione, R. Sersale, The influence of the chemical composition of the clinker on the strength properties of blast furnace slag cements, *Cement and Concrete Research*, 15 (1985) 159-166.
- [63] A.L.A. Fraay, J.M. Bijen, Y.M. de Haan, The reaction of fly ash in concrete a critical examination, *Cement and Concrete Research*, 19 (1989) 235-246.
- [64] F. Lagier, K.E. Kurtis, Influence of Portland cement composition on early age reactions with metakaolin, *Cement and Concrete Research*, 37 (2007) 1411-1417.
- [65] B. Lothenbach, K. Scrivener, R.D. Hooton, Supplementary cementitious materials, *Cement and Concrete Research*, 41 (2011) 1244-1256.
- [66] M. Cyr, M. Trinh, B. Husson, G. Casaux-Ginestet, Effect of cement type on metakaolin efficiency, *Cement and Concrete Research*, 64 (2014) 63-72.
- [67] B. Mota Gassó, Impact of alkali salts on the kinetics and microstructural development of cementitious systems, EPFL, 2015.
- [68] I. Jawed, J. Skalny, Alkalies in cement: A review, *Cement and Concrete Research*, 8 (1978) 37-51.
- [69] N. Smaoui, M.A. Bérubé, B. Fournier, B. Bissonnette, B. Durand, Effects of alkali addition on the mechanical properties and durability of concrete, *Cement and Concrete Research*, 35 (2005) 203-212.
- [70] F. Avet, R. Snellings, A. Alujas Diaz, M. Ben Haha, K. Scrivener, Development of a new rapid, relevant and reliable (R3) test method to evaluate the pozzolanic reactivity of calcined kaolinitic clays, *Cement and Concrete Research*, 85 (2016) 1-11.
- [71] A. Quennoz, K.L. Scrivener, Interactions between alite and C3A-gypsum hydrations in model cements, *Cement and Concrete Research*, 44 (2013) 46-54.
- [72] B. Mota, T. Matschei, K. Scrivener, Impact of NaOH and Na₂SO₄ on the kinetics and microstructural development of white cement hydration, *Cement and Concrete Research*, 108 (2018) 172-185.
- [73] S. Alahrache, F. Winnefeld, J.-B. Champenois, F. Hesselbarth, B. Lothenbach, Chemical activation of hybrid binders based on siliceous fly ash and Portland cement, *Cement and Concrete Composites*, 66 (2016) 10-23.
- [74] D.A. Kulik, Improving the structural consistency of C-S-H solid solution thermodynamic models, *Cement and Concrete Research*, 41 (2011) 477-495.
- [75] G.W. Scherer, Stress from crystallization of salt, *Cement and Concrete Research*, 34 (2004) 1613-1624.
- [76] C.W. Hargis, B. Lothenbach, C.J. Müller, F. Winnefeld, Further insights into calcium sulfoaluminate cement expansion, *Advances in Cement Research*, (2018) 1-18.
- [77] J.L. Poole, Riding, K.A., Folliard, K.J., Juenger, M.C.G., and Schindler, A.K., Methods for Calculating Activation Energy for Portland Cement, *Materials Journal*, 104 (2007).
- [78] M. Broda, E. Wirquin, B. Duthoit, Conception of an isothermal calorimeter for concrete—Determination of the apparent activation energy, *Materials and Structures*, 35 (2002) 389-394.
- [79] J.L. Poole, Riding, K.A., Folliard, K.J., Juenger, M.C.G., and Schindler, A.K., Effects of Supplementary Cementitious Materials on Apparent Activation Energy, *Journal of ASTM International*, 7 (2010) 1-16.
- [80] I. Pane, W. Hansen, Investigation of blended cement hydration by isothermal calorimetry and thermal analysis, *Cement and Concrete Research*, 35 (2005) 1155-1164.
- [81] K.S. Anton, Effect of Temperature on Hydration of Cementitious Materials, *Materials Journal*, 101.

- [82] H. Kada-Benameur, E. Wirquin, B. Duthoit, Determination of apparent activation energy of concrete by isothermal calorimetry, *Cement and Concrete Research*, 30 (2000) 301-305.
- [83] V.G. Papadakis, Effect of supplementary cementing materials on concrete resistance against carbonation and chloride ingress, *Cement and Concrete Research*, 30 (2000) 291-299.
- [84] R. Folic, D. Zenunović, *Durability design of concrete structures, Part 2: Modelling and structural assessment*, 2010.
- [85] G.M. Sabnis, *Green Building with Concrete: Sustainable Design and Construction*, Second Edition, CRC Press, Boca Raton, 2015.
- [86] T. H. Wee, Arvind K. Suryavanshi, S.S. Tin, Evaluation of Rapid Chloride Permeability Test (RCPT) Results for Concrete Containing Mineral Admixtures, *Materials Journal*, 97.
- [87] M. Balonis, B. Lothenbach, G. Le Saout, F.P. Glasser, Impact of chloride on the mineralogy of hydrated Portland cement systems, *Cement and Concrete Research*, 40 (2010) 1009-1022.
- [88] Z. Shi, M.R. Geiker, B. Lothenbach, K. De Weerd, S.F. Garzón, K. Enemark-Rasmussen, J. Skibsted, Friedel's salt profiles from thermogravimetric analysis and thermodynamic modelling of Portland cement-based mortars exposed to sodium chloride solution, *Cement and Concrete Composites*, 78 (2017) 73-83.
- [89] <https://http://www.understanding-cement.com/alkali-silica.html>, 2018.
- [90] M. Abdelrahman, M.K. ElBatanouny, P. Ziehl, J. Fasl, C.J. Larosche, J. Fraczek, Classification of alkali-silica reaction damage using acoustic emission: A proof-of-concept study, *Construction and Building Materials*, 95 (2015) 406-413.
- [91] T. Kim, J. Olek, H. Jeong, Alkali-silica reaction: Kinetics of chemistry of pore solution and calcium hydroxide content in cementitious system, *Cement and Concrete Research*, 71 (2015) 36-45.
- [92] F. Rajabipour, E. Giannini, C. Dunant, J.H. Ideker, M.D.A. Thomas, Alkali-silica reaction: Current understanding of the reaction mechanisms and the knowledge gaps, *Cement and Concrete Research*, 76 (2015) 130-146.
- [93] T. Chappex, K. Scrivener, Alkali fixation of C-S-H in blended cement pastes and its relation to alkali silica reaction, *Cement and Concrete Research*, 42 (2012) 1049-1054.
- [94] T. Chappex, K.L. Scrivener, The influence of aluminium on the dissolution of amorphous silica and its relation to alkali silica reaction, *Cement and Concrete Research*, 42 (2012) 1645-1649.
- [95] E. L'Hôpital, B. Lothenbach, K. Scrivener, D.A. Kulik, Alkali uptake in calcium alumina silicate hydrate (C-A-S-H), *Cement and Concrete Research*, 85 (2016) 122-136.
- [96] M. Antoni, L. Baquerizo, T. Matschei, Investigation of Ternary Mixes Made of Clinker Limestone and Slag or Metakaolin: Importance of Reactive Alumina and Silica Content, in: K. Scrivener, A. Favier (Eds.) *Calcined Clays for Sustainable Concrete*, Springer Netherlands, Dordrecht, 2015, pp. 545-553.
- [97] A. Favier, F. Zunino, I. Katrantzis, K. Scrivener, The Effect of Limestone on the Performance of Ternary Blended Cement LC3: Limestone, Calcined Clays and Cement, in: F. Martirena, A. Favier, K. Scrivener (Eds.) *Calcined Clays for Sustainable Concrete*, Springer Netherlands, Dordrecht, 2018, pp. 170-175.
- [98] A. Alujas, J. Fernando Martirena, Influence of Calcination Temperature in the Pozzolanic Reactivity of a Low Grade Kaolinitic Clay, in: K. Scrivener, A. Favier (Eds.) *Calcined Clays for Sustainable Concrete*, Springer Netherlands, Dordrecht, 2015, pp. 331-338.
- [99] R.L. Berger, J.D. McGregor, Influence of admixtures on the morphology of calcium hydroxide formed during tricalcium silicate hydration, *Cement and Concrete Research*, 2 (1972) 43-55.
- [100] K.S. Anton, J.F. Kevin, Heat of Hydration Models for Cementitious Materials, *Materials Journal*, 102.

References

- [101] B.H. Zaribaf, K.E. Kurtis, Addressing Key Challenges in MK-PLC Blends at Early Ages: Workability, Slump Retention, and Heat of Hydration, in: F. Martirena, A. Favier, K. Scrivener (Eds.) *Calcined Clays for Sustainable Concrete*, Springer Netherlands, Dordrecht, 2018, pp. 500-506.
- [102] K. A. Riding, J. L. Poole, K. J. Folliard, M. C. G. Juenger, A.K. Schindler, Modeling Hydration of Cementitious Systems, *Materials Journal*, 109.
- [103] K. A. Riding, J. L. Poole, K. J. Folliard, M. C. G. Juenger, A.K. Schindler, New Model for Estimating Apparent Activation Energy of Cementitious Systems, *Materials Journal*, 108.

Curriculum Vitae

Wilasinee Hanpongpun

Email: wilasinee.hanpongpun@epfl.ch, wilasin@scg.com

PERSONAL DETAILS

Date of Birth: December 03, 1982

Gender: Female

Nationality: Thai

EDUCATION

2015 - Present Swiss Federal Institute of Technology of Lausanne (EPFL), PhD student
Thesis topic: Investigation of the use of Limestone Calcined Clay Cement (LC3) applied to Thailand

2004 - 2006 Chulalongkorn University, Bangkok, Thailand
Master's Degree in Science, Department of Materials Science,
Major Ceramics Technology
Thesis topic: Utilization of zinc hydrometallurgy waste for artificial marble

2000 - 2004 Chiang Mai University, Chiang Mai, Thailand
Bachelor's Degree in Science, Department of Physics,
Major Materials Science
Senior project topic: Microstructure and wear of alloy coatings prepared by flame spray and spray and fuse techniques

EXPERIENCE

2013 - 2014 Product Development Specialist, Clinker and Cement Technology, Cement Application Technology,
SCG Cement Co., Ltd., Saraburi, Thailand

2007 - 2013 Researcher, Cement and Cementitious Research Group,
Siam Research and Innovation Co., Ltd.,
SCG Cement, Saraburi, Thailand

PUBLICATIONS

- 2017 Hanpongpun, W. and Scrivener, K., "The effect of alkali on the properties of Limestone Calcined Clay Cement (LC³)", 2nd International Conference on Calcined Clays for Sustainable Concrete, Habana, Cuba.
- 2017 Hanpongpun, W. and Scrivener, K., "The influence of calcined clay substitution on the properties of Limestone Calcined Clay Cement (LC³)", 71st RILEM Week & ICACMS 2017, Chennai, India.
- 2017 Hanpongpun, W. and Scrivener, K., "The effect of alkali on the microstructure of LC³ system" The 16th Euroseminar on Microscopy Applied to Building Materials, Les Diablerets, Switzerland.
- 2015 Hanpongpun, W. and Scrivener, K. "The effect of alkali on the hydration of Limestone Calcined Clay Cement (LC³)", 35th Cement & Concrete Science Conference 2015, Aberdeen, Scotland.

